Wave-driven recovery of sandy beaches following storm erosion

Author:
Phillips, Matthew

Publication Date:
2018

DOI:
https://doi.org/10.26190/unsworks/20313

Wave-driven recovery of sandy beaches following storm erosion

Matthew Sean Phillips

A thesis in fulfillment of the requirements for the degree of

Doctor of Philosophy

School of Civil and Environmental Engineering

Faculty of Engineering

UNSW Sydney

February, 2018

THE UNIVERSITY OF NEW SOUTH WALES
Thesis/Dissertation Sheet

Surname or Family name: **Phillips**

First name: **Matthew** Other name/s: **Sean**

Abbreviation for degree as given in the University calendar: **Ph.D.**

School: **School of Civil and Environmental Engineering** Faculty: **Faculty of Engineering**

Title: **Wave-driven recovery of sandy beaches following storm erosion**

Abstract

Following the rapid and destructive impacts of storm erosion, beach recovery is a key natural process of restoration, returning eroded sediment to the subaerial beach and rebuilding coastal morphology to continue to support the needs of modern-day coastal communities. While more detailed understanding of storm erosion has been developed, this thesis advances insight into wave-driven recovery processes of the subaerial beach following storms on microtidal, wave-dominated sandy beaches.

The onshore return of nearshore sediment back to the shoreline is a primary wave driven process of beach recovery. Shoreline recovery is analysed following 82 individual storms using a 10-year coastal imaging dataset of daily shoreline and sandbar positions. Shoreline recovery rates are quantified, highlighting temporal variability significantly correlated with parameters related to nearshore wave steepness and sandbar morphodynamics. A new conceptual model is presented, describing phases and rates of shoreline recovery through various stages of onshore sandbar migration following storms, from fully detached storm-deposited sandbar morphology through to complete sandbar welding with the shoreline.

After nearshore sediment has returned to the shoreline, swash processes then rework sediment up onto the subaerial beach to rebuild the berm. Following complete removal by a significant storm event, the entire rebuilding of a berm is examined at tide by tide timescales, using high resolution (5 Hz) swash and subaerial beach profile measurements obtained from a continuously scanning Lidar. Tide-by-tide rates of subaerial volume change, berm crest growth and subaerial profile variability are quantified and examined. The findings identify behavioural modes of subaerial profile variability throughout berm recovery, distinguished by swash, nearshore wave and ocean water level conditions.

Finally, alongshore variability in subaerial volume recovery on an embayed coastline is evaluated at distinct spatial scales both within and between four closely-situated embayments following a significant storm event. The range of variability in net rates of subaerial volume recovery within individual embayments was found to be substantially larger (by a factor of 10) than between embayments. This variability was observed between embayment extremities and also locations spaced only a few hundred metres apart, considered to be driven by subaqueous morphodynamics and alongshore gradients in nearshore wave energy.

Originality Statement

‘I hereby declare that this submission is my own work and to the best of my knowledge it contains no materials previously published or written by another person, or substantial proportions of material which have been accepted for the award of any other degree or diploma at UNSW or any other educational institution, except where due acknowledgement is made in the thesis. Any contribution made to the research by others, with whom I have worked at UNSW or elsewhere, is explicitly acknowledged in the thesis. I also declare that the intellectual content of this thesis is the product of my own work, except to the extent that assistance from others in the project's design and conception or in style, presentation and linguistic expression is acknowledged.’

Matthew Sean Phillips

February 2018

Copyright Statement

Authenticity Statement

This research was funded by the Australian Research Council [DP150101339]. The author was supported by an Australian Postgraduate Award and in part by the Coastal Processes and Responses Node Research Hub of the NSW Office of Environment and Heritage.

Abstract

Following the rapid and destructive impacts of storm erosion, beach recovery is a key natural process of restoration, returning eroded sediment to the subaerial beach and rebuilding coastal morphology to continue to support the needs of modern-day coastal communities. While more detailed understanding of storm erosion has been developed, this thesis advances insight into wave-driven recovery processes of the subaerial beach following storms on microtidal, wave-dominated sandy beaches.

The onshore return of nearshore sediment back to the shoreline is a primary wave-driven process of beach recovery. Shoreline recovery is analysed following 82 individual storms using a 10-year coastal imaging dataset of daily shoreline and sandbar positions. Shoreline recovery rates are quantified, highlighting temporal variability significantly correlated with parameters related to nearshore wave steepness and sandbar morphodynamics. A new conceptual model is presented, describing phases and rates of shoreline recovery through various stages of onshore sandbar migration following storms, from fully detached storm-deposited sandbar morphology through to complete sandbar welding with the shoreline.

After nearshore sediment has returned to the shoreline, swash processes then rework sediment up onto the subaerial beach to rebuild the berm. Following complete removal by a significant storm event, the entire rebuilding of a berm is examined at tide-by-tide timescales, using high resolution (5 Hz) swash and subaerial beach profile measurements obtained from a continuously scanning Lidar. Tide-by-tide rates of subaerial volume change, berm crest growth and subaerial profile variability are quantified and examined. The findings identify behavioural modes of subaerial profile variability throughout berm recovery, distinguished by swash, nearshore wave and ocean water level conditions.

Finally, alongshore variability in subaerial volume recovery on an embayed coastline is evaluated at distinct spatial scales both within and between four closely-situated embayments following a significant storm event. The range of variability in net rates of subaerial volume recovery within individual embayments was found to be substantially larger (by a factor of 10) than between embayments. This variability was observed between embayment extremities and also locations spaced only a few hundred metres apart, considered to be driven by subaqueous morphodynamics and alongshore gradients in nearshore wave energy.

Acknowledgements

I would like to begin by acknowledging the Traditional Custodians of the land on which this study took place, the **Garigal** people, and recognise their continuing connection to land, water and community. I pay respect to Elders past and present, and extend this to any Aboriginal and Torres Strait Islander person on this land today.

I want to thank my supervisor **Prof. Ian Turner** for making it possible for myself, and so many others, to be taught in the field of coastal engineering. To be given the opportunity to undertake this thesis, learning and studying the beaches I've been blessed to grow up on, was an offer he gave that was too good to turn down. It has been a privilege to have had this opportunity and to study under his insight, guidance and support throughout all stages of this work. He once told me *"...at the end of a PhD what you really learn is how much you don't know"*. I couldn't agree more.

I would also like to thank my joint supervisors, **Dr. Kristen Splinter** and **Dr. Mitchell Harley** for their valued input and dedicated supervision of this thesis. I am grateful for all the insightful feedback, encouragement and the constant willingness to give time and thought to problems, figures, writing and key ideas. Also thanks to my secondary supervisor, **A/Prof. Ron Cox** whose experience and knowledge gave direction during the initial stages of this work. I am grateful to have also collaborated with **Dr. Chris Blenkinsopp** in developing Chapters 3 and 5 of this thesis, to which he has given valued understanding, feedback and enthusiasm.

There are many who have been involved in the various datasets presented in this thesis. In particular I would like to thank those who contributed to the procurement and deployment of the Fixed Lidar monitoring system presented in Chapter 5. This has included **Dr. Kristen Splinter**, **Dr. Chris Blenkinsopp**, **Larry Paice, Dr. Daniel Howe**, **Dr. Michael Allis, Robert Thompson** and **Karina Taylor.** Thanks also to **Flight Deck** apartment building, Collaroy, for their cooperation. Additionally, I would like to acknowledge the efforts of all those involved in the support, development, operation, maintenance and data processing of the Narrabeen ARGUS Coastal Imaging station presented in Chapter 4. Wave and tide data was kindly provided by **Manly Hydraulics Laboratory** on behalf of the **NSW Office of Environment and Heritage** (OEH). Nearshore wave modelling and lookup table was undertaken by **Dr. Thomas Mortlock**, Macquarie University.

I have been grateful to have completed this thesis at the supportive, experienced and collaborative environment of the **Water Research Laboratory** (WRL). Thank you to all the WRL staff and students who make this such a great place to work and team to be a part of.

A special mention to **Joshua Simmons**, to who I am thankful to have shared the journey of a PhD with from day one to completion. Whether it was signing our names in the tracks of the quad bike data, chasing storms, post-conference downhill mountain biking, lunch time runs around the dam, measuring in excess of 2800 beach profiles, or just an ordinary day of slowly going insane; thanks for your friendship. It couldn't have been more fun.

To **Mum** and **Dad**, thanks for taking me to the beach all those years. Thanks for putting sunscreen on my face, holding my hand under that first wave, washing my sand-covered body under the shower while I squirmed, pushing me onto the biggest “wave of the day” while I screamed, the 50c icy poles from Long Reef surf club kiosk, my first blue foam surfboard, taking me surfing, waving at me from the beach when I was obliviously drifting with the current, holidays to Evans Head, looking for shells, digging for pippies, untangling my fishing line, pulling off the blue bottles, filming/commentating our surf movies, and so much more. To my sister **Ami** and brother **Dan**, thanks for waiting for me at the car while I got that last, just one more, wave in.

To my wife **Kezia**, thank you for your affirming love, faithful companionship, patience and prayer.

Most importantly, to **God**, whom I could never thank enough for the gift that it is to be his child, bought by the death and resurrection of **Jesus**. Without using a word, every wave proclaims the greatest of his power and each grain of sand declares the intricacies of his wisdom.

O LORD, our Lord, how majestic is your name in all the earth!

Psalm 8:1

Relevant Publications

Journal Publications

Phillips, M. S., Harley, M. D., Turner, I. L., Splinter, K. D. and Cox, R. J., 2017. Shoreline recovery on wave-dominated sandy coastlines: the role of sandbar morphodynamics and nearshore wave parameters. Marine Geology, 385, 146-159. doi: 10.1016/j.margeo.2017.01.005.

Phillips, M. S., Harley, M. D., Blenkinsopp, C. E., Turner, I. L., Splinter, K. D. and Cox, R. J., *in prep*. Timescales and rates of post-storm beach recovery: a synthesis. Coastal Engineering.

Phillips, M. S., Blenkinsopp, C. E., Splinter, K. D., Harley, M. D., Turner, I. L. and Cox, R. J., *in prep*. Beachface and berm morphodynamics during post-storm beach recovery: observations from a continuous scanning Lidar. Geophysical Research Letters.

Phillips, M. S., Harley, M. D., Splinter, K. D., and Turner, I. L., *in prep*. Alongshore variability in post-storm beach recovery at spatial scales within and between embayments. Marine Geology.

Turner, I. L., Harley, M. D., Short, A. D., Simmons, J. A., Bracs, M. A., **Phillips, M. S**. and Splinter, K. D., 2016. A multi-decade dataset of monthly beach profile surveys and inshore wave forcing at Narrabeen, Australia. Scientific Data, 3, 160024. doi: 10.1038/sdata.2016.24.

Harley, M. D., Turner, I. L., Kinsela, M. A., Middleton, J. H., Mumford, P. J., Splinter, K. D., **Phillips, M. S**., Simmons, J. A., Hanslow, D. J. and Short, A. D., 2017. Extreme coastal erosion enhanced by anomalous extratropical storm wave direction. Scientific Reports, 7(1), 6033. doi: 10.1038/s41598-017-05792-1.

Peer-reviewed Conference Publications

Phillips, M. S., Turner, I. L., Cox , R. J., Splinter, K. D. and Harley, M. D., 2015. Will the sand come back? Observations and characteristics of beach recovery In Procceedings: Australasian Coasts & Ports Conference, Auckland, New Zealand.

Phillips, M. S., Blenkinsopp, C. E., Splinter, K. D., Harley, M. D., Turner, I. L. and Cox, R. J., 2017. High-frequency observations of berm recovery using a continuous scanning Lidar. In Procceedings: Australasian Coasts & Ports, Cairns, Australia.

Harley, M. D., Turner, I. L., Short, A. D., Bracs, M. A., **Phillips, M. S.**, Simmons, J. A. and Splinter, K. D., 2015. Four decades of coastal monitoring at Narrabeen-Collaroy Beach: the past, present and future of this unique dataset. In Procceedings: Australasian Coasts & Ports Conference, Auckland, New Zealand.

Harley, M. D., Turner, I. L., Splinter, K. D., **Phillips, M. S**. and Simmons, J. A., 2016. Beach response to Australian East Coast Lows: A comparison between the 2007 and 2015 events, Narrabeen-Collaroy Beach. Journal of Coastal Research, SI(75), 388-392. doi: 10.2112/SI75-078.1.

Contents

List of Figures

List of Tables

Nomenclature

Symbol	Description	Units
d_{50}	Median grain size	mm
dv/dt	Rate of subaerial volume change	m^3/m/day
dv_{bf}/dt	Rate of beachface volume change	m^3/m/day
dv_{bm}/dt	Rate of berm volume change	m^3/m/day
dx_b/dt	Cross-shore rate of sandbar change	m/day
dx_s/dt	Cross-shore rate of shoreline change	m/day
E	Wave energy	J/m^2
H/L	Wave steepness	-
H_s	Significant wave height	m
L	Wavelength	m
P	Wave power	W/m
r	Pearson correlation coefficient	-
$R_{2\%}$	2% wave runup exceedance elevation	m
T_p	Peak wave period	s
x_b	Cross-shore sandbar position	m
x_{bs}	Cross-shore sandbar position relative to the concurrent shoreline position	m
x_s	Cross-shore shoreline position	m
Δx_s	Cross-shore accuracy of the daily video-derived shoreline position	m
θ	Wave direction	°TN
Ω	Dimensionless fall velocity	-
$\Delta\Omega$	Temporal disequilibrium in dimensionless fall velocity	-

Abbreviation	Description
ECL	East Coast Low
LBT	Longshore bar and trough
LTT	Low tide terrace
MHW	Mean high water
MHWS	Mean high water springs
MSL	Mean sea level
OWL	Ocean water level
PIC	Pixel intensity clustering
RBB	Rhythmic bar and beach
RTK-GPS	Real time kinematic global positioning system
TBR	Transverse bar and rip
TWL	Total water level

Chapter 1

Introduction

"Is there anyone who can watch without fascination the struggle for supremacy between sea and land? ... A fresh look always awaits the student, and every wave is a masterpiece of originality. It will ever be so. Go and see."

Willard Bascom, 1964 - Waves and Beaches

1.1 Motivation

Often situated at the interface of the ocean and growing human settlements, coastlines are dynamic environments that support the multifaceted demands of modern-day coastal communities. Coastal regions have attracted the settlement of a large proportion of the world's population, with nearly one quarter living within 100 km of the coast (Small and Nicholls, 2003). Infrastructure assets in coastal regions are estimated at a value of US$13 trillion worldwide (Jongman et al., 2012). In these locations it is often beaches and their dune systems that provide a primary natural buffer of protection, separating settlements and infrastructure from inundation by ocean waters (CERC, 1984). Beaches also provide prized public amenity, as well as critical habitats supporting coastal ecology (Defeo et al., 2009; Frampton, 2010). In Australia, these ecosystem services of protection and amenity have been valued on the order of several millions of dollars per kilometre of shoreline (Blackwell, 2007).

The capacity of a beach to meet the present and future needs of a coastal community is primarily governed by its dynamic response to changes in water level and waves (Bascom, 1954; Wright and Short, 1984). Beaches are composed of a thin veneer of unconsolidated sediment that is continually being reshaped by wind, waves and currents. As described in Cowell et al. (1994), these dynamic changes occur at spatial scales of centimetres (e.g., bed ripples) to several hundreds of kilometres (e.g., regional storm erosion), and at temporal scales of seconds (e.g., wave-by-wave) to millennia (e.g., barrier island evolution).

The dynamic nature of beaches is most evident during storms. Within a period of hours to several days, energetic wave forcing and elevated water levels, can lead to widespread regional erosion of subaerial beach morphology, displacing millions of cubic metres of sediment at varying extents offshore in the subaqueous beach (often deposited as sandbars), and potentially also onshore as overwash deposition (e.g., Morton and Sallenger, 2003; Scott et al., 2016; Harley et al., 2017). This erosion typically results in a landward retreat of the shoreline, removal of berm morphology, and potentially the loss of dune systems in the backshore. After a storm, the natural buffer of the subaerial beach (in terms of cross-shore width, height and volume of sediment) separating coastal infrastructure from the ocean, is left narrower, lower and depleted of volume such that the risk of coastal inundation during subsequent storm activity increases (e.g., Forbes et al., 2004). A reduction in usable beach width, large unstable erosion scarps, storm debris and unsafe access points create hazards for beach users and lower beach amenity (e.g., Silva et al., 2008). Additionally, beach ecology can also be disrupted due to storm erosion (e.g., Rakocinski et al., 2000; Revell et al., 2011). As such, the drastic impact of a storm may leave a beach, at least temporarily, in a degraded condition that poorly meets the demands of a coastal community.

However, storm erosion is not the only component adding to the variability of beaches with time. Counter-acting the destructive impact of storms is the onshore return of eroded sediment and associated rebuilding of the subaerial beach (i.e., the shoreline, berm and dunes) after storms due to forces of waves and wind (aeolian). This post-storm rebuilding process is often referred to in the literature as 'beach recovery' (e.g., Morton et al., 1994; Corbella and Stretch, 2012). In contrast to rapid instances of storm erosion, beach recovery is typically observed as a more gradual process, occurring over several months to years (e.g., Thom and Hall, 1991; Kobayashi and Jung, 2012; Phillips et al., 2015). Importantly as a beach recovers, the depleted post-storm buffer of the subaerial beach protecting adjacent coastal settlement and infrastructure from coastal inundation, is progressively restored in width, volume and height (CERC, 1984). Additionally, during recovery the usable width of a beach is restored to satisfy beach goers (Frampton, 2010) and impacted beach ecology returns to a former state of health (Revell et al., 2011). In this regard, beach recovery is a component of beach variability restoring the impacts of storms and returning the beach to a condition that is often more desired by a coastal community.

An informed understanding into the dynamic nature of beaches is critical to managing densely populated and asset-rich coastal regions (Bascom, 1954). While a more detailed empirical and process-based technical understanding of storm erosion has been developed (e.g., Larson and Kraus, 1989; Roelvink et al., 2009), scientific insight into beach recovery and physical parameters governing its occurrence are less well understood (Jensen et al., 2009; Corbella and Stretch, 2012). Scientific investigations into beach recovery processes are surprisingly limited relative to the vast majority of research focused on understanding and predicting erosion. At present this poses a limitation to risk assessment, planning and design for coastal hazards as coastlines evolve over timescales of multiple storms, years and decades (Coco et al., 2014; Masselink and van Heteren, 2014; Wainwright et al., 2015). Process-based models developed to predict erosion have been applied in various attempts to model beach recovery (Pender and Karunarathna, 2013; Karunarathna et al., 2014). With limited success, these attempts highlight the likelihood of different physics to that of storm erosion. As an alternative, a number of studies have used simplistic fits of beach recovery with limited field data validation or insight into governing parameters in an attempt to capture beach recovery processes (Kriebel and Dean, 1993; Callaghan et al., 2008; Callaghan et al., 2013; Wainwright et al., 2015).

Field investigation to quantify (in terms of rates and durations) beach recovery processes and provide insight into key governing parameters is necessary for the accurate prediction of beach evolution and improved coastal risk assessment. In particular, new scientific insight is warranted into the recovery of the subaerial beach in regions seaward of the foredune, where processes related to waves (termed *wave-driven* recovery processes) drive the post-storm return of subaerial sediment volume deposited offshore and rebuild the shoreline, beachface and berm. This insight can be valuable to post-storm beach remediation works, informing coastal management how to work with natural recovery processes to enhance the return of the beach to a desired condition that serves the economic, social and ecological values of coastal communities.

1.2 Wave-dominated sandy beaches

The world's coastlines can be classified into different wave climates and tidal settings. The global distribution of deepwater significant wave heights, H_s, is shown in Figure 1.1. Mid-latitude cyclones tracking east to west generate large waves ($H_s \approx 2$ - 5 m) between latitudes of 40° to 60° N/S (Davies, 1980; Short, 1999). In the northern hemisphere, these storms predominately occur during the winter (October - March). In the southern hemisphere, these larger wave events occur all year-round with $H_s > 6$ m for 10% of the time and $H_s > 2$ m for 90% of the time (Young and Holland, 1996; Short, 1999). High energy coastlines situated at these latitudes include the west coast of Canada, NW coast of the United States, NW Europe, southern Chile, SW Tasmania in Australia and the South Island of New Zealand. At latitudes of 25° to 40° N/S, mid-latitude cyclones generate moderate to high energy ($H_s \approx 1$ - 3 m) west coast swell and east coast swell that propagates to many exposed west-facing coastlines (e.g., Peru, northern Chile, west coast of America, west coast of Africa, and south coast of Australia) and east-facing coastlines (e.g., Brazil, east coast of Africa, SE Australia) respectively (Young and Holland, 1996; Short, 1999). Closer toward the equator, at latitudes of 0° to 25° N/S, low to moderate wave energy ($H_s \approx 0.5$ - 1.5 m) is generated by year-round trade winds and seasonal monsoons as well as intermittent higher waves by tropical cyclones, hurricanes and typhoons. Low wave energy ($H_s \approx 0$ - 0.5) is

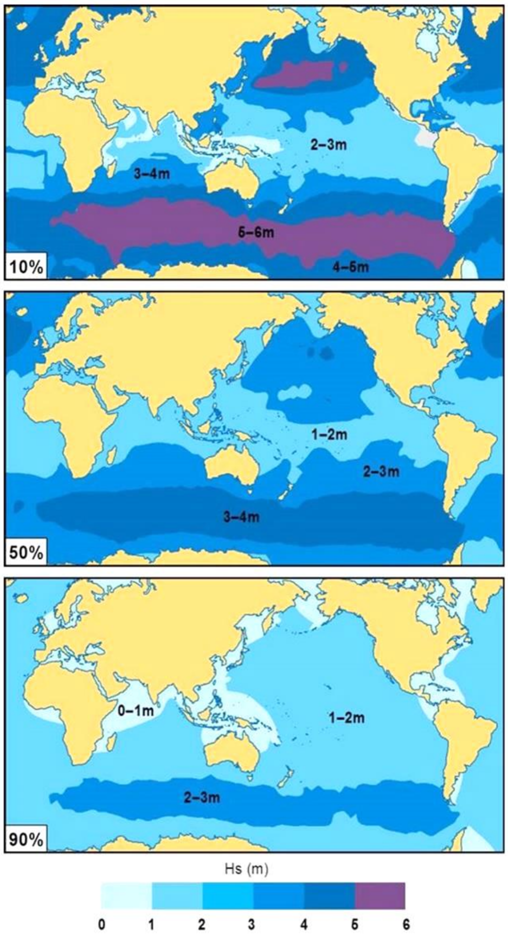

Figure 1.1: Global distribution of significant wave heights H_s, exceeded 10% (top), 50% (middle) and 90% (bottom) of the time. From Short and Woodroffe (2009). Source: The Coast of Australia, Short, A. D. and Woodroffe, C. D., Cambridge University Press. © Andrew D. Short & Colin D. Woodroffe 2009. (Reproduced with permission)

also generated in high latitudes (70° to 90° N/S) by polar easterlies, light winds in the tropics (0° to 10° N/S) as well as local winds in regions of land-locked seas, island arcs, and coral reefs (Short, 1999). Examples of low wave energy coastlines include those along the Caribbean, Gulf of Mexico, Mediterranean, Black Sea, northern Australia and southern China.

Additionally, coastlines can also be classified by the magnitude of the mean spring tidal range shown in Figure 1.2 as microtidal (mean spring tidal range < 2 m), mesotidal (2 - 4 m) and macrotidal (> 4 m) (Davies, 1964). Tidal range is controlled by regional coastal topography including continental shelf characteristics and coastline configuration (Masselink and Hughes, 2003). Microtidal coasts are common on open ocean coasts and enclosed seas, whereas macrotidal coasts are typically situated in semi-enclosed seas and funnel-shaped coastline topography (Davies, 1980).

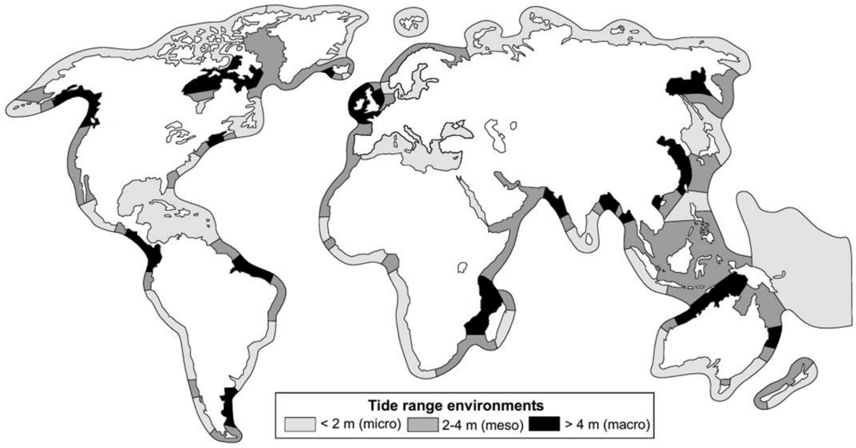

Figure 1.2: Global distribution of mean spring tidal range. From Masselink and Hughes (2003), modified from Davies (1980). Source: Geographical Variation in Coastal Development, Davies, J. L., Pearson Education Limited. © J.L. Davies 1980. (Reproduced with permission)

The dominance of tidal processes relative to wave processes is particularly important in classifying beach morphology (Davis and Hayes, 1984; Masselink and Short, 1993). The relative tidal range (*RTR*), is calculated by the ratio of the mean spring tidal range (*MSR*) to breaker wave height (H_b),

$$RTR = \frac{MSR}{H_b} \tag{1.1}$$

Relative tidal range is used to distinguish wave-dominated (*RTR* < 3), mixed wave-tide (*RTR* < 3 - 15) and tide-dominated beaches (*RTR* > 15) (Masselink and Short, 1993; Short, 1999). Wave-dominated sandy beaches are common worldwide on moderate to high wave energy, microtidal coasts (Figures 1.1 and 1.2). In Australia, wave-dominated beaches account for 47% of the nation's approximately 7000 kilometres of sandy beach coastline (Short, 2006).

1.3 Thesis objectives and outline

The aim of this thesis is to *provide quantitative and parametric insight into wave-driven recovery processes of the subaerial beach following storms on microtidal, wave-dominated sandy beaches*. To achieve this, specific research objectives are to quantify in terms of rates, durations and behavioural characteristics, targeted wave-driven processes of beach recovery and to investigate related governing parameters. Research objectives are chosen to give insight into the wave-driven recovery of the subaerial beach, from interactions with onshore sandbar migration at the shoreline through to the complete swash rebuilding of berm morphology, as well as spatial variability along an embayed coastline. The following research objectives are addressed:

1. *Examine the influence of sandbar morphodynamics and nearshore wave parameters on shoreline recovery at a microtidal, wave-dominated sandy beach.*

   The temporal variability of shoreline recovery rates is quantified and characterised by different nearshore parameters related to sandbar morphodynamics and nearshore wave properties. This is undertaken using a 10-year dataset of daily shoreline and sandbar positions extracted from time-exposure images obtained by an Argus Coastal Imaging system. Temporal phases and rates of shoreline recovery through various stages of onshore sandbar migration are examined following storms, from fully detached storm-deposited sandbar morphology through to complete sandbar welding with the shoreline.

2. *At the timescale of individual tides, classify and evaluate parameters governing beachface and berm morphodynamics throughout the entire recovery of a berm following a significant storm event at a microtidal, wave-dominated sandy beach.*

   The entire rebuilding of berm morphology after removal by a significant storm is analysed at tide-by-tide timesteps (i.e., from low tide to low tide) using high frequency (5 Hz) Lidar measurements of a single profile location spanning 76 days. Tide-by-tide rates of subaerial volume change, patterns of berm crest growth and behavioural modes of subaerial profile variability are quantified throughout berm recovery and distinguished by swash, nearshore wave and ocean water level conditions.

3. *Evaluate the alongshore variability in subaerial volume recovery within and between embayments following a significant storm event along a microtidal, wave-dominated, embayed coastline.*

   The extent to which subaerial volume recovery durations and net rates vary alongshore is examined and compared both within and between embayments. This is undertaken using subaerial profile measurements of beach recovery following a significant storm at four separate embayments. Factors driving alongshore variability in net rates of subaerial volume recovery are evaluated.

A detailed literature review synthesising previous field investigations of post-storm beach recovery processes is undertaken in Chapter 2. The regional setting and field study sites at which beach recovery processes are investigated in this thesis are described in Chapter 3. Research objectives 1, 2 and 3, are then individually addressed in Chapters 4, 5 and 6, respectively. As each objective addresses specific wave-driven processes of beach recovery, a brief literature review is also provided in the introduction of these chapters related to each recovery process that is examined. Different datasets used to address each objective are described in the methodology of corresponding chapters. Overall conclusions of this study and suggested further research are provided in Chapter 7.

Chapter 2

Quantifying post-storm beach recovery: a review

"…waves transport sand from the offshore bar, built during the storm, and place material on the beach. Winds then transport the sand onto the dunes where it is trapped by the vegetation. In this manner the beach begins to recover from the storm attack…"

Shore Protection Manual, 1984

Content of this chapter is in preparation for publication in:

Phillips, M. S., Harley, M. D., Blenkinsopp, C. E., Turner, I. L., Splinter, K. D. and Cox, R. J., *in prep*. Timescales and rates of post-storm beach recovery: a synthesis. Coastal Engineering.

Chapter overview: While the research objectives of this thesis (Section 1.3) focus on wave-driven recovery processes of the subaerial beach (i.e., recovery of the shoreline, beachface and berm) it is important to first understand the broader context of these processes within the overall progression of post-storm beach recovery, from the return of offshore storm deposits to the rebuilding of dunes in the backshore. In this regard, this chapter provides a synthesis of published field measurements quantifying durations and rates of the varying processes that take place throughout beach recovery. Background information is given as to how beach recovery has been defined in the literature, as well as outlining the main processes and indicators that have been used to quantify its occurrence. Durations and rates of recovery are synthesised from over 70 studies worldwide in a range of wave climates (from low to high wave energy) and tidal settings (from micro- to macrotidal), with a focus primarily on sandy beach coastlines. A holistic perspective of the different processes and indicators that constitute beach recovery is presented, including those in the subaqueous beach related to the post-storm onshore migration of sandbars and storm deposits in deeper offshore waters, as well as processes in the subaerial beach related to the recovery of subaerial sediment volume, shorelines, berms, and dunes.

2.1 Defining beach recovery

In general terms, the word recovery is defined as "*a return to a normal state of health, mind or strength*" or "*the action or process of regaining possession or control of something stolen or lost"* (Oxford Dictionary of English, 2010). When applied to beaches, the phrase "beach recovery" is typically used to describe the return of beach sediment and morphology following the impact of a storm, back to pre-storm conditions without human intervention (e.g., artificial nourishment). In the literature, reports of beach recovery and related concepts are noted back to early studies addressing the temporal variability of beach morphology (Bagnold, 1940; Shepard and LaFond, 1940; Shepard, 1950). Beach recovery has been described as a post-storm process of 'restoration' (Mackenzie, 1939), 'rebuilding' (CERC, 1984), 'reconstruction' (Morton et al., 1994), 're-establishment' (Maspataud et al., 2009) and 'reversing' (List et al., 2006). It has also been described as a process of morphological 'resilience' to storm activity (e.g., Masselink and van Heteren, 2014; Houser et al., 2015).

A series of images depicting beach recovery are shown in Figure 2.1, captured by a Coastal Imaging station located at Narrabeen-Collaroy Beach, south-east Australia (described later in Chapter 3). In this example, a major storm event caused the

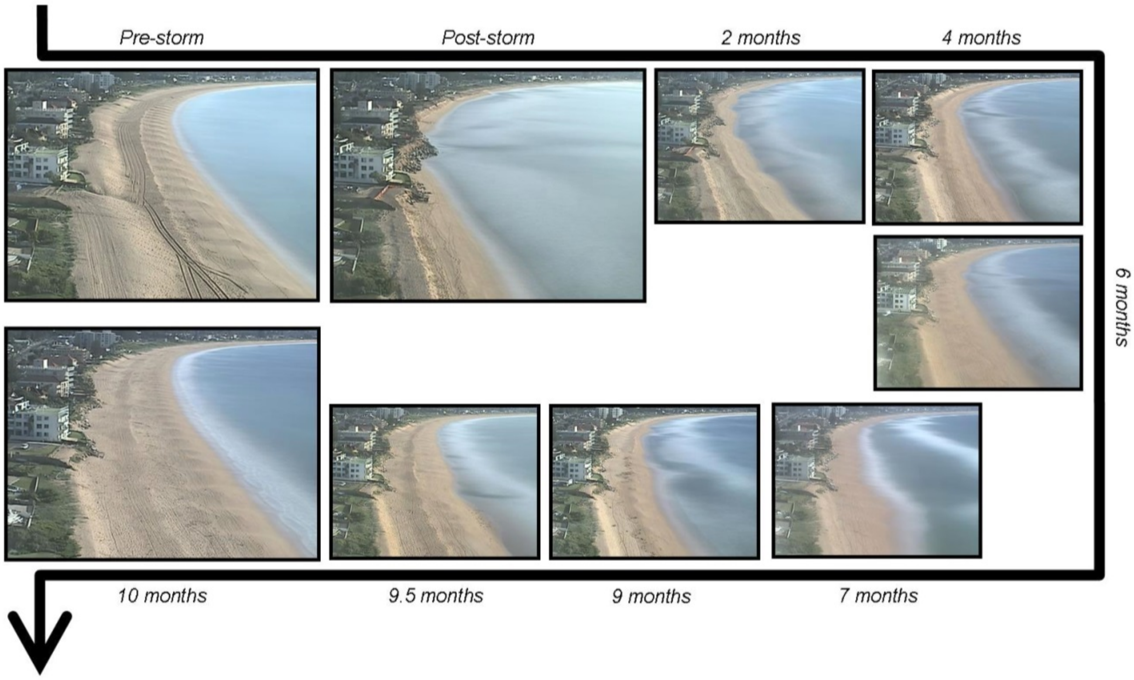

Figure 2.1: Beach recovery and the return of shoreline and berm morphology to pre-storm conditions following storm erosion at Narrabeen-Collaroy Beach, SE Australia in June 2007. Images show progressive changes during recovery over the initial 10 months following the storm, showing the recovery of the shoreline and berm. Note the removal of nourished sediment by the storm in the upper profile that does not recover over this period.

shoreline to rapidly retreat up to 31 m landwards with erosion of the subaerial beach in the order of 78 m^3/m (Harley et al., 2016). Following this storm event, the sequence of images show the progressive regrowth of the shoreline in the seaward direction and rebuilding of the berm in the subaerial beach. The final panel in Figure 2.1 depicts the beach after the complete wave-driven recovery of the shoreline and berm, 10 months following the storm. Note that in addition to shoreline and volume changes in the subaerial beach, the images depict varying sandbar patterns in the subaqueous beach (evident by bands of white in the time-averaged images) throughout the recovery process. Relationships between the subaerial and subaqueous beach during recovery are examined in Chapter 4.

The completion of beach recovery is aptly described by Morton et al. (1994) as having occurred when all the impacts of a storm on a beach have been restored and pre-storm conditions have returned. Quoting Morton et al. (1994):

> *"… ideal complete recovery of an eroded beach would include replacing the volume of sand eroded from the beach and restoring the positions of the shoreline, berm crest and vegetation line to pre-storm conditions"*

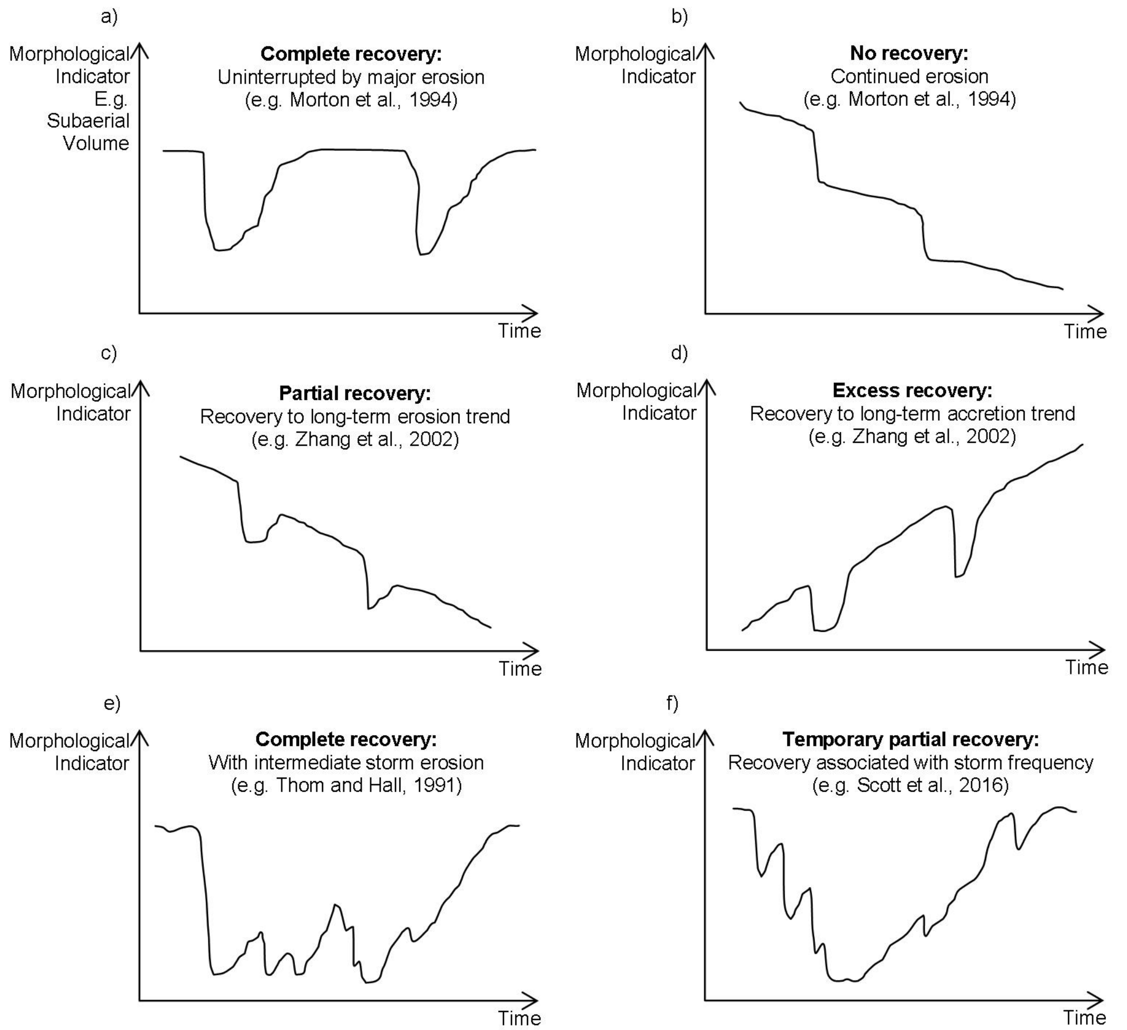

Figure 2.2: Different scenarios of post-storm beach recovery. a) Complete recovery, b) continued erosion, c) partial recovery and d) excess recovery relative to pre-storm conditions. Also illustrated are additional scenarios of e) complete recovery with intermediate storm activity and f) recovery associated with phase of varying storm frequency.

Morton et al. (1994) makes reference to "ideal" beach recovery. It is important to note however that complete beach recovery to pre-storm conditions is not always observed to occur following a storm. Four different post-storm recovery scenarios were noted by Morton et al. (1994) along a 30 km stretch of barrier island coastline in Texas, United States following Hurricane Alicia in 1983. These four scenarios are illustrated in Figure 2.2a-d and include: complete recovery (Figure 2.2a); no recovery with continued erosion (Figure 2.2b); partial recovery (Figure 2.2c); and excess recovery (Figure 2.2d) relative to pre-storm conditions. Beach recovery can also be intermixed with subsequent storm activity as shown in Figure 2.2e. Intermediate storm activity during recovery can result in smaller sub-cycles of erosion and recovery in the subaerial beach. This is particularly noted on higher energy coastlines where larger wave events may occur more frequently compared to lower energy coastlines (e.g., Corbella and Stretch, 2012). During periods of more frequent storm activity, beach recovery can be partial, returning to pre-storm conditions only after subsequent periods of less frequent storm activity as in Figure 2.2f (e.g., Houser and Hamilton, 2009; Coco et al., 2014).

Beach recovery differs from other natural accretionary processes, such as longer-term trends of accretion due to additional sediment sources (e.g., river mouth, continental shelf) or littoral drift, which occur without the disturbance of a storm (e.g., Zhang et al., 2002). Though beyond the scope of this study, it is noted that beach recovery has also been documented following the impact of tsunamis (e.g., Choowong et al., 2009; Liew et al., 2010) and coastal lagoon entrance openings (e.g., Costas et al., 2005; Baldock et al., 2008).

2.2 Morphological processes and indicators of beach recovery

The temporal progression of beach recovery encompasses a broad range of quantifiable processes driven by varying wave and aeolian (wind) forcing, extending from the lower shoreface through to the backshore and dunes. The main wave-driven and aeolian-driven processes of beach recovery are illustrated in Figure 2.3 and listed in Table 2.1. In the subaqueous beach, recovery processes include the onshore transport of storm deposits from deeper offshore waters and the onshore migration of sandbars in shallower nearshore waters (Wright et al., 1985; Lee et al., 1998). At the subaerial beach, processes include shoreline and berm recovery of the foreshore, as well as backshore and dune recovery (Wearne, 1977; Morton et al., 1994). Since the mid-20th century, studies have quantified these different processes of beach recovery, by measuring a return to pre-storm conditions of a range of beach morphological features and indicators following storms. Table 2.1 lists a total of 16 morphological indicators identified in the literature that have been adopted by previous studies to measure and quantify varying processes of beach recovery. Other non-morphological indicators including sediment properties (e.g., Terwindt et al., 1984) and ecological indices (see Section 2.2.3) have also been reported (not listed in Table 2.1).

Coastal practitioners are often required to interpret between various indicators of beach morphology in light of a desired beach condition based on the economic, social and ecological values of a coastal community. From a coastal protection perspective, beach recovery would ideally result in a return of beach sediment and/or morphology to provide a natural buffer of protection sufficient to absorb the impact of future storm activity (CERC, 1984).

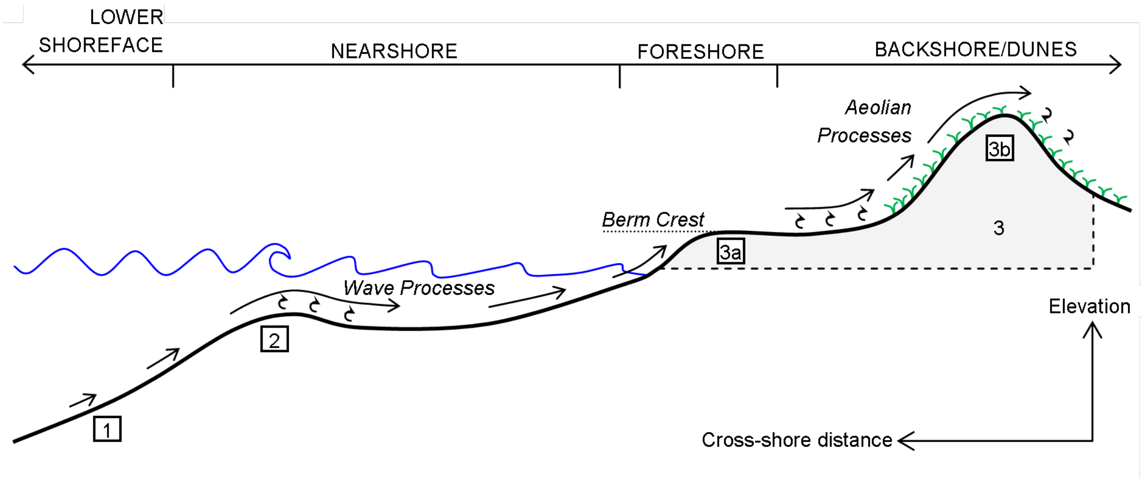

Figure 2.3: The main wave-driven and aeolian-driven processes of post-storm beach recovery with labels corresponding to Table 2.1. The region of the subaerial beach is shaded.

Table 2.1: The main wave-driven and aeolian-driven processes (as in Figure 2.3) of post-storm beach recovery including measured indicators used to quantify their occurrence.

No.	Process	Cross-shore region	Predominant forcing	Measured indicators	Example reference
1	Onshore transport of lower shoreface storm deposits	Lower shoreface	Wave-driven	Lower shoreface volume Lower shoreface elevations	(Lee et al., 1998) (Shepard and LaFond, 1940)
2	Onshore sandbar migration	Nearshore	Wave-driven	Beach state transitions Sandbar position Nearshore volume	(Wright et al., 1985) (Senechal et al., 2015) (Aubrey, 1979)
3	Subaerial beach recovery	Subaerial		Subaerial volume (often above MSL)*	(Morton et al., 1994)
3a	Shoreline and berm recovery	Foreshore	Wave-driven	Shoreline position* Berm width Berm crest height Subaerial volume (following predominantly berm erosion) Foreshore slope Berm concavity/convexity Intertidal 3D morphology	(Phillips et al., 2017) (Hine, 1979) (Jensen et al., 2009) (Dubois, 1988) (Wang et al., 2006) (Sonu and Beek, 1971) (Poate et al., 2014)
3b	Backshore aggradation and dune recovery	Backshore and dunes	Aeolian-driven	Backshore elevations Dune volume* Dune crest height* Vegetation line	(Wearne, 1977) (Suanez et al., 2012) (Houser et al., 2015) (Morton and Paine, 1985)

** More common indicator*

Additional criteria such as usable beach area and user safety may also be considered to account for amenity to beach goers (Frampton, 2010). Furthermore post-storm ecological recovery measures and criteria might also be adopted, particularly in areas of environmental significance (Revell et al., 2011; Witmer and Roelke, 2014). Coastal remediation works should aim to assist a beach where natural recovery processes are insufficient to return the beach to a desired condition or criteria within a specified timeframe following a storm. As such, it is recommended that coastal management select and interpret indicators of beach recovery from field studies based on site-specific criteria that best characterise the desired state of a beach according to community values. Alongside quantitative insight into beach recovery, this requires a local community understanding of the values attributed to a beach. The following sections outlines the main processes and various indicators from the literature shown in Figure 2.3 and Table 2.1 that have been used to measure and characterise beach recovery.

2.2.1 Recovery processes and indicators in the subaqueous beach

Equally important, though often not measured concurrently with the recovery of the subaerial beach, are subaqueous processes of beach recovery, including onshore transport of lower shoreface storm deposits and onshore sandbar migration (Figure 2.3 and Table 2.1). During storm activity the nearshore and lower shoreface become regions of deposition that subsequently act as a primary sediment source during beach recovery (Aubrey, 1979; Houser et al., 2015). As such, consideration of subaqueous processes provide a broader and more holistic description of beach recovery in addition to the more commonly observed subaerial region.

Onshore transport of lower shoreface storm deposits

During larger storm events, eroded beach sediment may be displaced to depths beyond the usual breaker zone on the lower shoreface. On high energy embayed beaches, this can occur due to the formation of megarips which control embayment-wide circulation during extreme events and have been observed to deposit sediment at depths of 10 - 30 m (Short, 1985; Nielsen and Lord, 1993; Coutts-Smith, 2004; Smith et al., 2010; Loureiro et al., 2012). Following a storm, as wave conditions become milder, offshore storm deposits beyond the breaker zone can be left stranded in the relatively low energy environment of the lower shoreface (Wearne, 1977; Leadon, 1999; Splinter et al., 2011a; Scott et al., 2016). Sufficient energy associated with wave shoaling is required during recovery to mobilise this sediment and return it back onshore into shallower waters (Hallermeier, 1980; Nielsen and Lord, 1993).

Post-storm onshore sandbar migration

Beach recovery processes at shallower depths in the nearshore are commonly measured by the onshore migration and associated beach state transitioning of nearshore sandbars (Wright et al., 1985; van Enckevort and Ruessink, 2003; Ranasinghe et al., 2012). During beach recovery, Wright et al. (1985) observed that sandbars move onshore by undergoing consecutive downstate transitions from more dissipative beach states immediately post-storm, to more reflective beach sates associated with a return of mild wave conditions characterised by a decrease in the dimensionless fall velocity (Gourlay, 1968). The sandbar may eventually semi-attach to the shoreline, forming transverse bar and rip morphology. With sustained mild wave conditions, a low tide terrace state occurs prior to complete welding of the sandbar onto the beachface to form steep and reflective beach morphology (Short, 1999). A number of sediment transport processes have been attributed to the onshore migration of sandbars including wave skewness (e.g., Gallagher et al., 1998; Hoefel and Elgar, 2003; Walstra et al., 2007), two dimensional morphology and flow patterns (e.g., Splinter et al., 2011a), weakening undertow (e.g., Aagaard et al., 2013), wave breakpoint (e.g., Plant et al., 1999; Pape et al., 2009), bed load transport (e.g., Ruessink et al., 2007; Dubarbier et al., 2015) and boundary layer streaming and Stokes drift (e.g.,Henderson et al., 2004).

2.2.2 Recovery processes and indicators in the subaerial beach

As illustrated in Figure 2.3 and described by Morton et al. (1994), recovery processes in the subaerial beach involve the return of subaerial volume to restore shoreline, berm and dune morphology to pre-storm conditions. During recovery, sediment is initially deposited by wave-processes at lower foreshore elevations of the subaerial beach, up to the vertical limit of wave run-up. With time this sediment is reworked landward by aeolian processes to higher elevations above the vertical limit of wave run-up into the backshore and dunes.

Subaerial volume recovery

The recovery of subaerial beach sediment volume to a pre-storm value is one of the more common approaches used to quantify beach recovery (e.g., Kana, 1977; Birkemeier, 1979; Thom and Hall, 1991; Vousdoukas et al., 2012). Subaerial volume is measured using two-dimensional (2D) profile or three dimensional surface (3D) elevation data. It is calculated as the volume above a specified elevation contour, usually mean sea level (MSL) and seaward of a fixed cross-shore reference point in the backshore or dunes. It is typically expressed in cubic metres per linear alongshore metre of shoreline (m^3/m).

A volumetric measure of beach recovery is particularly practical for the budgeting of sediment volume fluxes within broader coastal sediment compartments, as well as managing a sufficient subaerial sediment volume to buffer against coastal inundation (e.g., Cooper et al., 2001; Rosati, 2005; Mulder et al., 2011). This informs the design of nourishment works that provide added subaerial volume where natural recovery processes are insufficient in returning the subaerial volume required to absorb future storm demand. Additionally, subaerial volume recovery marks the return of sediment that can readily be reworked by artificial means (e.g., beach scraping) into the backshore and dunes to expedite longer aeolian-driven recovery and enhance beach amenity (Gordon, 2015).

Shoreline and berm recovery

Shoreline and berm recovery is the most immediate response of the subaerial beach during recovery, as depicted in Figure 2.1 (Morton et al., 1994). Representative elevations contours, often MSL or mean high water (MHW), are commonly used to measure the cross-shore return of the shoreline to a pre-storm position. Shoreline and berm recovery involves swash zone deposition resulting in the seaward translation of the shoreline and rebuilding of the berm. This includes processes of onshore sandbar migration interacting with the foreshore (Phillips et al., 2017), steepening of the beachface (Wang et al., 2006), the seaward growth (progradation) of berm width and vertical growth (aggradation) of the berm crest (Hine, 1979; Dubois, 1988; Jensen et al., 2009).

Shoreline and berm recovery is particularly important on coastlines lacking dune morphology due to urban encroachment on pre-existing foredune systems (e.g., at Narrabeen-Collaroy, Figure 2.1). In these regions shoreline and berm morphology provide the primary natural buffer to storm erosion with no additional buffer from a dune system. Additionally, the recovery of berm morphology restores the dry beach plan area desired for sun bathing and beach user amenity (Frampton, 2010).

Backshore and dune recovery

Backshore aggradation and dune recovery mark the latter, aeolian-driven (wind-driven) stages of post-storm recovery in the subaerial beach (Morton et al., 1994). This is typically measured via the return to pre-storm conditions of dune crest height, dune volume (sediment volume measured above the dune toe or vegetation line elevation contour) or dune vegetation indicators. Backshore and dune recovery is driven by onshore winds when the width of the dry berm surface provides a suitable fetch length for aeolian transport processes to occur (Short and Hesp, 1982; Davidson-Arnott, 1988; Davidson-Arnott and Law, 1990; Bauer and Davidson-Arnott, 2003; McLean and Shen, 2006; Houser, 2009; Houser and Mathew, 2011). Short and Hesp (1982) noted that the potential for this is highest on wide, flat, dissipative beaches and lower on narrower, reflective beaches where fetch may be limited. Storms with strong onshore winds can also act to enhance backshore and dune recovery (Delgado-Fernandez and Davidson-Arnott, 2011). During dune recovery, aeolian processes work simultaneously with the growth and recolonization of dune vegetation to promote dune re-establishment (Priestas and Fagherazzi, 2010; Suanez et al., 2012).

The elevation and volume of the upper beach profile in the backshore and dunes is particularly important where low-lying coastal settlements and infrastructure are susceptible to high storm surge, erosion and flooding often via storm impact regimes of overwash and inundation (Sallenger, 2000). This is particularly the case for barrier islands coastlines, such as those along the Gulf of Mexico and mid-Atlantic coasts of the United States (e.g., Day et al., 2007).

2.2.3 Recovery of beach ecology

In addition to the recovery of beach morphology described above, the return of healthy beach ecology following a storm is particularly important in areas of environmental significance (e.g., Maccarone and Mathews, 2011; Revell et al., 2011; Witmer and Roelke, 2014; Machado et al., 2016). In these areas, beach ecosystems may provide critical habitats supporting threatened or endangered species (e.g., Bamford et al., 2008). A study by Revell et al. (2011) following storm erosion during El Nino years in 1997-98 in Isla Vista, United States, measured the recovery of a number of ecological indices, including macrophyte wrack abundance, macrofauna biomass, shorebird abundance and shorebird species richness. Ecological indices may also focus on the recovery of an individual species population (e.g., Maccarone and Mathews, 2011). Although beyond the scope of this study, integrating an applied recovery understanding of both beach ecology and morphology is warranted toward informing best practice in coastal management.

2.3 Documented durations and rates of beach recovery processes

This section provides an extensive review of previous field studies in order to document and assimilate observed durations and rates of the various processes of beach recovery outlined in Section 2.2.

2.3.1 Observation of recovery processes in the subaqueous beach

2.3.1.1 Onshore transport of lower shoreface storm deposits

Durations and rates of the onshore sediment transport of lower shoreface storm deposits are shown in Table 2.2. In depths greater than -10 m below MSL, storm deposits have been observed to return onshore over several years. In shallower waters just offshore of the breaker zone above -10 m, shorter duration onshore migration of storm deposits has been observed over several months. In some instances lower shoreface storm deposits have been observed to gradually feed back into the nearshore during recovery (Lee et al., 1998) while in other cases these have remained stationary until mobilised by subsequent high wave energy (Scott et al., 2016).

2.3.1.2 Post-storm onshore sandbar migration

Durations and rates of post-storm onshore sandbar migration at sandy beaches are shown in Table 2.3. Across all these previous studies, rates of onshore sandbar migration have been typically observed on the order of 1 m/day with the potential for higher rates at some sites of up to the order of 10 m/day. Durations of onshore sandbar migration on microtidal single bar coastlines have been typically observed within the range of days to a few weeks following a storm. Longer durations of several weeks to months have been observed on mesotidal, macrotidal and multiple sandbar coastlines. A more prolonged onshore sandbar migration on coastlines with higher tidal ranges and flatter nearshore profiles is described by Masselink et al. (2006). This has been attributed to a higher degree of tidal-induced shifting of wave processes across the nearshore and intertidal profile, thereby limiting the time window for onshore movement of the sandbar. Smaller tidal ranges and steeper beach profiles reduce this effect and have greater potential for morphological change in the nearshore. In general, durations of onshore sandbar migration are the shortest amongst the main morphological processes of beach recovery described in Sections 2.2, highlighting the dynamic response of the nearshore following storms. The influence of onshore sandbar migration on shoreline recovery processes in the foreshore is further explored in Chapter 4.

Table 2.2: Durations and rates of onshore sediment transport of outer storm deposits on sandy beach coastlines

Environmental setting Modal wave energy	Tidal range	Selected references	Location	Subaerial erosion magnitude	Depth of storm deposition relative to MSL	Observed durations	Observed onshore migration rates
Low energy	Micro-tidal	(Leadon, 1999)	Florida Panhandle Coast, United States	13 to 95 m^3/m	Offshore limit -12 m	Incomplete after 3 years	Minimal/static
Moderate to High energy	Microtidal	(Shepard and LaFond, 1940)	La Jolla, United States	Seasonal erosion	-10 to -16 ft (-3 to -5 m)	7 months	Steady 3 ft decline in sand level over 200 ft profile chainage /7 months (≈ 90 $m^3/m/year$)
		(Lee et al., 1998)	Duck, United States	Not stated, associated with storm groups	-5 to -8 m	Several years	Steady 30 $m^3/m/year$
		Chapter 6, this thesis	**Bilgola and Narrabeen, Australia**	**30 - 82 m^3/m**	**Above -10 m**	**Several months**	
		(Thom and Hall, 1991) (Nielsen and Lord, 1993)	Moruya, Australia	150 to 250 m^3/m	Offshore limit for extreme storms -22 m (±4 m)	Several years	
	Macro-tidal	(Scott et al., 2016)	Perranporth, United Kingdom	165 m^3/m	-6 to -14 m		Static and rapid phases associated with high wave events

Table 2.3: Durations and rates of post-storm onshore sandbar migration on sandy beach coastlines

Environmental setting						
Modal wave energy	**Tidal range**	**No. of sand-bars**	**Selected references**	**Location**	**Observed durations**	**Observed onshore migration rates/state transitioning**
Low energy	Non-tidal	Single	(Davis et al., 1972)	Lake Michigan, United States	7 to 10 days	
Low energy	Non-tidal	Single	(Ostrowski et al., 1990)	Black Sea, Bulgaria	Few days	4m/day
Low energy	Micro-tidal	Single	(Dabrio, 1982)	Gulf of Cadiz, Spain	6 to 8 days	
Low energy	Mesotidal	Single	(Dabrio, 1982)	Bay of Mazarron, Spain	6 to 8 weeks	
Low energy	Mesotidal	Single	(Davis et al., 1972)	Northern Massachusetts, United States	5 to 6 weeks	
Moderate to high energy	Microtidal	Single	(Wright et al., 1985)	Narrabeen, Australia		Mean of 8.1 days per downstate transition of beach state
Moderate to high energy	Microtidal	Single	(Ranasinghe et al., 2004b; Splinter et al., 2011a; Ranasinghe et al., 2012)	Palm Beach (Sydney), Australia	11 days	36 to 42 h (1.5 - 1.75 days) per downstate transition of beach state 0 to 10 m/day
Moderate to high energy	Microtidal	Single	(van Maanen et al., 2008)	Tairua Beach, New Zealand		3.5 m/day
Moderate to high energy	Microtidal	Single	(Owens and Frobel, 1977)	Magdalen Islands, Canada	Few days	0.8 to 10 m/day
Moderate to high energy	Microtidal	Single	(Sonu, 1968)	Nags Head, United States	Several days	Up to 30 m/day
Moderate to high energy	Microtidal	Single	(Sallenger et al., 1985; Lippmann and Holman, 1990; Gallagher et al., 1998; Plant et al., 1999; Ranasinghe et al., 2012; Fernández-Mora et al., 2015)	Duck, United States	5 to 16 days	0 to 29 m/day
Moderate to high energy	Microtidal	Multiple Inner	(Sunamura and Takeda, 1984)	Naka Beach, Japan		1.2 to 11.5 m/day
Moderate to high energy	Microtidal	Multiple Outer & Inner	(Ruessink et al., 2009; Pape et al., 2010)	Gold Coast, Australia	Several weeks	O(1 m/day)
Moderate to high energy	Microtidal	Multiple Outer & Inner	(van Enckevort and Ruessink, 2003)	Noordwijk, Netherlands	Several weeks	Up to 8 m/day Mean 1 m/day
Moderate to high energy	Micro/ meso-tidal	Single	(Orme, 1985)	Ventura, United States	Days to few weeks	8.9 to 30 m/day
Moderate to high energy	Meso/ macro-tidal	Multiple Inner	(Senechal et al., 2015)	Biscarrosse, France	Seasonal	3 m/day
Moderate to high energy	Macro-tidal	Multiple Outer[1] & Inner[2]	(Masselink et al., 2014; Poate et al., 2014)	Perranporth, United Kingdom	[1]Several months [2]2 to 3 months	[1]50 to 100 m over 5 months (0.3 to 0.7 m/day)

2.3.2 Observation of recovery processes in the subaerial beach

2.3.2.1 Subaerial volume recovery

Documented durations and rates of post-storm subaerial volume recovery to pre-storm conditions from a wide variety of sandy beaches worldwide are summarised in Table 2.4. Previous studies have been undertaken on coastlines with modally low to high wave energy exposure, predominantly in microtidal settings. Across all studies, durations of subaerial volume recovery have been observed in a broad range, spanning several months to multiple years. On modally low wave energy coastlines, durations of multiple years are commonly observed and rates of subaerial volume recovery typically range from 0.01 - 0.08 m^3/m/day. On modally moderate to high wave energy coastlines, durations of subaerial volume recovery range from months to several years, with relatively faster rates typically between 0.1 - 0.6 m^3/m/day. Durations of subaerial volume recovery spanning several years are most often observed following more extreme erosion (>100 m^3/m).

The results of some studies have observed rapid rates of subaerial volume accretion of up to 10 m^3/m/day, within the first few days of beach recovery immediately following a storm (e.g., Zeigler et al., 1959; Birkemeier, 1979; Vousdoukas et al., 2012). This has typically been observed on modally moderate to high wave energy coastlines following relatively minor storm erosion (< 30 m^3/m). These observations of rapid post-storm accretion are likely to be associated with the rapid post-storm re-attachment of the sandbar to the shoreline that can occur over similar timescales as shown in Table 2.3. Some studies have also observed alongshore variability in subaerial volume recovery, suggesting the influence of site-specific factors (Morton et al., 1994; Corbella and Stretch, 2012; Yu et al., 2013; Scott et al., 2016). Alongshore variability of subaerial volume recovery is quantified and examined in further detail in Chapter 6 of this thesis.

Comparably fewer studies have measured subaerial volume recovery on gravel and mixed sand/gravel beaches (Bramato et al., 2012; Roberts et al., 2013; Bergillos et al., 2016; Scott et al., 2016). At mixed sand/gravel beaches on the microtidal, low energy coast of southern Spain, rapid recovery to pre-storm conditions has been observed within days to weeks after storms, with rates between 0.5 and 1.8 m^3/m/day (Bramato et al., 2012; Bergillos et al., 2016). In contrast, Scott et al. (2016) observed minimal recovery and multi-year recovery durations on two macrotidal high energy gravel beaches following extreme erosion in south-west England, suggested to be linked to effects of overwash and alongshore storm deposition.

Table 2.4: Durations and rates of post-storm subaerial volume recovery on sandy beach coastlines

Environmental setting: Modal wave energy	Environmental setting: Tidal range	Selected references	Location	Magnitude of storm erosion	Observed recovery duration	Observed recovery rates
Low energy	Non-tidal	(Tătui et al., 2014)	Sulina-Sfantu Gheorghe, Romania	16 to 50+ m^3/m	1.5 to 6 years	8 to15 $m^3/m/year$ (0.02 to 0.04 $m^3/m/day$)
Low energy	Microtidal	(Kriebel, 1987)	Clearwater Beach, United States	No pre-storm data	Interrupted by storm after 2 months	Initially up to 2.7 $m^3/m/day$* Following 2 months: 3 m^3/m (0.05 $m^3/m/day$)
Low energy	Microtidal	(Yu et al., 2013)	Hong Kong Island, China	10 to 30 m (shoreline erosion)	4 months at one site Incomplete at other	Up to 700m^3/4 months for 170m beach length (0.03 $m^3/m/day$)
Low energy	Microtidal	(Morton et al., 1994; Morton et al., 1995)	Galveston Island, United States	51 to 73 m^3/m	4 to 5 years	5 to 30 $m^3/m/year$ (0.01 to 0.08 $m^3/m/day$)
Low energy	Microtidal	(Houser and Hamilton, 2009; Houser et al., 2015)	Santa Rosa Island (Florida), United States	146 m^3/m (mean)	2 to 7 years	Mean 28 $m^3/m/year$ (0.08$m^3/m/day$)
Low energy	Microtidal	(Priestas and Fagherazzi, 2010)	St. George Island, United States	7 m^3/m	Incomplete after 1 year	-18 to16$m^3/m/year$ (-0.05 to 0.04 $m^3/m/day$)
Moderate to High energy	Microtidal	(Birkemeier, 1979)	Long Beach Island, Ludlam Island, Dare County, United States	8 to 26 m^3/m	4 days at one site Incomplete at others	-1 to 10 $m^3/m/day$*
Moderate to High energy	Microtidal	(Everts and Czerniak, 1978)	Absecon Island and Ludlam Island, United States	7 to 20 m^3/m (per storm) 20 to 38 m^3/m (per season)	Seasonal	20 to 38 m^3/m per season (≈ 0.11 to 0.21 $m^3/m/day$)
Moderate to High energy	Microtidal	(Kana, 1977)	Debidue Island, United States	Up to 15 m^3/m	Incomplete after 4 days	Up to 6.5 m^3/m/4days (1.6 $m^3/m/day$)*
Moderate to High energy	Microtidal	(Quartel et al., 2008)	Noordwijk, Netherlands	19 m^3/m	Seasonal	19 $m^3/m/season$ (0.11 $m^3/m/day$)
Moderate to High energy	Microtidal	(Kobayashi and Jung, 2012)	Rehoboth and Dewey Beach, United States	37 to 91 m^3/m	Several months	38 to 86 m^3/m/7months (0.18 to 0.41 $m^3/m/day$)
Moderate to High energy	Microtidal	(Katuna, 1991)	Isle of Palms, United States	31 m^3/m (mean)	Incomplete after 8 months	
Moderate to High energy	Microtidal	(Thom and Hall, 1991)	Moruya, Australia	150 to 250 m^3/m	7 years 4 phases of 6, 8, 12 and 42 months respectively	0.12 to 0.42 $m^3/m/day$
Moderate to High energy	Microtidal	**Chapter 6, this thesis**	**Bilgola, Mona Vale, Narrabeen, Dee Why, Australia**	**5 to 82 m^3/m**	***Individual profiles:*** **Days to 1+ year** ***Embayments:*** **2 to 8 months** ***Overall:*** **Several months**	***Individual profiles:*** **0.1 to 1.6 $m^3/m/day$** ***Embayments:*** **0.1 to 0.3 $m^3/m/day$** ***Overall median:*** **0.24 $m^3/m/day$**
Moderate to High energy	Microtidal	(Corbella and Stretch, 2012)	Durban, South Africa	120 to 250 m^3/m	*Individual profiles:* 0.5 - 6 years *Alongshore-averaged:* 1.5 to 3 years *Overall mean:* 2 years	*Individual profiles:* 40 to 520 $m^3/m/year$ (0.11 to 1.42 $m^3/m/day$) *Alongshore-averaged:* 45 to 204 $m^3/m/year$ (0.12 to 0.56 $m^3/m/day$) *Overall mean:* 90 $m^3/m/year$ (0.25 $m^3/m/day$)
Moderate to High energy	Meso-tidal	(Vousdoukas et al., 2012)	Faro Beach, Portugal	Up to 30 m^3/m	Incomplete after 24 days	Up to 10$m^3/m/day$*
Moderate to High energy	Meso-tidal	(Castelle et al., 2017)	Truc Vert Beach, France	180 m^3/m	1.5 years	12 $m^3/m/month$ (0.4 $m^3/m/day$) between winters
Moderate to High energy	Macro-tidal	(Scott et al., 2015) (Scott et al., 2016)	Perranporth Beach, England	165 m^3/m	3 to 5 years	Mean 95 $m^3/m/year$

**Observed immediately within days following a storm*

2.3.2.2 Shoreline and berm recovery

Measured durations and rates of post-storm shoreline and berm recovery on sandy beach coastlines are shown in Tables 2.5 and 2.6 respectively. Durations of shoreline (commonly the MHW or MSL contour) recovery to a pre-storm position, have typically been observed in the range of a few months to 1 - 2 years, with rates of 0.04 - 0.16 m/day. Reports of higher rates of shoreline recovery have been more commonly observed on moderate to high modal wave energy coastlines. Rapid rates of shoreline recovery (on the order of metres per day) have also been observed either immediately following a storm (List et al., 2006; Quartel et al., 2008; Angnuureng et al., 2017) or during later phases of shoreline recovery with sandbar attachment to the shoreline (Phillips et al., 2015; Phillips et al., 2017). Chapter 4 of this thesis further examines the temporal variability in rates during shoreline recovery on a sandy microtidal high energy beach, determining the influence of nearshore wave parameters and sandbar migration in the subaqueous beach.

The concurrent rebuilding of the berm to pre-storm conditions has typically been observed to occur within similar durations as shoreline recovery, of several months to a year (Table 2.6). Different patterns of berm growth in width (progradation) and height (aggradation) have been identified and are noted in Table 2.6. These are further evaluated and characterised on a tide-by-tide basis throughout the complete rebuilding of a berm following a significant storm in Chapter 5.

2.3.2.3 Backshore and dune recovery

Documented durations and rates of backshore and dune recovery from numerous studies on sandy beaches are presented in Table 2.7. In comparison to wave-driven processes of shoreline and subaerial volume recovery, this predominantly aeolian-driven process of recovery has been observed with typically longer durations of several years to 1 - 2 decades following storms. Following extreme erosion in south-east Australia in May-June 1974, the recovery of subaerial volume to a pre-storm value completed within several years while dune re-establishment was noted roughly two decades after the storm (Thom and Hall, 1991; McLean and Shen, 2006). Vertical dune crest recovery rates are generally noted in the literature in the range of 0.1 - 0.6 m/year and dune volume rates typically on the order of several cubic metres per year. Alongshore variability in dune recovery is also noted in studies of post-storm dune recovery and has been related to storm overwash deposition and the presence/absence of vegetation growth during the recovery process (Priestas and Fagherazzi, 2010; Weymer et al., 2015).

Table 2.5: Durations and rates of post-storm shoreline recovery on sandy beach coastlines

Environmental setting: Modal wave energy	Environmental setting: Tidal range	Selected references	Location	Shoreline contour	Shoreline erosion magnitude	Observed recovery duration	Observed recovery rates
Low energy	Microtidal	(Morton et al., 1994)	Galveston Island, United States	MSL	Up to 30 m	Few months to 1 year	
		(Houser and Hamilton, 2009)	Santa Rosa Island (Florida), United States	MSL	64 m (mean)	Incomplete after one year	19 m/year (0.05 m/day)
		(Mulcahy et al., 2016)	NE Yucatan Peninsula, Mexico	MHW	10+ m	8 months	Up to 7.6 m/8months (0.03 m/day)
		(Yu et al., 2013)	Hong Kong Island, China	HWL	10 to 30 m	4 months at one site Incomplete at other	Up to 5 m/4 months (0.04 m/day)
Moderate to High energy	Microtidal	(Quartel et al., 2008)	Noordwijk, Netherlands	MHW/ MSL	10 to 30 m	Few days	
		(List et al., 2006)	North Carolina United States	MHW	10 to 20 m	Days to weeks	O (m/day)*
		(Splinter et al., 2011b)	Gold Coast, Australia	MSL	15 to 22 m	6 to 12+ months	0.3 to 0.7 m/week (0.04 to 0.1 m/day)
		(Sexton and Hayes, 1991)	South Carolina, United States	HWL	23 to 29 m	12 months	23 to 29 m/year (0.06 to 0.08 m/day)
		(Phillips et al., 2015) Chapter 4, this thesis (Phillips et al., 2017)	**Narrabeen, Australia**	**MHW**	**20 to 30 m**	**Several months to a year**	**0.05 to 0.15m/day with weekly variability up to O (m/day)**
		(Corbella and Stretch, 2012)	Durban, South Africa	Upper Swash Lower Swash	≈50 m	1.8 years 1.3 years	27 m/year (0.07 m/day) 39 m/year (0.11 m/day)
	Mesotidal	(List et al., 2006)	Cape Cod, United States	MHW	10 to 20 m	Days to weeks	O (m/day)*
		(Ruggiero et al., 2005)	Oregon and Washington, United States	MHW	6 to 36 m	Seasonal	11 to 29 m/season (0.06 to 0.16 m/day)
	Meso/ macrotidal	(Senechal et al., 2015) (Angnuureng et al., 2017)	Biscarrosse, France	MHW	10 to 30 m	Seasonal	Rapid 10 to 15 m/month (0.3 to 0.5 m/day) and stable phases. Immediate recovery up to 3.7 m/day*

**Observed immediately within days following storm*

Table 2.6: Durations and rates of post-storm berm recovery on sandy beach coastlines

Environmental setting: Modal wave energy	Environmental setting: Tidal range	Selected references	Location	Berm indicator	Observed recovery duration	Observed recovery rates
Low energy	Microtidal	(Morton et al., 1994)	Galveston Island, United States	Foreshore slope Berm crest elevation	Few months to a year	
		(Wang et al., 2006)	Fort Walton Beach to St. George Island, United States	Foreshore slope Berm crest elevation	1 month 3 months	1 m /90 days (0.01 m/day)
		(Yu et al., 2013)	Hong Kong Island, China	Berm elevations	4 months	1 m /4 months (0.008 m/day)
Moderate to High energy	Microtidal	(Bascom, 1954)	Carmel Beach, United States	Berm width	Seasonal	40 to 60 feet/month (0.4 to 0.6 m/day)
		(Wearne, 1977)	Stuarts Point and Bonville Creek, Australia	Berm elevations	Incomplete after 12 months	0.77 to 0.90 m/year (≈0.002 m/day)
		Chapter 5, this thesis	**Narrabeen, Australia**	**Subaerial volume following berm erosion**	**2.5 months**	**0.67 m^3/m/day** **Up to 3.5 m^3/m/tide** **(7 m^3/m/day)**
		(Dubois, 1988)	Dewey Beach, United States	Subaerial volume following berm erosion 1) Aggradation 2) Progradation	6 months First 3 months Second 3 months	40 m^3/m/3 months (0.44 m^3/m/day) Up to 5.3 m^3/m/day 20 m^3/m/3 months (0.22 m^3/m/day)
	Micro/mesotidal	(Hine, 1979)	Nauset Beach, United States	Berm width 1) Neap berm 2) Swash bar welding 3) Berm-ridge		Over 16 weeks: 8m (0.5 m/day) 22m (1.4 m/day) 115m (7.2 m/day)
		(Aubrey and Ross, 1985)	Torrey Pines, United State	Eigenfunctions of beach profile	Seasonal (5 to 6 months) 3 month lag in start of berm recovery	

Table 2.7: Durations and rates of post-storm backshore and dune recovery on sandy beach coastlines

Environmental setting: Modal wave energy	Environmental setting: Tidal range	Selected references	Location	Dune indicator	Observed recovery duration	Observed recovery rates
Low energy	Microtidal	(Priestas and Fagherazzi, 2010)	St. George Island, United States	Dune height	Incomplete after 1 year.	3 to 4 cm/month (0.36 to 0.48 m/year)
Low energy	Microtidal	(Stone et al., 2004; Houser and Hamilton, 2009; Houser et al., 2015)	Santa Rosa Island, United States	Dune height	Incomplete after 6 years. 1 to 3 year lag in dune growth Expected to complete in 10 years	Sigmoid growth with rates of 0.05 to 0.55 m/year Mean 0.25 m/year
Low energy	Microtidal	(Morton and Paine, 1985; Morton et al., 1994)	Galveston Island, United States	Dune vegetation	4 to 5 years	
Low energy	Microtidal	(Ritchie and Penland, 1988)	Caminada-Moreau, United States	Dune vegetation	10 years	
Low energy	Macro-tidal	(Maspataud et al., 2009)	Dunkirk, France	Dune volume	Incomplete after 4 months	1.2 m^3/m/58 days 2.0 m^3/m/41 days (8 to 18 m^3/m/year)
Moderate to High energy	Microtidal	(Ruessink and Jeuken, 2002)	Delta, Holland and Wadden Coasts, Netherlands	Dune toe position		Up to 5m/year
Moderate to High energy	Microtidal	(McLean and Shen, 2006)	Moruya, Australia	Dune height and vegetation	≈ 2 decades for established dune. 6-9 years lag in dune growth	2m /15 years (0.13 m/year)
Moderate to High energy	Microtidal	(Zhang et al., 2002)	Cotton Patch Hill, United States	Dune height	2 to 3 decades	
Moderate to High energy	Microtidal	(Aagaard et al., 2004)	Skallingen, Denmark	Dune volume	3 decades of accretion	5 m^3/m/year
Moderate to High energy	Meso/ Macro-tidal	(Castelle et al., 2017)	Truc Vert Beach, France	Dune volume	Incomplete after 1.5 years	
Moderate to High energy	Macrotidal	(Suanez et al., 2012)	Vougot Beach, France	Dune height	Incomplete after 2.5 years	4 to 4.5 cm/month (0.48 to 0.54 m/year)
Moderate to High energy	Macrotidal			Dune volume		Up to 2 m^3/m/month (24 m^3/m/year) 1800 m^3 /650m beach length/ 2.5 years (1.1 m^3/m/year)

2.4 The varying recovery of post-storm beach morphology: a synthesis

As highlighted in detail in the previous section, beach recovery is comprised of differing processes and morphological adjustments that have been observed to occur over varying durations and rates. Following on from this extensive synthesis of previous observations, a holistic representation of typical post-storm recovery durations of sandy beach morphology is presented in Figure 2.4, extending across the entire beach profile from the lower shoreface through to the backshore and dunes. The subaqueous beach is divided into shallower (shaded red to orange) nearshore regions that mobilise onshore sediment transport more rapidly (days to weeks for single sandbar, microtidal coastlines) following a storm, compared to deeper (shaded green to blue) lower shoreface regions that are typically slower to recover (up to several years).

In Figure 2.4, the recovery of the subaerial beach is likewise composed of two differing regions corresponding to wave-driven shoreline and berm recovery (shaded yellow to green) and predominantly aeolian-driven backshore aggradation and dune recovery (shaded green to blue). These recovery processes form two distinct regions in a recovered beach profile, separated by the elevation of the berm crest, defined by maximum wave runup during mild conditions (Bagnold, 1940; Russell et al., 2009). Shoreline and berm recovery below the berm crest is more immediate, typically completing within durations of months to 1 - 2 years. At elevations above the berm crest in the backshore and dunes, the beach takes longer to recover, with typical durations of several years to 1 - 2 decades.

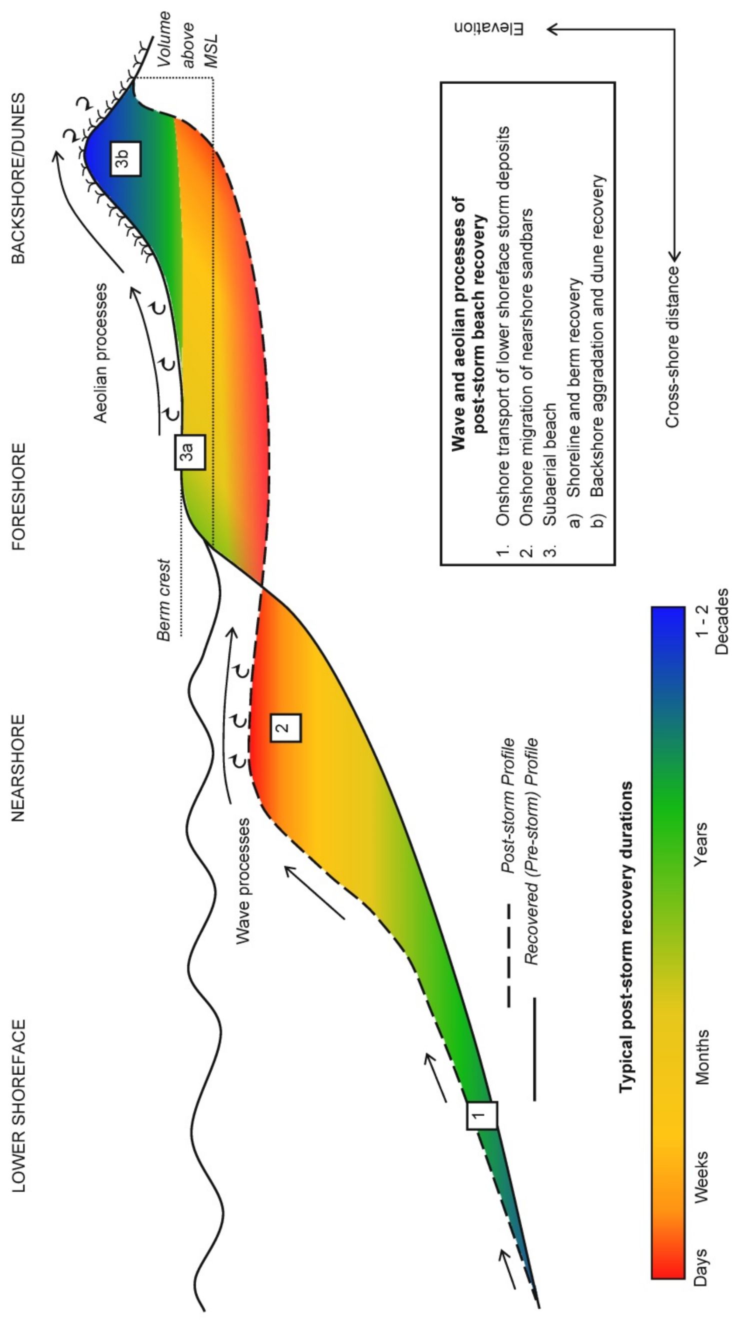

Figure 2.4: The post-storm recovery of sandy beach morphology from the lower shoreface to the backshore and dunes. Typical recovery durations for sandy beach coastlines are illustrated.

2.5 Summary

The term ‘beach recovery’ is typically used to describe the natural return of beach sediment and morphology back to pre-storm conditions following the impact of a storm. Since the mid-20th century, field studies have quantified a range processes and indicators of beach recovery following storms. This chapter has provided a synthesis of observations previously reported in the literature, assimilating recovery durations and rates for a variety of beach morphology, from subaqueous beach processes on the lower shoreface returning offshore storm deposits, through to the aeolian-driven rebuilding of the backshore and dunes.

When viewed holistically, beach recovery is seen to be comprised of differing processes (and driving mechanisms) observed to recover over a range of durations and rates. Recovery durations may vary from a matter of days to weeks (e.g., onshore sandbar migration) to decades (dune recovery) depending on the choice of morphological indicator and recovery process of interest being observed. It is important to note that while a given indicator might completely recover to a pre-storm value, other indicators quantifying a different recovery process (with different driving mechanisms) may be still ongoing. For instance, the wave-driven recovery of the shoreline will often complete prior to the longer-term aeolian-driven recovery of the backshore and dunes. Likewise, durations of onshore sandbar migration may not necessarily correspond to recovery in the subaerial beach. Determining a single measure or relationship to quantify the varying morphological responses and processes of beach recovery is a particularly onerous task.

In this light, field investigation is warranted providing quantitative and parametric understanding of targeted beach recovery processes. In particular, research examining wave-driven recovery processes of the subaerial beach should consider the progression and interaction with subaqueous beach processes of beach recovery, as well as the role of key hydrodynamic parameters. In this regard the remaining chapters of this thesis examine targeted wave-driven processes of beach recovery related to the research objectives in Section 1.3: shoreline recovery and the role of sandbar morphodynamics and nearshore wave parameters (Chapter 4); berm recovery and the swash conditions responsible for the rebuilding of the broader beach profile (Chapter 5); and alongshore variations in subaerial volume recovery at differing spatial scales along an embayed coastline (Chapter 6). In the overall progression of post-storm beach recovery, the specific wave-driven recovery processes addressed in this thesis are amongst the primary phases of recovery in the subaerial beach, and are followed by latter stages of aeolian-driven recovery in the backshore and dunes (Figure 2.4). An example from field data further illustrating the differing wave-driven and aeolian-driven stages of recovery in the subaerial beach is provided in Appendix A.

Chapter 3

Regional setting and study sites

3.1 Regional setting: the south-east Australian coastline

The study sites of Narrabeen-Collaroy Beach, Bilgola Beach, Mona Vale-Warriewood Beach and Long Reef-Dee Why Beach are situated in the broader regional setting of the south-east (SE) Australian coastline (Figure 3.1a), which exhibits a wave-dominated relative tidal range (*RTR*) on the order of 0.8. Tides in the region are microtidal with mean spring and neap ranges of 1.3 m and 0.8 m respectively (Couriel et al., 2012). The regional wave climate is of moderate to high energy. Deepwater wave data collection has been undertaken off the coastline near Sydney from 1987 initially with non-directional measurements and since 1992 with directional measurements, shown in the wave rose in Figure 3.1b. Waves are predominantly from the SSE direction with an average significant wave height (H_s) of 1.6 m and peak wave period (T_p) of 10 s. Waves in the region are generated from synoptic systems that track over the southern Coral and Tasman Seas. These systems are described in detail by Short and Trenaman (1992) as well as Speer et al. (2009) and include tropical cyclones, extratropical cyclones, zonal anticyclones and local sea breezes. Deepwater H_s exceeds 3 m for approximately 5 % of the time and have been observed to reach up to 9 m during high energy events, most commonly driven by intense extratropical cyclones known as East Coast Lows (ECLs) that track further north in the Tasman Sea (e.g., Harley et al., 2016; Harley et al., 2017). For the remaining 95% of the time, waves are of mild to moderate energy (H_s < 3 m) and are predominantly generated from mid-latitude cyclones that track further south across the Tasman Sea, as well as zonal anticyclones and local north-easterly breezes (Short and Trenaman, 1992).

The SE Australian coastline is approximately 1600 km long, consisting of ~60% sandy beach shoreline and ~40% rocky headlands and cliffs (Short, 2007). Geology of headlands and cliffs vary within the region, including metamorphic formations of the New England and Lachlan Fold Belts, as well as clastic sedimentary formations of the Sydney Basin. These rocky shores partition the open coastline into 757 embayed beaches, ranging in length from 20 m to 30 km (average of approx. 1 km), and predominantly composed of medium-grained quartz sand with a 30% carbonate fraction (Short, 2007). Most beaches were deposited during the mid-Holocene, approximately 6500 years ago, as rising sea levels began to stabilise to their present-day level (Roy et al., 1980; Thom, 1984). During this period, continental shelf marine sand was transported onshore and deposited in embayments between rocky protrusions of headlands and cliffs. Many of these deposits formed barrier beaches backed by estuaries that have progressively infilled with fluvial sediments. Offshore, the

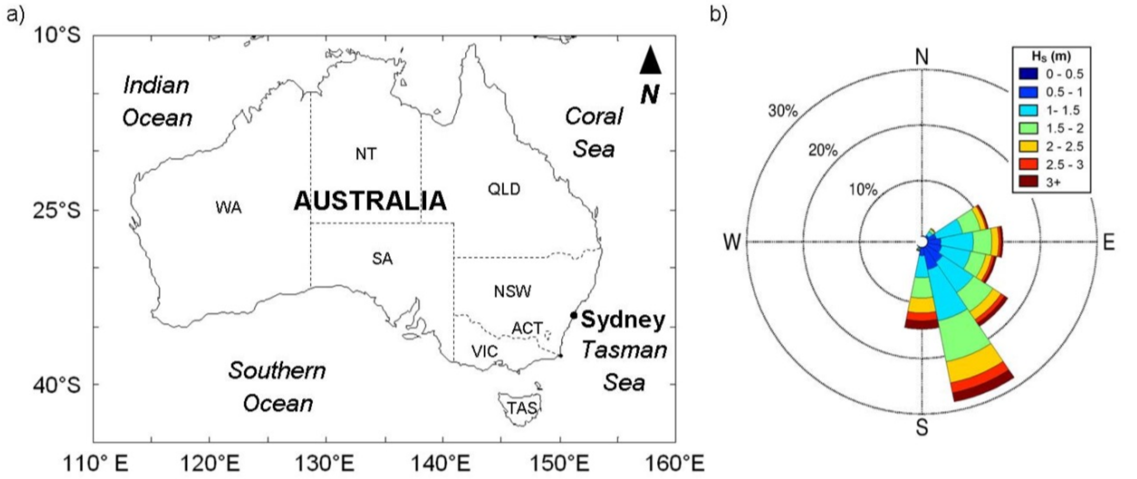

Figure 3.1: a) Map of regional setting on the SE Australian coastline. b) Wave rose of deepwater wave directions and significant wave heights H_s, off the SE Australian coastline near Sydney.

coastline has a steep and narrow (20 - 70 km) continental shelf (Short and Trenaman, 1992).

While the coastline has on average a shore-normal orientation of approximately 110º TN (ESE), locally beaches are swash-aligned with varying shore-normal orientations and exposure to the predominant SSE wave energy. Shore-normal orientations typically range between 90° TN and 150° TN (E to SSE) (You et al., 2014) but also include more north-facing orientations, particularly toward the southern end of curved embayments (Harley and Turner, 2008). Sheltering effects of headlands and reefs also induce alongshore gradients in nearshore wave exposure (Harley et al., 2015). As such, modal beach morphology varies along the coastline and is classified using beach states as defined by Wright and Short (1984), with 9% reflective (REF), 13% low tide terrace (LTT), 65% transverse bar and rip (TBR), and 13% rhythmic bar and beach (RBB) (Short, 2007).

3.2 Study site descriptions

The four study sites that are utilised in this thesis are situated north of the Port Jackson (Sydney Harbour) inlet and south of Broken Bay in the Sydney metropolitan region as shown in Figure 3.2. The Sydney coast contains numerous sandy beach embayments, bounded by prominent rocky headlands (mostly sandstone) and reefs. Narrabeen-Collaroy Beach is the primary study site of this thesis, at which beach recovery processes are examined in detail in Chapters 4 and 5, and compared with

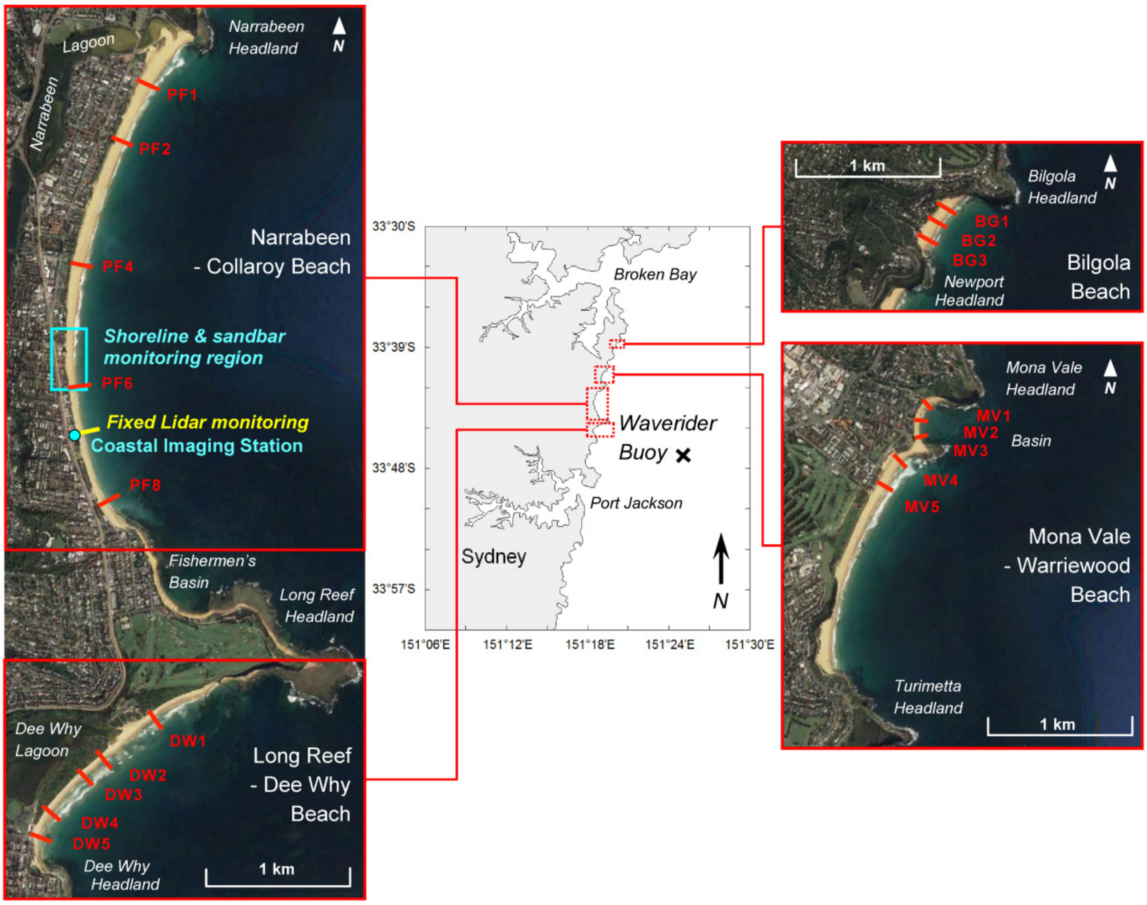

Figure 3.2: Study site locations situated on the embayed Sydney coastline between Broken Bay and Port Jackson, SE Australia. Beach recovery processes at Narrabeen-Collaroy Beach are examined in detail using data collected from an ARGUS Coastal Imaging station (location shown in blue, analysed in Chapter 4) and a continuously scanning Fixed Lidar monitoring system (profile location shown in yellow, analysed in Chapter 5). Furthermore, RTK-GPS beach profile measurements (profile locations shown in red) spanning this embayment as well as three closely-situated embayments (Bilgola Beach, Mona Vale-Warriewood Beach, and Long Reef-Dee Why Beach) are used to examine alongshore variability in recovery (Chapter 6).

three additional surrounding embayments in Chapter 6; Bilgola Beach, Mona Vale-Warriewood Beach and Long Reef-Dee Why Beach (Figure 3.2). A detailed site description of each of the four studied embayments is presented below.

Hourly deepwater wave measurements of significant wave height H_s (m), peak wave period T_p (s), and wave direction θ (°), were collected from the Sydney waverider buoy shown in Figure 3.2, situated in 80 m water depth and approximately 11 km directly offshore of the study sites. A MIKE21 spectral wave model (DHI, 2014) was used to generate a lookup table to transform deepwater H_s and θ to the -10 m depth contour at each of the study sites shown in Figure 3.2 (Mortlock and Goodwin, 2016). Peak wave period T_p, was assumed to remain unchanged between the deepwater and nearshore locations.

Table 3.1: Study site characteristics.
RBB = rhythmic bar and beach, TBR = transverse bar and rip, LTT = low tide terrace and REF = reflective.

Location	**Bilgola Beach**			**Mona Vale-Warriewood**					**Narrabeen-Collaroy Beach**						**Dee Why-Long Reef Beach**				
				Basin			Beach												
Profile	BG1	BG2	BG3	MV1	MV2	MV3	MV4	MV5	PF1	PF2	PF4	PF6	PFLD	PF8	DW1	DW2	DW3	DW4	DW5
Embayment length (km)	0.5			2.2					3.6						1.8				
d_{50} (mm)	0.28			0.30					0.30						0.24				
Upper nearshore slope (rise/run) [a]	0.028			-			0.020		0.029						0.017				
	.030	.028	.027	-	.011	-	.021	.019	.020	.039	.036	.033	.030	.015	.012	.022	.018	.018	.017
Shore-normal orientation (°TN)	125			-			117		95						139				
	125	125	125	140	100	84	130	117	118	114	100	84	74	60	144	138	138	135	100
Mean nearshore H_s (m)	1.2			-			1.2		0.95						1.2				
	1.20	1.20	1.18	-	-	-	1.18	1.18	1.12	0.97	1.01	0.88	0.80	0.78	1.31	1.09	1.12	1.13	1.13
Modal beach state [b]	TBR			REF			TBR		TBR			LTT			RBB/TBR				

[a] Slope of linear regression fit of bathymetry data (28th April 2015) between 0 m and -10 m depth contours
[b] From Short (2007)

3.2.1 Narrabeen-Collaroy Beach

Narrabeen-Collaroy Beach shown in Figure 3.2 is a 3.6 km-long east-facing embayment (average shore-normal orientation of ~95 °TN), and one of the longest on the Sydney coastline (Table 3.1). The embayment consists of Narrabeen Beach toward the north and Collaroy Beach toward the south. The embayment is confined at the northern extremity by the shale and sandstone Narrabeen Headland, and at the southern extremity by the claystone Long Reef Headland, both of which formed during the Triassic Period. Sediment within the embayment is much younger, having been deposited in the mid-Holocene as a regressive barrier (Roy et al., 1980; Thom, 1984). This barrier prograded roughly 300 m as Holocene sea levels stabilized, where it reached its current position approximately 3000 years ago.

Narrabeen-Collaroy Beach is composed of fine to medium grained (d_{50} ≈ 0.3 mm) quartz sand with a 30% carbonate composition. The upper nearshore slope (between the 0 m and -10 m bathymetry contours) of approximately 0.03 is one of the steepest amongst the four studied embayments listed in Table 3.1. Bathymetry contours in the embayment are plotted in Figure 3.3. At shallower depths above -10 m, contours are

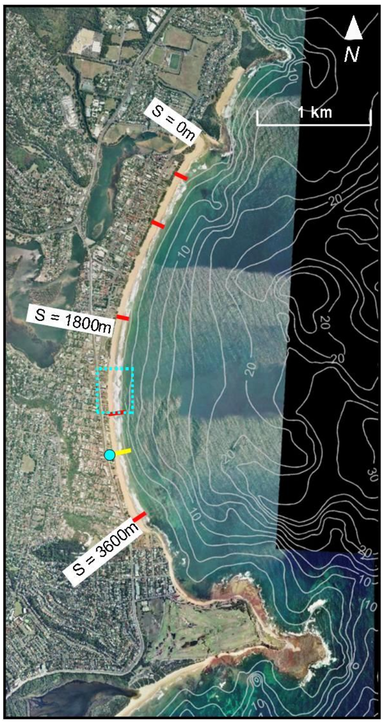

Figure 3.3: Bathymetry contour map of Narrabeen-Collaroy Beach. Contours are closely-spaced and shore-aligned at shallower depths above -10 m. In deeper offshore waters contours become more irregularly spaced and aligned to rock outcrops. Monitoring locations correspond to those in Figure 3.2.

closely-spaced and shore-aligned, becoming more irregularly spaced and aligned to rock outcrops in deeper offshore waters contours. Beach morphology is predominantly of intermediate state, tending more dissipative and reflective under higher and lower wave conditions, respectively (Wright et al., 1985). The embayment has a depth of closure of approximately 22 m for extreme storms and 12 m for less extreme beach fluctuations (Nielsen and Lord, 1993). In the very northern end of the embayment is the entrance to Narrabeen Lagoon (Figure 3.2), which is approximately 50 m in width and intermittently closed by the infilling of embayment sediment (Morris and Turner, 2010).

As a result of the predominant SSE direction of the deepwater Sydney wave climate (Figure 3.1) nearshore waves in the embayment are to a large degree sheltered by Long Reef Headland at the southern extremity (i.e., Collaroy). The resultant alongshore gradient in wave energy is evident in recorded mean nearshore H_s shown in Table 3.1, varying from 0.8 m to 1.1 m at the -10 m depth contour from south to north along the embayment. As such, beach morphology also varies alongshore, with predominantly low tide terrace (LTT) state toward the sheltered southern end and transverse bar and rip (TBR) state toward the north.

Analyses based on a multi-decade monthly profile dataset along the embayment (refer Turner et al., 2016) have found that the primary mode of shoreline variability at Narrabeen-Collaroy, accounting for 60% of the overall shoreline variability, is a cross-shore sediment exchange between the subaerial and subaqueous beach. This primary mode of shoreline variability is predominantly a result of changes in the frequency and intensity of wave energy/storms from the modal SSE direction. A secondary rotational signal (accounting for approximately 25% of the overall shoreline variability) has been observed between the northern and southern ends of the embayment and is linked to alongshore variability in cross-shore sediment fluxes as well as sediment exchanges in the alongshore direction (Harley et al., 2011b; Harley et al., 2015). These rotation cycles of the shoreline have been observed at both seasonal timescales (Harley et al., 2011b) as well as inter-annually due to influences by the El Niño-Southern Oscillation (Ranasinghe et al., 2004a; Barnard et al., 2015). The average curvature of the shoreline orientation within the embayment (evident in Figure 3.2), has been shown to match a log-spiral form, and can be readily transformed for data analysis purposes (Harley and Turner, 2008).

3.2.2 Bilgola Beach

Bilgola Beach is a 0.5 km long pocket beach, located 8 km north of Narrabeen, and the shortest embayment monitored in this thesis (Table 3.1). The embayment is bounded by Bilgola Headland to the north and Newport Headland to the south, with an average shore-normal orientation of approximately 125 °TN. Rocky reefs at the base of Newport Headland provide minimal sheltering from predominant SSE waves, such that H_s is on average 1.2 m in the nearshore at the -10 m depth contour. Modal beach morphology as classified by Wright and Short (1984) is characterised by a transverse bar and rip (TBR) state with a single sandbar often divided by 2 - 3 alongshore migrating beach rips within the embayment (Short, 2007). Sediment is composed of medium-grained sand with an upper nearshore slope (between the 0 m and -10 m bathymetry contours) of approximately 0.03, one of the steepest amongst the four embayments studied.

3.2.3 Mona Vale-Warriewood Beach

Mona Vale-Warriewood Beach is a 2.2 km long embayment, situated just north of Narrabeen-Collaroy Beach (Figure 3.2, Table 3.1). It is bounded by Mona Vale Headland to the north and Turimetta Headland to the south. Beach monitoring in this thesis was concentrated at the northern end of the embayment. At this location, a tombolo in the lee of a rocky reef and ocean rock pool, separates the highly refracted wave environment and reflective morphology of Mona Vale Basin, from the more exposed and transverse bar and rip (TBR) morphology of Mona Vale Beach to the south (Short, 2007). Mona Vale has an average ESE shore-normal orientation of 117 °TN and is relatively exposed to predominant SSE waves (mean H_s = 1.2 m at the -10 m depth contour). The nearshore slope is approximately 0.02 with d_{50} (≈ 0.3 mm) similar to that of Narrabeen-Collaroy Beach.

3.2.4 Long Reef-Dee Why Beach

Long Reef-Dee Why beach is situated immediately south of Narrabeen-Collaroy on the southern, more exposed side of Long Reef Headland (Figure 3.2). The embayment is 1.8 km in length with a distinct SE average shore-normal orientation of 138 °TN (Table 3.1). It is bounded in the south by Dee Why Headland and fringed by offshore reefs in the north. At the -10 m depth contour, H_s averages 1.1 m along the majority of the embayment and 1.3 m on the more exposed reefs in the north. Modal beach morphology varies from transverse bar and rip (TBR) to rhythmic bar and beach (RBB) states. In comparison to the other study embayments listed in Table 3.1, sand at Dee Why is slightly finer-grained (d_{50} ≈ 0.24 mm) and the upper nearshore mildly flatter with a slope (≈ 0.017) approximately half that of Narrabeen-Collaroy Beach.

3.3 Summary

This thesis utilises field data collected from four closely-situated sandy beach embayments located in Sydney on the SE Australian coastline to investigate wave-driven recovery processes of the subaerial beach. Narrabeen-Collaroy Beach is the primary study site of this thesis, at which shoreline recovery is examined in the following Chapter 4 using Argus coastal imaging, and berm recovery analysed in Chapter 5 using a continuously scanning Fixed Lidar monitoring system. Alongshore variability in subaerial volume recovery along the broader Narrabeen-Collaroy embayment, as well as three closely-situated embayments (Bilgola Beach, Mona Vale-Warriewood Beach, and Long Reef-Dee Why Beach) is investigated in Chapter 6 using RTK-GPS beach profile measurement.

Chapter 4

Shoreline recovery: the role of sandbar morphodynamics and nearshore wave parameters

Content of this chapter has been published in:

Phillips, M. S., Harley, M. D., Turner, I. L., Splinter, K. D. and Cox, R. J., 2017. Shoreline recovery on wave-dominated sandy coastlines: the role of sandbar morphodynamics and nearshore wave parameters. Marine Geology, 385, 146-159. doi: 10.1016/j.margeo.2017.01.005.

Chapter overview: The onshore return of nearshore sediment back to the shoreline is a primary wave-driven process of post-storm beach recovery (Chapter 2). In this chapter shoreline recovery following 82 individual storm events is analysed using a 10-year dataset of daily shoreline and sandbar positions on a high energy sandy coastline. Temporal variations in rates of shoreline recovery are quantified and characterised by nearshore wave and sandbar conditions. A new conceptual model is presented, describing phases and rates of shoreline recovery through various stages of onshore sandbar migration following storms, from fully detached storm-deposited sandbar morphology through to complete sandbar welding with the shoreline.

4.1 Introduction

On coastlines lacking established dune systems (e.g., due to urban encroachment on pre-existing foredunes), shoreline and berm morphology provide a primary natural buffer to coastal inundation. In particular, the recovery of the shoreline and berm following the impact of a storm, shown in Figure 2.1, restores the width separating coastal infrastructure and the ocean. In this chapter, the temporal variability of shoreline recovery is examined and key governing parameters are evaluated.

Shoreline recovery, namely the cross-shore return of a representative shoreline contour to a pre-storm position following a storm, is a commonly measured component of post-storm beach recovery. At many locations, cross-shore changes in shoreline position have been shown to provide a useful proxy for the corresponding changes in subaerial sand volume (e.g., Farris and List, 2007; Harley et al., 2011c). Previously described in Section 2.3.2.2 and synthesised in Table 2.5, shoreline recovery has been observed with a range of durations (months to years) and rates (centimetres to metres per day). Some studies with broader spatial coverage have revealed that variability in rates of shoreline recovery can occur spatially alongshore and between locations (List et al., 2006; Corbella and Stretch, 2012). The spatial variability in subaerial beach recovery is addressed in further detail in Chapter 6. In contrast, the temporal variability of shoreline recovery rates is less well reported. Studies are often limited to the monitoring of shoreline recovery following an individual storm and lack sufficient survey frequency to observe potential day-to-day variability in rates during this period. In addition, multi-year shoreline monitoring programs that capture shoreline recovery following multiple storms are rare (Corbella and Stretch, 2012; Phillips et al., 2015).

Preliminary work by Phillips et al. (2015) using a unique decade long dataset of high resolution (daily) shoreline observations remotely captured from video images, identified temporal variability in shoreline recovery rates during 10 post-storm shoreline recovery periods. This work revealed a high degree of variability in rates at timescales of days to weeks during shoreline recovery, despite relatively consistent net rates for recovery recorded over longer periods extending from several months to a year (Table 2.1). Phases of more gradual and rapid shoreline recovery rates were identified, but the hydrodynamic and/or morphodynamic processes that underlie these observations remained unclear.

For shoreline recovery to occur, sediment deposited in the nearshore (or further offshore) by the preceding storm must first be transported back onshore. Though morphodynamic relationships between shoreline and sandbar morphology are noted in the literature, the potential role of sandbar morphodynamics on shoreline recovery rates is yet to be fully explored. Wright and Short (1984) classified beaches into dissipative, intermediate and reflective states. As previously described in Section 2.2.1, nearshore morphology during recovery is frequently observed to systematically undergo a series of downstate transitions in beach state, characterised by different sandbar configurations and attachment to the shoreline including longshore bar and trough (LBT), rhythmic bar and beach (RBB), transverse bar and rip (TBR), low tide terrace (LTT) and reflective states.

Wright and Short (1984) and others (e.g., Sonu and Beek, 1971) proposed a coupling of the sandbar and shoreline that more recently has been explored with new insight through the use of video imaging (Coco et al., 2005; Price and Ruessink, 2013; van de Lageweg et al., 2013). For example, on an embayed microtidal sandy beach in New Zealand, van de Lageweg et al. (2013) found an increased degree of sandbar-shoreline coupling with closer sandbar-shoreline proximity. At the meso-to-macrotidal, high energy sandy beach of Biscarrosse, France, sandbars were observed to migrate onshore at shorter timescales and a rate 6 times faster than concurrent shoreline recovery response (Senechal et al., 2015). Despite this, post-storm field investigation of shoreline recovery (Section 2.3.2.2) and onshore sandbar migration (Section 2.3.1.2) are often conducted separately from one another.

Addressing research objective 1 of this thesis (Section 1.3), this chapter uses a 10-year daily shoreline and sandbar position dataset obtained at Narrabeen-Collaroy Beach in SE Australia (refer to Chapter 3) to quantify and characterise the temporal variability of shoreline recovery rates. The shoreline and sandbar dataset and study methodology is further detailed in Section 4.2. Following a total of 82 storms, rates of cross-shore shoreline change are quantified and examined in Section 4.3, as the shoreline returns to its observed pre-storm position. The influence of nearshore wave forcing and sandbar morphodynamics on the variability of shoreline recovery rates are explored. Correlation analysis for the observed shoreline recovery rates was undertaken with eight nearshore wave and related morphodynamic parameters, plus sandbar-shoreline proximity and cross-shore sandbar migration rates. The results are discussed and a new conceptual model is presented in Section 4.4, that encapsulates differing phases and rates of shoreline recovery under favourable wave forcing for detached, semi-attached, attached and absent sandbar morphology. Conclusions of the chapter are summarised in Section 4.5.

4.2 Methodology

To examine the temporal variability of shoreline recovery rates, this study uses a high frequency video image dataset collected over a 10-year period at Narrabeen-Collaroy Beach. Extraction of daily shoreline and mid-tide sandbar positions from this dataset is described in Section 4.2.1. Steps undertaken in the analysis of shoreline recovery rates from the shoreline data are outlined in Section 4.2.3. In addition, correlation analysis described in Section 4.2.4, was performed to investigate controls of shoreline recovery rates with consideration given to parameters related to nearshore wave conditions and also sandbar morphodynamics.

4.2.1 Study site

The analysis undertaken in the present chapter was located along a 400 m alongshore stretch of Narrabeen-Collaroy Beach just south of the midpoint of the embayment, corresponding to the location of the Narrabeen-Collaroy Coastal Imaging station (Figure 3.2). For a detailed site description of the Narrabeen-Collaroy embayment refer to Section 3.2.1. This 400 m-long monitoring region where sufficiently high resolution images of the shoreline and sandbar are available is partially exposed to the predominant SSE wave energy, with nearshore significant wave heights at the -10 m depth contour averaging ~0.9 m and exceeding 1.8 m approximately 5% of the time. Beach morphology at this location is predominantly of transverse bar and rip state in contrast to the higher (lower) energy intermediate states that characterise modal beach morphology further north (south) in the embayment (Wright and Short, 1984). The analysis in the present chapter focusses on cross-shore sediment exchange between the subaerial and subaqueous beach, which is the dominant mode of shoreline variability at Narrabeen-Collaroy with a secondary signal of shoreline rotation (see Section 3.2.1). The 400 m monitoring region is located southwards of the pivot point of shoreline rotation, such that the secondary rotation signal within the monitoring region can be considered uniform.

4.2.2 Video-derived shoreline and sandbar data

Video monitoring of the southern half of Narrabeen-Collaroy Beach has been undertaken for over a decade via operation of an Argus Coastal Imaging station (Holman and Stanley, 2007). The Coastal Imaging station is located on the roof of a beach side building at 44 m above mean sea level (MSL) and comprises five video cameras that combine to span a 180° view of the southern end of the embayment (Figure 3.2). From August 2004 to April 2015, a suite of oblique image products (snapshot, 10-minute time-exposure and variance images) were captured every daylight hour by the Coastal Imaging station. In the present study, time-exposure images were used from the north-facing camera (Camera 5) from which the sandbar and shoreline positions can be readily identified (Figure 4.1). In order to obtain quantitative information from this camera, oblique images were corrected for lens-distortion and geo-rectified to a map projection using a series of ground control points distributed throughout the image (Holland et al., 1997). The pixel resolution following geo-rectification in the 400 m study site ranged from 0.3 - 1 m in the cross-shore direction and 1.5 - 7 m in the alongshore direction.

4.2.2.1 Shoreline data

Hourly shoreline positions were detected from geo-rectified time-exposure images using the Pixel Intensity Clustering (PIC) technique (Aarninkhof et al., 2003) and combined with an empirical shoreline elevation model to account for tide and wave runup effects (Harley et al., 2011c). An automated algorithm (Harley et al., 2007; Uunk et al., 2010) was developed to repeat this process and systematically remove any erroneous shoreline positions detected by the PIC technique. These erroneous positions occur due to issues such as shadows on the beach, poor visibility or sun glare on the water surface. A total of 24,168 hourly daylight shoreline positions were mapped and quality controlled over the 10-year period by this automated algorithm, forming an extensive shoreline dataset obtained at a range of elevations within the intertidal zone. For each day, all the available hourly daylight shorelines were then used to linearly interpolate a daily shoreline position at a constant elevation

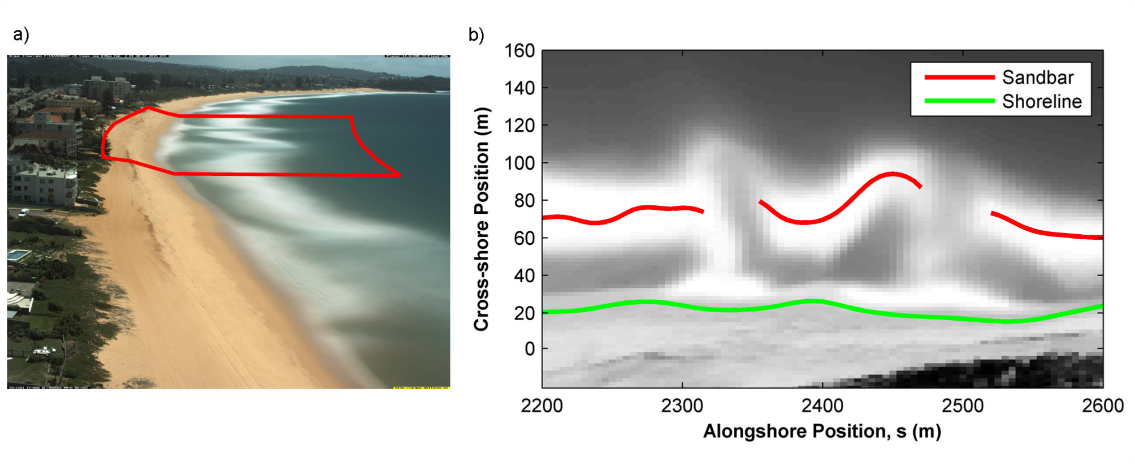

Figure 4.1: a) 10-minute mid-tidal time-exposure image taken from the Argus Coastal Imaging station with the 400 m-long study site shown in red. b) Corresponding geo-rectified time-exposure image of the study site in local alongshore and cross-shore coordinates with the concurrent mid-tidal sandbar and daily shoreline positions.

corresponding to mean high water springs (0.7 m above MSL contour, Figure 4.1b). The cross-shore uncertainty of the daily video-derived shoreline position in the study site, termed Δx_s, has previously been shown to be of the order of ± 2 m (Harley et al., 2011c).

In order to distinguish trends of shoreline recovery from other forms of variability in the daily shoreline time series, two pre-processing steps specific to this study were applied to the shoreline data. First, alongshore variability due to localised features such as rip heads and beach cusps were minimized in the analysis by alongshore averaging the daily shoreline data along the 400 m study site. At the study site this 400 m length corresponds to 4 - 10 times the length-scales of accretionary rips (more commonly observed during shoreline recovery), and twice the length-scales of typical erosion-type rips that may temporarily persist after storm activity (Short, 1979; Short, 1985; Davidson et al., 2013). Additionally, a longer-term (several years) rotation signal towards the southern end of the embayment (i.e., a counter-clockwise rotation) was evident in the shoreline data. This was characterised by approximately a linear trend towards a wider beach and was removed from the data. The resulting alongshore-averaged and detrended time series of daily shoreline position is hereafter denoted x_s (m) in this study.

4.2.2.2 Sandbar data

In addition to shoreline data, geo-rectified time-exposure images over the same 10-year study period were also used to extract sandbar position data at mid-tide (Figure

4.1b). The detection of sandbar data was undertaken in three steps. First, pixel intensities along cross-shore transects spaced 10 m alongshore were detrended following the method outlined by Splinter et al. (2011a). This step was undertaken to remove any lighting effects associated with sun glare on the water surface and to enhance contrast between regions of breaking and non-breaking waves. Second, pixels landward of the shorebreak, identified as the pixel intensity maximum within 10 m of the shoreline (as detected in Section 4.2.2.1), were removed from the analysis. Finally, the cross-shore position of the sandbar at each cross-shore transect was taken as the maximum pixel intensity along each cross-shore transect (Figure 4.1b) following Lippmann and Holman (1989) and other authors (e.g., Plant et al., 1999; Splinter et al., 2011a).

Consistent with pre-processing of the shoreline data, sandbar positions were alongshore-averaged at the 400 m-long study site and detrended using the same embayment rotation trend applied to the shoreline data. The resulting alongshore-averaged and detrended sandbar position time series is hereafter denoted x_b (m). This was also expressed in terms of sandbar proximity relative to the concurrent shoreline position, denoted by x_{bs} (m) where

$$x_{bs} = x_b - x_s \tag{4.1}$$

Sandbar positions detected from wave breaking using video imaging techniques may deviate from actual sandbar positions depending on tidal water level and wave height over the sandbar (van Enckevort and Ruessink, 2001). At low tide, waves may break on the seaward edge of the bars compared to high tide where they may break more landward. This induces a tidally driven cross-shore migration of the sandbar if water levels vary between images. For example, at the Gold Coast, also located in a microtidal setting on the east coast of Australia and exposed to a similar wave climate, Ruessink et al. (2009) found these errors to be 10 - 15 m landward per metre of increasing water depth over a tidal cycle. In an effort to minimise these errors in the present study, sandbar positions were only obtained from images at a relatively constant tidal elevation within ± 0.2 m of mean sea level (approx. mid-tide). This translates to a potential horizontal error resulting from tidal variations on the order of 4 - 6 m, based on 0.4 m of depth variability between images and an equivalent error range per metre water depth to that observed by Ruessink et al. (2009). Images taken during low wave conditions when wave breaking on the sandbar was minimal were ignored. Further erroneous observations due to discontinuities in wave breaking, particularly around rip head features, were removed via a final manual inspection of the images. In total, 3,398 mid-tide sandbar positions were used in the analysis over the 10-year study period.

4.2.3 Shoreline recovery period classification

In order to classify from the daily shoreline data periods of recovery following storms, two steps were undertaken. Firstly, individual storm events were identified by applying a peak-over-threshold technique (Harley et al., 2009; Masselink et al., 2014) to the hourly wave height time series (refer to Section 4.2.5.1), with a 95th percentile ($H_s \approx$ 1.8 m) nearshore (-10 m depth contour) significant wave height threshold. The pre-storm shoreline position was taken as the maximum shoreline position within 3 days before the start of storm and the post-storm position was taken as the minimum shoreline position within 3 days after the storm. Only storms that resulted in shoreline erosion greater than twice the accuracy of the shoreline dataset (i.e., $2\Delta x_s$ = 4 m) were included in the analyses. Secondly, a shoreline recovery period for each storm was classified from the time of the post-storm position until the time when the shoreline was observed to return to its pre-storm position (within a tolerance defined by the shoreline detection accuracy, Δx_s). Examples of shoreline recovery periods are illustrated in Figure 4.2 following three storms during late 2004 and early 2005. Note from this figure that the second storm (mid-October) occurs during the recovery of the first storm (early October). Intermediate storm activity during shoreline recovery is a common occurrence at the study site and on other high energy coastlines (e.g., Corbella and Stretch, 2012). In these cases, the recovery period is deemed to have ended when the shoreline returns to the pre-storm position of the initial storm event, as shown in Figure 4.2.

4.2.4 Shoreline recovery rate calculation

To examine temporal variability during shoreline recovery periods, cross-shore rates of shoreline recovery, dx_s/dt (m/day), were calculated by dividing the full duration of each recovery period into smaller temporal windows and calculating the slope of a linear regression line fitted (using least-squares) to the cross-shore shoreline position time series (x_s) for each window. A range of temporal window sizes used to divide shoreline recovery periods were explored, with the most informative found to be 7, 14, 30 and 60 days. For an example recovery period with a total duration of 28 days and partitioning into 7-day windows, four shoreline recovery rates were calculated for days 1-7, 8-14, 15-21 and 22-28 respectively. This was repeated for all windows sizes less

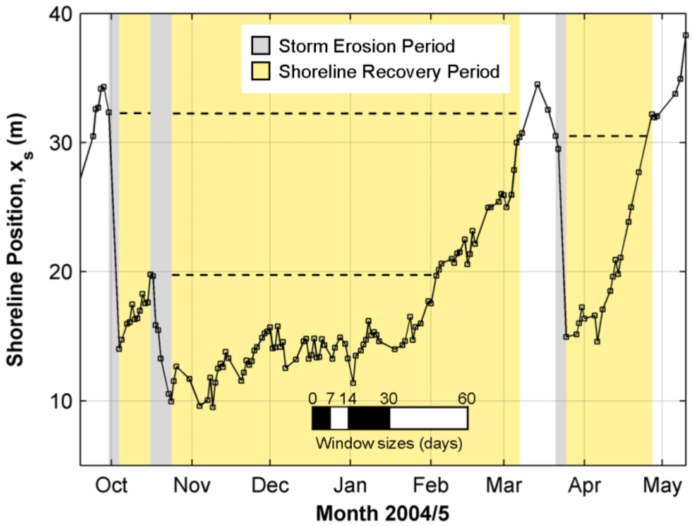

Figure 4.2: Example of storm erosion and shoreline recovery periods for October 2004 to May 2005. Pre-storm shoreline positions are marked by dashed lines. Rates of shoreline recovery were calculated by dividing shoreline recovery periods into smaller temporal windows (7, 14, 30 and 60 days) and applying linear regression.

than or equal to the duration of the recovery period. Window sizes of less than 7 days were not considered in the analysis due to poor signal-to-noise ratios influencing sub-weekly observations of shoreline change in the data (Harley et al., 2011c).

4.2.5 Correlation analysis with nearshore wave parameters and sandbar morphodynamics

Parameters that may influence the temporal variability of the observed shoreline recovery rates were examined using linear correlation analysis. A broad range of potential parameters were considered in the first-pass analysis, including several parameters describing nearshore wave conditions and also sandbar morphodynamics. These are outlined in the following section. The correlation coefficient, r, was calculated between each shoreline recovery rate and forcing parameter statistic for the window during which the rate was calculated. A 95% confidence level, $r_{95\%}$, was adopted to assess the statistical significance of the results.

4.2.5.1 Nearshore wave parameters

Hourly deepwater wave data H_s, T_p and θ, for the 10-year study period were acquired from the Sydney waverider buoy and transformed to the -10 m depth contour in the nearshore of the shoreline and sandbar monitoring region using a MIKE21 spectral wave model as described in Section 3.2. These three fundamental nearshore wave parameters (H_S, T_p and θ) plus the local sediment properties (d_{50}, sediment fall velocity, *w*) were used to consider five additional nearshore wave and related morphodynamic parameters, described in further detail below.

Wave steepness, *H/L*, has been widely recognised as an important parameter governing the direction of cross-shore sediment transport on the beach profile (e.g., Rector, 1954; Iwagaki and Noda, 1963; Dean, 1973; Larson and Kraus, 1989). In this study hourly wave steepness was calculated at the -10 m depth contour using significant wave height and the corresponding peak wave period.

Similarly, the dimensionless fall velocity, Ω (Gourlay, 1968; Dean, 1973) has been commonly adopted to empirically classify sediment transport direction (Larson and Kraus, 1989) and also morphological beach states (Wright and Short, 1984). In this study dimensionless fall velocity was calculated at the -10 m depth contour by

$$\Omega = \frac{H_S}{wT_P} \tag{4.2}$$

where *w* is the fall velocity (m/s) of the beach sediment.

Wright et al. (1985) also suggested that rates of morphological change are influenced by weighted antecedent values of the dimensionless fall velocity parameter. More recently, this concept has been applied by Davidson et al. (2013) to empirically predict shoreline rates of change, by adopting a temporal disequilibrium term ΔΩ,

$$\Delta\Omega = \Omega_{eq} - \Omega \tag{4.3}$$

where Ω_{eq} is the weighted average of antecedent dimensionless fall velocity values following Wright et al. (1985)

$$\Omega_{eq} = \frac{\sum_{j=0}^{\frac{D}{\Delta t}} \Omega_j 10^{-j\Delta t/\phi}}{\sum_{j=0}^{\frac{D}{\Delta t}} 10^{-j\Delta t/\phi}} \tag{4.4}$$

In Equation 4.4, *Δt* is the wave data sampling interval in units of days and *j* the number of observations prior to the time at which the equilibrium term is being calculated. The memory decay term, *ϕ*, and the window size over which the equilibrium term is calculated, *D*, were taken as 30 days and 2*ϕ* respectively in this study, following the results of Davidson et al. (2013) at the Narrabeen-Collaroy Beach study site.

Nearshore wave conditions can be characterised using nearshore wave energy E (J/m^2) given by

$$E = \rho g \frac{{H_S}^2}{16} \tag{4.5}$$

where ρ is the density of ocean water (1025 kg/m^3), g is the gravitational acceleration (9.8 m/s^2).

Similarly nearshore wave energy flux or wave power P (W/m) is given by

$$P = c_g E \tag{4.6}$$

It describes the power per unit crest length of a train of waves in water depth d (m) and moving at a group velocity c_g (m/s) given by

$$c_g = \frac{L}{T_P}\frac{1}{2}\left[1 + \frac{4\pi d/L}{sinh[4\pi d/L]}\right] \tag{4.7}$$

For interest, bulk statistics of these eight parameters (i.e., H_s, T_P, θ, H/L, Ω, $\Delta\Omega$, E, P) calculated over the full 10-year study period are shown in Table 4.1. When undertaking correlation analysis, three statistics from hourly values of the specified parameters were evaluated for each window over which a shoreline recovery rate was calculated. Firstly the mean, μ, of the hourly values within each time-window was taken. Secondly, to observe the influence of larger values within a given time-window, the number of hourly observations exceeding the 75th percentile value in Table 4.1, n_{high}, was taken. Thirdly, to observe the influence of smaller values within a given time-window the number of hourly observations below the 25th percentile value in Table 4.1, n_{low}, was recorded. For $\Delta\Omega$ only the first approach was used.

Table 4.1: Nearshore wave and related morphodynamic parameter statistics recorded during shoreline and sandbar monitoring from August 2004 to April 2015.

Parameter	**Study site characteristics**		
	25th percentile	**Mean**	**75th percentile**
H_s (m)	0.57	0.90	1.13
T_p (s)	8.2	9.8	11.5
θ (°)	92	101	111
H/L	0.006	0.011	0.014
Ω	1.5	2.6	3.3
E (kJ/m^2)	0.20	0.65	0.80
P (kW/m)	1.6	5.1	6.1

4.2.5.2 Sandbar morphodynamics

The correlation analysis also examined two additional parameters relating specifically to sandbar morphodynamics as potential controls of the observed rates of shoreline recovery. The proximity of the sandbar to the shoreline x_{bs} (m) as defined in Section 4.2.2.2 was included in the analysis. For each time-window over which a shoreline recovery rate was calculated, the initial (mean of the first 25% of observations), final (mean of the last 25% of observations), and overall mean of observed sandbar-shoreline distances were determined. This sandbar-shoreline proximity was related to the degree of attachment with the shoreline with reference to observed morphological states as defined by Wright and Short (1984). Also included was the rate of cross-shore sandbar migration dx_b/dt (m/day) calculated using the time series of x_b and following the same procedure described in Section 4.2.4. Positive values of both dx_b/dt (m/day) and dx_s/dt (m/day) indicate a seaward movement of the sandbar and shoreline, respectively.

4.3 Results

4.3.1 Shoreline and sandbar variability

Changes in shoreline position x_s and sandbar-shoreline proximity x_{bs} over the 10 years of monitoring are shown alongside daily mean nearshore wave power in Figure 4.3. In Figure 4.3a, the detrended shoreline (i.e., multi-year embayment rotation trend removed) is observed to fluctuate in response to storm erosion and recovery cycles within a 55 m cross-shore envelope, about a mean of 21 m from the landward benchmark. A total of 82 storm erosion events (equivalent to 7.7 events per year) were identified in the time series, coinciding with spikes in nearshore wave power and offshore displacement of the sandbar in Figures 4.3c and 4.3b, respectively. Magnitudes of shoreline erosion due to identified storm events ranged up to 31 m, with a mean of 10 m. Storm erosion occurred most often in Austral autumn and winter months (i.e., between May and August). Erosion was observed due to either clusters of smaller storm events (e.g., in mid-2006), or larger, isolated storm events (e.g., June 2007). Considering the total summation of shoreline change over the monitoring period, the shoreline experienced 820 m of erosion due to storms. This however was equally matched by cumulative magnitudes of shoreline recovery between storms, such that the longer-term inter-annual net impact of storm erosion on the shoreline was minimal.

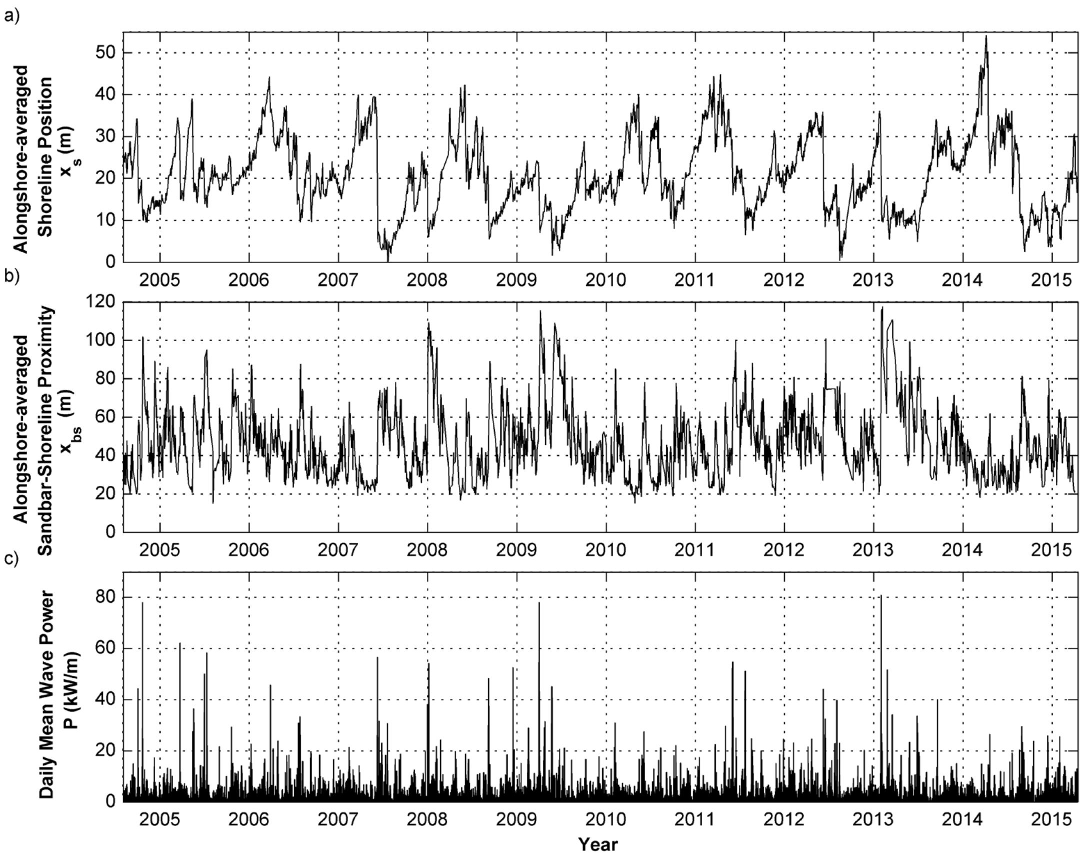

Figure 4.3: Time series of study period from August 2004 to April 2015 showing a) daily alongshore-averaged shoreline position (x_s), b) mid-tidal (daylight) alongshore-averaged sandbar-shoreline proximity (x_{bs}), and c) daily mean nearshore wave power at the -10 m depth contour of the study site. The time series depicts a high energy sandy coastline with dynamic shoreline and sandbar morphology.

In Figure 4.3b, sandbar positions with respect to the shoreline (x_{bs}) were observed to fluctuate between 20 and 120 m from the shoreline, spanning a range that was approximately twice that of the shoreline variability. On average, storms displaced the sandbar 66 m from the shoreline. Over the study period, the mean sandbar-shoreline proximity was 46 m, with an upper quartile of observations greater than 56 m and a lower quartile of observations less than 34 m. Upper quartile observations are shown in Figure 4.4a and were characterised by a prevalence of detached, rhythmic bar and beach sandbar morphology as described by Wright and Short (1984). In contrast and as would be expected, in Figure 4.4c lower quartile observations were characterised by a prevalence of attached low tide terrace and more reflective morphology. Remaining interquartile observations of sandbar-shoreline proximity (Figure 4.4b) were characterised by predominantly semi-attached, transverse bar and rip morphology. Lower quartile, interquartile and upper quartile observations of sandbar-shoreline proximity are hereafter referred to as attached, semi-attached and detached sandbar conditions respectively.

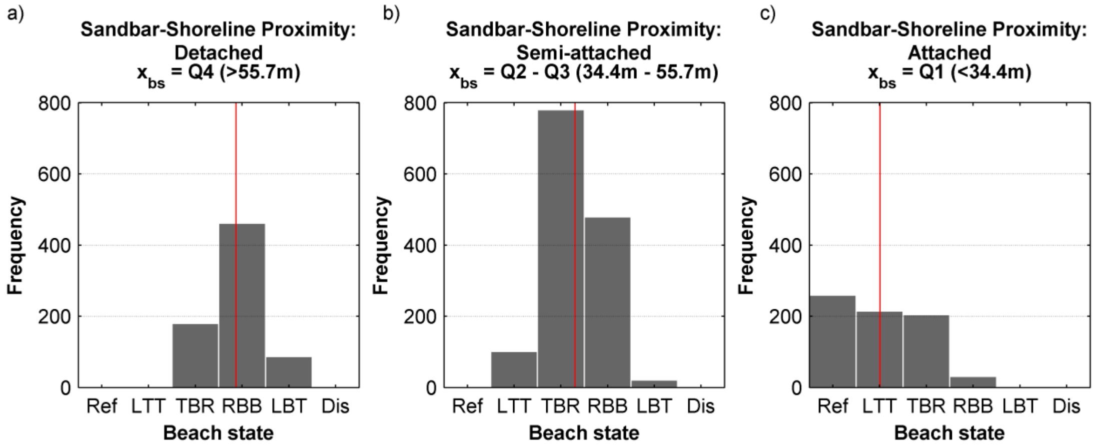

Figure 4.4: Visual classification of morphological beach states corresponding with a) upper quartile (*Q4*) b) intermediate quartiles (*Q2* & *Q3*), and c) lower quartile (*Q1*) observations of sandbar-shoreline proximity (x_{bs}) over the monitoring period. Ref = Reflective, LTT = low tide terrace, TBR = transverse bar and rip, RBB = rhythmic bar and beach, LBT = longshore bar and trough and Dis = Dissipative. Mean beach states are shown by the red line. Detached sandbar morphology becomes more prevalent with greater cross-shore separation of the sandbar and the shoreline.

4.3.2 Temporal variability of shoreline recovery rates

The distributions of shoreline recovery rates are shown in Figure 4.5 for shoreline recovery periods corresponding to temporal window sizes of 7, 14, 30 and 60 days. As expected during shoreline recovery, mean rates were observed to be positive for all window sizes, in the range of 0.15 m/day (60-day window) to 0.22 m/day (7-day window), characterising an overall net seaward movement. However variances in rates between window sizes were significantly different (95% confidence level) as assessed by a Levene's Test for homoscedasticity ($F = 23.7$, $p < 0.0001$). For shoreline recovery periods divided into shorter 7 and 14-day windows (Figures 4.5a and 4.5b respectively), higher variability in observed recovery rates was evident, with greater spread and increased weighting in tail distributions. This shorter-term variability during shoreline recovery included observations of rates more frequently between 0 - 0.3 m/day, less frequent more rapid progradation with rates in excess of 1 m/day, and also minor landward shoreline movements (i.e., rates < 0 m/day not associated with storm activity). The maximum observed rate during shoreline recovery was 1.8 m/day for a 7-day window, equivalent to more than 12 m of beach widening during one week. On the other hand, for shoreline recovery periods divided into longer 30 and 60-day windows (Figures 4.5c and 4.5d respectively), rates were less variable, characterised by more uniform distributions of gradual seaward progradation, predominantly in the range of 0 - 0.3 m/day.

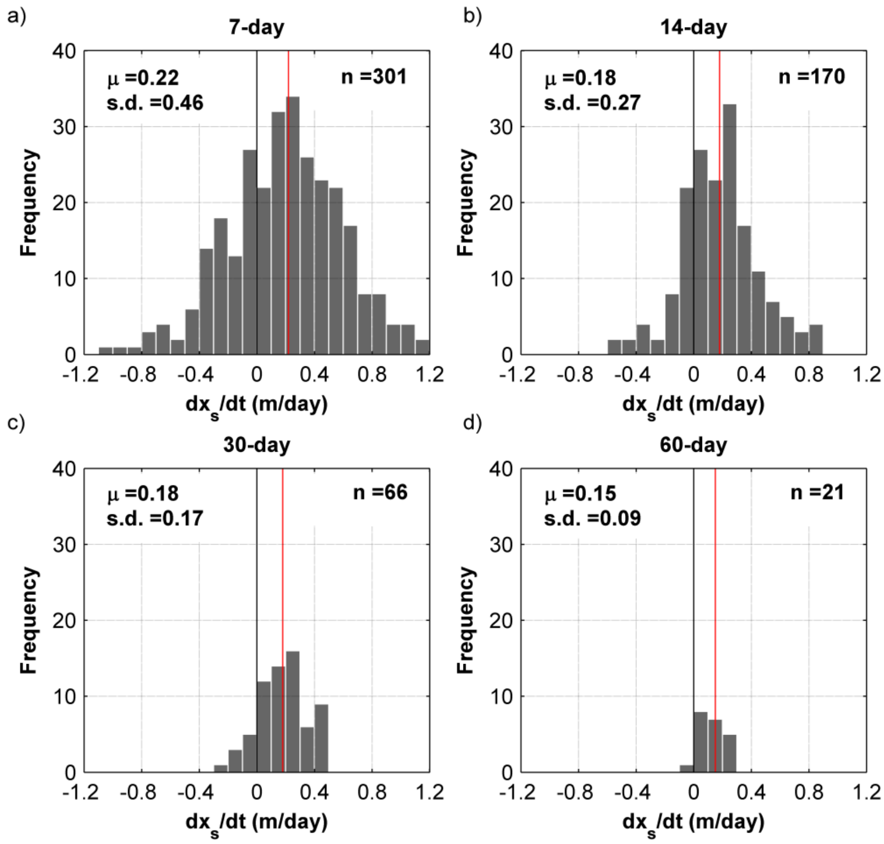

Figure 4.5: Distributions of shoreline recovery rates for recovery periods divided into window sizes of a) 7 days, b) 14 days, c) 30 days and d) 60 days. Mean rates (red) are characterised by gradual progradation with increased temporal variability evident at finer window sizes, including more rapid progradation and minor landward movement. Differences in variances in rates between window sizes are statistically significant (95% confidence level) as assessed by a Levene's Test for homoscedasticity ($F = 23.7$, $p < 0.0001$).

4.3.3 Correlation analysis

Linear correlation results of shoreline recovery rates with nearshore wave parameter statistics, related morphodynamic parameter statistics, sandbar-shoreline proximity and cross-shore sandbar migration rates are summarised in Figure 4.6 In general, nearshore wave and related morphodynamic parameter statistics were better correlated to observed shoreline recovery rates for recovery periods divided into shorter 7 and 14-day windows shown in Figures 4.6a and 4.6b, respectively. In both cases, a statistically significant (95% confidence level) negative relationship was observed for both mean wave steepness (H/L) and dimensionless fall velocity (Ω). Correlations with rates for 14-day windows during shoreline recovery also suggest that the occurrence of less common high and low magnitudes of such parameters were of significance.

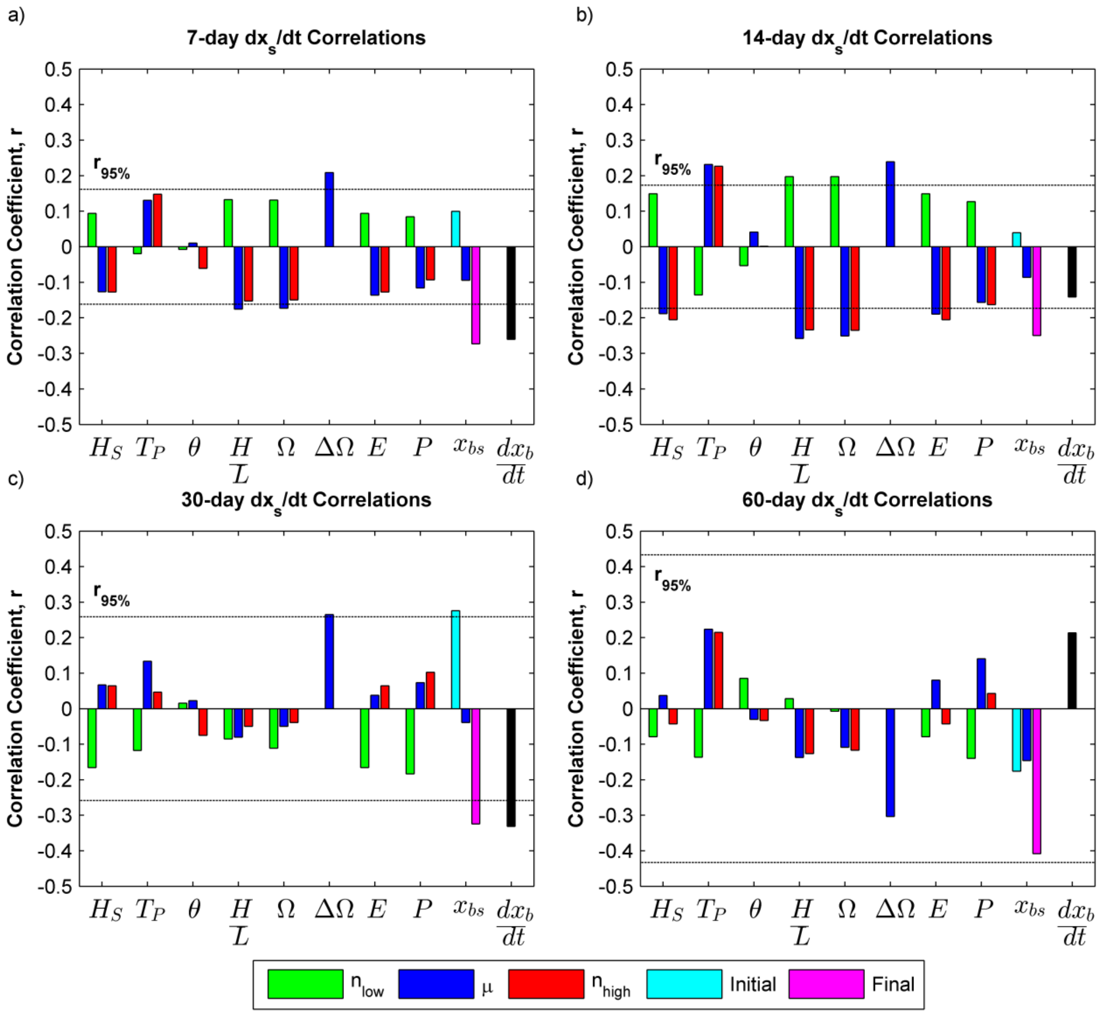

Figure 4.6: Linear correlation results of shoreline recovery rates with nearshore wave and related morphodynamic parameter statistics (H_s, T_P, θ, H/L, Ω, $\Delta\Omega$, E, P), sandbar-shoreline proximity (x_{bs}) and sandbar migration rates (dx_b/dt). Results are shown for shoreline recovery periods divided into a) 7-day, b) 14-day, c) 30-day, and d) 60-day window sizes, and using various statistics for each parameter (outlined Sections 4.2.5.1 and 4.2.5.2). The dotted line indicates correlation for a 95% confidence level. Parameters describing sandbar morphodynamics (x_{bs}, dx_b/dt) and nearshore wave height to period (H/L, Ω, $\Delta\Omega$) were observed to best account for the temporal variability of shoreline recovery rates at finer time-window sizes.

Additionally, a significant positive correlation with the mean dimensionless fall velocity disequilibrium (ΔΩ) was observed for shoreline recovery rates for 7, 14 and 30-day windows. Wave direction at the -10 m depth contour was poorly correlated with shoreline recovery rates for all window sizes during shoreline recovery. Correlation results with rates for 60-day windows in Figure 4.6d were likely influenced by limited sample size and low variability in rates for this longer time-window duration. Overall, parameters incorporating the ratio of wave height to wave period (H/L, Ω, ΔΩ) were found to be most correlated to the observed temporal variability in rates of shoreline recovery. In addition to significant relationships identified for H/L, Ω, and ∆Ω, it is seen that parameters describing sandbar morphodynamics account equally well for the temporal variability of shoreline recovery rates. The last two parameters in each of the plots in Figure 4.6 describe morphodynamic relationships of shoreline recovery rates with the proximity of the sandbar to the shoreline (x_{bs}) and the rate of cross-shore sandbar migration (dx_b/dt), respectively. A significant negative relationship was observed between shoreline recovery rates and final sandbar proximity for 7, 14 and 30-day windows during shoreline recovery. The results indicate that for a given time-window during recovery, the rate of shoreline recovery increases as the sandbar approaches the shoreline. Furthermore, significant negative correlations between shoreline recovery rates and sandbar migration rates for 7 and 30-day windows also suggest a morphodynamic coupling with concurrent rates of onshore sandbar migration.

4.3.4 Shoreline recovery rates and sandbar attachment

Based on the highest number of significant correlation results presented in Figure 4.6, 14-day windows during shoreline recovery were adopted to explore the influence of sandbar-shoreline proximity on shoreline recovery rates in further detail. Results plotted in Figure 4.7 show correlations with the wave-based parameters H/L, Ω, $\Delta\Omega$ as well as sandbar migration rates dx_b/dt, separated into 3 cases (as in Figure 4.4) of detached, semi-attached and attached sandbar-shoreline proximity. For semi-attached sandbars, shoreline recovery rates were significantly (95% confidence level) negatively correlated with Ω and H/L, and significantly positively correlated with $\Delta\Omega$. Also, a significant negative correlation was observed with dx_b/dt, indicating a coupling with onshore sandbar migration rates. The same relationships were evident with attached sandbars, but not all were significant at the 95% level. However, for conditions with detached sandbars such relationships were not apparent, with shoreline recovery rates observed to be poorly correlated to H/L, Ω, $\Delta\Omega$ and dx_b/dt.

The effect on shoreline recovery rates (14-day time-windows) of sandbar-shoreline proximity and corresponding cases of sandbar attachment is shown in Figure 4.8. Differences between mean shoreline recovery rates for cases of sandbar attachment are statistically significant (95% confidence level) as assessed by one-way analysis of variance (ANOVA). When the sandbar was detached from the shoreline, shoreline recovery tended to be more gradual with a mean rate of 0.12 m/day. Shoreline recovery where the sandbar was semi-attached was slightly higher with a mean rate of 0.23 m/day. In contrast, shoreline recovery with attached sandbars was much more

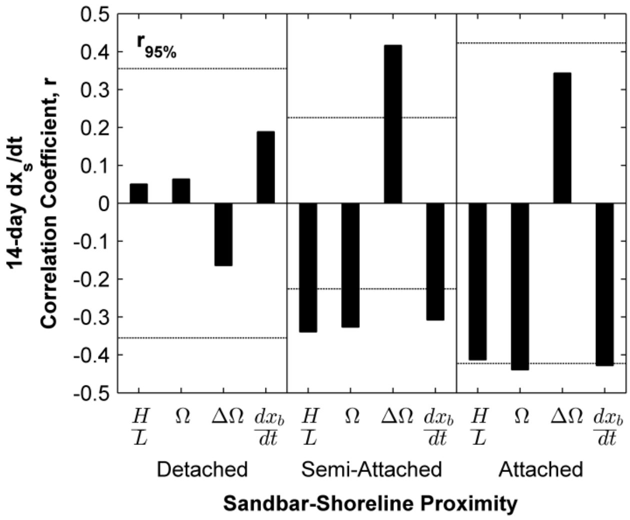

Figure 4.7: Linear correlation results (14-day windows) of shoreline recovery rates with mean nearshore forcing parameters (*H/L*, *Ω*, Δ*Ω*) and sandbar migration rates (dx_b/dt), for detached (n = 31), semi-attached (n = 76) and attached (n = 22) sandbars. Relationships evident for conditions with attached and semi-attached sandbars were not observed with detached sandbar morphology.

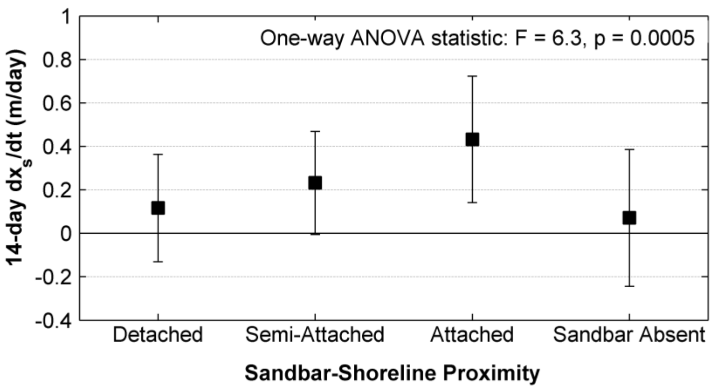

Figure 4.8: Variability in shoreline recovery rates for 14-day windows during recovery with sandbar-shoreline proximity associated with detached, semi-attached, attached and sandbar absent conditions. The mean rate is plotted with error bars equivalent to standard deviations. Differences in means are statistically significant (95% confidence level) as assessed by one-way analysis of variance (ANOVA). Mean shoreline recovery rates increase as a storm-deposited sandbar progressively moves within closer proximity (and attachment) to the shoreline.

rapid, with a mean rate of 0.43 m/day, approximately 3.5 times greater than for detached sandbar conditions. Shoreline recovery rates when the sandbar had entirely welded onto the subaerial beach (i.e., sandbar absent) and was no longer present in the nearshore are also shown. In this case, shoreline recovery rates were minimal with a mean of 0.07 m/day, and observations more evenly split between rates of beach widening and narrowing. The results distinguish the variability in shoreline recovery rates through the various stages of post-storm onshore sandbar migration, from an offshore storm-deposited sandbar to the final attachment to the shoreline.

4.4 Discussion and conceptual model

The daily shoreline time series shown in Figure 4.3 (top panel) demonstrates that, despite episodic and rapid storm erosion occurring multiple times each year, the predominance of recovery between these events is such that over the entire 10-year study period, minimal net erosion due to storm activity was observed. The dynamic shoreline fluctuations provide a clear example of what is described by Masselink and van Heteren (2014) as a characteristic of the sustainable resilience of a beach to storm impact, with shoreline recovery enabling the continual restoration and long-term maintenance of subaerial beach width. Consistent with studies investigating storm clustering (Ferreira, 2006; Coco et al., 2014; Karunarathna et al., 2014) and longer-term beach evolution (Zhang et al., 2002), results from the present study indicate the importance of beach recovery processes in assessing the net impact of storms through time at high energy sandy coastlines.

Significant temporal variability in shoreline recovery rates at this site (Figure 4.5) is evident at finer temporal resolutions of days to a few weeks during shoreline recovery. For shoreline recovery periods divided into shorter 7 and 14-day windows, shoreline recovery rates were most frequently observed between 0 - 0.3 m/day, with less frequent more rapid rates of up to 1.8 m/day (for 7 days) and also minor landward movements of the shoreline (i.e., rates < 0 m/day). Landward movement of the shoreline during shoreline recovery not associated with storm activity may arise due to a number of reasons, such as temporary post-storm persistence of rip cells with significant length scales (e.g., Loureiro et al., 2012), phases of higher wave steepness (Figure 4.6), and also a steepening response of the foreshore with phases of berm aggradation (e.g., Dubois, 1988). When observed at temporal resolutions of days to a few weeks, post-storm shoreline recovery is found to be characterised by a net progradation of the shoreline to a pre-storm position with time, rather than solely observations of seaward shoreline migration rates. The observed integrated effect of this short-term variability in rates during shoreline recovery was a gradual progradation of the shoreline to a pre-storm position with overall mean rates of ~0.2 m/day. In this study, rates observed for 60-day (i.e., two-month) windows during shoreline recovery ranged between 0 - 0.3 m/day, in comparison to preliminary work with shoreline recovery rates observed for longer periods of several months to a year between 0.05 - 0.15 m/day (Phillips et al., 2015).

When observed at different temporal resolutions, shoreline recovery at the single Narrabeen-Collaroy Beach study site is interestingly found to exhibit close to the full range of rates listed in Table 2.5 observed at other high energy sandy beaches worldwide. On high energy mesotidal beaches at Cape Cod and North Carolina in the USA, List et al. (2006) found rapid rates of shoreline recovery of the order of a few metres per day, for days to weeks immediately following storm erosion. In contrast, at the high energy microtidal Gold Coast, Australia, Splinter et al. (2011b) observed more gradual shoreline recovery in the range of 0.04 to 0.1 m/day for two consecutive 6-month windows following a storm. In comparison, the findings in the present study highlight the dynamic foreshore morphology at Narrabeen-Collaroy Beach, likely associated with the frequent transitioning between a broad range of reflective and intermediate beach states at this site (Wright et al., 1985).

4.4.1 Conceptual Model

The correlation results summarised in Figures 4.6 - 4.8 suggest that the proximity of the sandbar to the shoreline can play a key role in governing rates of shoreline recovery. The sandbar-shoreline proximity parameter (x_{bs}) included in these analyses and the corresponding degree of sandbar attachment with the shoreline (Figure 4.4) is seen to usefully distinguish gradual from rapid rates of shoreline recovery (Figure 4.8). The proximity of the sandbar to the shoreline is also seen to influence the degree of dependence of shoreline recovery rates to a range of nearshore forcing parameters (Figure 4.7) that were found to be significant, namely wave steepness (H/L), dimensionless fall velocity (Ω), the temporal disequilibrium in the prevailing beach morphodynamic state ($\Delta\Omega$), as well as the observed rate of cross-shore sandbar migration (dx_b/dt). The results highlight the importance of parameters related to wave steepness and sandbar morphodynamics in governing the temporal variability of shoreline recovery on wave-dominated sandy coastlines. Phases of more gradual and rapid shoreline recovery observed by Phillips et al. (2015) are found in the present study to be governed by the forcing of these parameters.

These core findings are summarised in a new conceptual model presented in Figure 4.9, that takes as its starting point the beach state classification scheme of Wright and Short (1984). The observed temporal variability of shoreline recovery is characterised into four phases, each associated with stages of onshore sandbar migration following a storm, including detached, semi-attached, attached and sandbar absent nearshore morphology.

Shoreline recovery and detached sandbar morphology

Detached sandbar conditions, depicted in Figure 4.9a, is described by Wright and Short (1984) as longshore bar and trough or rhythmic bar and beach morphology in which a trough fully separates the sandbar from the shoreline. With these conditions, more gradual shoreline recovery is seen in Figure 4.8, with rates on average between 0 - 0.2 m/day. Rates were observed to be poorly correlated with changes in nearshore wave steepness, dimensionless fall velocity and cross-shore rates of sandbar migration.

These results may likely be due to the location of the sandbar (storm deposits) further from the shoreline in deeper outer surf zone waters and separated by an intermediate trough. For milder wave conditions, the onshore migration of sandbars located in deeper waters beyond the breaker zone is significantly reduced when compared to that of lower state attached sandbar morphology in shallower breaker zone waters (e.g., Lee et al., 1998; Splinter et al., 2011a). As cellular surf zone circulation develops, sediment deposition is concentrated in regions of the trough with onshore cellular flow, weaker undertow and the onshore migration of sandbars (Plant et al., 2006; Splinter et al., 2011a; Aagaard et al., 2013). Though post-storm onshore migration of detached sandbars can also be rapid with rates of up to *O(10 m/day)* (Sallenger et al., 1985; van Enckevort and Ruessink, 2003), the present findings indicate that this morphological change in the nearshore is decoupled from a shoreline recovery response in the foreshore. The response of the foreshore under cellular flow is noted by Sonu (1973) with alongshore variability including seaward excursions (mega-cusps) in the lee of onshore flow and landward excursions (embayments) in the lee of rip currents and offshore flow. This foreshore variability has been observed to develop over the days to weeks following a storm (Poate et al., 2014). Alongshore-averaged shoreline recovery observed in the present study with detached sandbar morphology (Figure 4.8) is likely the net cross-shore movement of this developing rhythmic variability following a storm, and in most cases was observed as a gradual progradation of the shoreline.

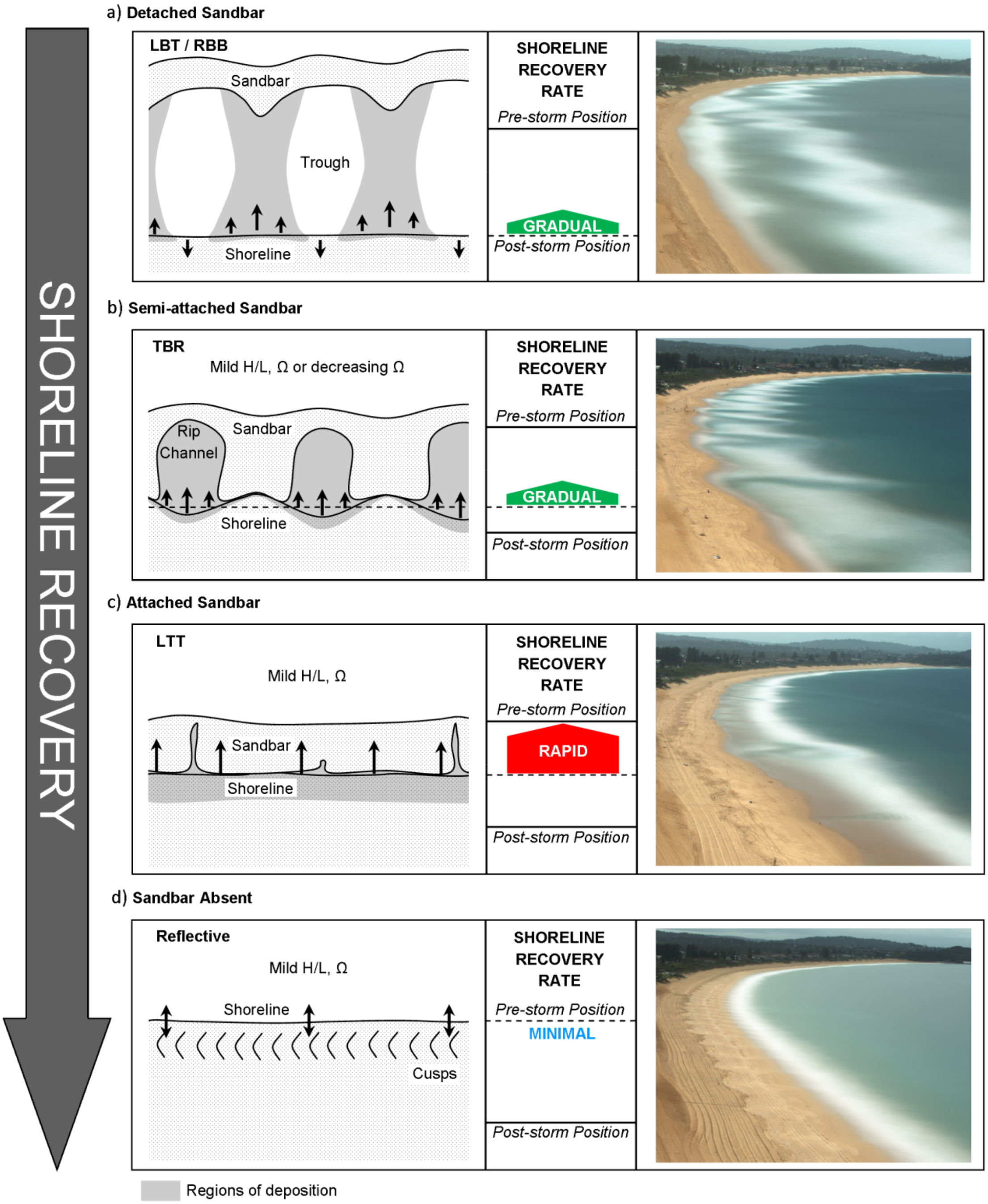

Figure 4.9: Conceptual model describing phases and rates of alongshore-averaged shoreline recovery occurring with post-storm onshore migration and attachment of sandbar morphology. Beach states are classified following Wright and Short (1984); LBT = longshore bar and trough, RBB = rhythmic bar and beach, TBR = transverse bar and rip, and LTT = low tide terrace. More rapid shoreline recovery rates are triggered by attached sandbar morphology under nearshore conditions of mild wave steepness/dimensionless fall velocity.

Shoreline recovery and semi-attached sandbar morphology

When in closer proximity to the shoreline, sandbars weld at mega-cusps, forming semi-attached, transverse bar and rip morphology (Wright and Short, 1984) depicted in Figure 4.9b. This can occur within 1 - 2 weeks following a storm (van Enckevort et al., 2004; Ranasinghe et al., 2012). For semi-attached sandbar conditions, shoreline recovery though still gradual, is observed to increase slightly, with rates on average between 0.1 - 0.3 m/day (Figure 4.8). This may be due to a modest increase in sediment availability at shallower depths in the inner nearshore as transverse sandbars move shoreward by expanding laterally, depositing sediment into weakening and narrowing rip channels (Short, 1999; Aagaard et al., 2013). In contrast to detached sandbar conditions, shoreline recovery with semi-attached sandbars is seen to be coupled with concurrent rates of onshore sandbar migration. The present findings suggest that the coupling of wave-driven beach recovery in the foreshore with concurrent onshore sediment transport in the nearshore, increases with closer sandbar proximity and attachment to the shoreline. Likewise, van de Lageweg et al. (2013) found increased coupling of planform variability in sandbar and shoreline morphology with closer proximity.

Shoreline recovery rates in the presence of semi-attached sandbars were found to be significantly (95% confidence level) negatively correlated to the forcing of nearshore wave steepness and dimensionless fall velocity (Figure 4.7). As expected, higher rates of shoreline recovery were associated with milder prevailing wave conditions. It was common for higher values of these parameters to slow rates of shoreline recovery, interrupting, resetting and prolonging the temporal progression of shoreline recovery, and associated onshore sandbar migration, depicted in Figure 4.9. These relationships with nearshore wave steepness and dimensionless fall velocity were expected considering the demonstrated importance of these parameters in classifying sediment transport direction with physical experimentation (Dean, 1973) and states of beach morphology in the field (Wright and Short, 1984). Shoreline recovery rates were also observed to be significantly positively correlated to a temporal disequilibrium in dimensionless fall velocity adopted by Davidson et al. (2013). The identified relationships with these nearshore wave parameters, not observed with detached sandbars, may be dependent on some degree of sandbar-shoreline attachment and depth of sandbar crest relative to a wave base for mild conditions.

Shoreline recovery and attached sandbar morphology

With persistent lower than average wave steepness/dimensionless fall velocity (i.e., mild wave conditions), the sandbar moves within closer proximity to the shoreline, attaching further by filling the lower intertidal zone and forming low-tide terrace/ridge-runnel morphology (Wright and Short, 1984) shown in Figure 4.9c. In this case, results from the present study as depicted in Figure 4.8, highlight a rapid increase in rates of shoreline recovery, with a mean 3.5 times greater than for detached sandbar conditions between 0.3 - 0.6 m/day and with maximum rates for 7 days in excess of 1 m/day. More rapid shoreline recovery rates correspond with sandbar welding events and are characterised by a higher sediment volume and flatter profile gradient in the inner nearshore associated with closer sandbar-shoreline proximity. Under continued mild wave conditions, this inner nearshore sediment is transported onshore with deposition concentrated in the foreshore as rip channels become exhausted of storage capacity (Aagaard et al., 2013). This is characterised by onshore migrating intertidal sandbars driven by the tidal shifting of wave and swash processes across the foreshore and inner nearshore profile (Hine, 1979; Masselink et al., 2006). A subsequent rebuilding of berm morphology occurs in the subaerial beach (e.g., Jensen et al., 2009). The shoreline rapidly recovers to a maximum seaward position as depicted in Figure 4.9d characteristic of reflective morphology, berm cusps and minimum surf zone width with no sandbar present (Wright and Short, 1984). For a reflective beach state with a steeper inner nearshore profile, onshore sediment transport potential with mild wave conditions reduces and observed rates of shoreline recovery are minimal, oscillating about equilibrium in response to small changes in incident wave conditions acting on the foreshore (Aagaard et al., 2013).

4.4.2 Temporal progression of shoreline recovery

The temporal progression of observed shoreline recovery is also summarised in Figure 4.9, associated with the onshore migration of the sandbar. With a detached and semi-attached sandbar during the initial weeks following a storm, an immediate shoreline recovery response proceeds steadily until attached sandbar conditions trigger a more rapid response. Similarly, Aubrey and Ross (1985) observed slower subaerial recovery response during the first half of recovery periods over a five year monitoring period at Torrey Pines Beach, United States. On the other hand, some studies have also observed rapid subaerial recovery immediately following storms (e.g., Kana, 1977; Birkemeier, 1979; Kriebel, 1987; List et al., 2006). Simplified fits of subaerial recovery used in modelling beach morphological change have also adopted a rapid initial response, decaying exponentially with time (Callaghan et al., 2008; Callaghan et al., 2013; Wainwright et al., 2015). The findings from the present study suggest that rapid shoreline recovery immediately following a storm requires a close post-storm sandbar-shoreline proximity, thereby allowing immediate reattachment of the sandbar with minimal rip persistence.

It is important to note that the temporal progression of nearshore and shoreline recovery in Figure 4.9 is for the 'ideal' case of uninterrupted mild wave conditions. Of course, it is common on storm-dominated coastlines for beach recovery processes to be interrupted by subsequent storm events (e.g., Kriebel, 1987; Morton et al., 1994; Corbella and Stretch, 2012). In the present study, 37% of shoreline recovery periods were interrupted by the occurrence of subsequent storm erosion. These events, in addition to higher values of wave steepness/dimensionless fall velocity, reset and prolong the temporal progression of shoreline recovery, and associated onshore sandbar migration, depicted in Figure 4.9. However, in deeper waters further offshore, smaller storm events during recovery may also mobilise stranded storm-deposits onshore (e.g., Scott et al., 2016).

The findings indicate that temporal variability in wave-driven recovery processes in the subaerial beach are particularly influenced by nearshore wave parameters related to wave steepness and also morphological interactions with changes (or lack of changes) in the subaqueous beach that occur concurrently during beach recovery. Further research examining the role of the subaqueous beach in driving spatial variability in wave-driven processes of subaerial beach recovery along the broader Narrabeen-Collaroy embayment and other nearby embayments is presented in Chapter 6.

4.5 Conclusion

A unique 10-year dataset of daily shoreline and sandbar positions collected by a Coastal Imaging station at Narrabeen-Collaroy Beach, Australia, were used to quantify and characterise the temporal variability of shoreline recovery rates on a high energy sandy coastline. Following 82 individual storm events, rates of the cross-shore movement of the shoreline as it returned to its pre-storm position were examined. Temporal variability in shoreline recovery rates were most evident at shorter timescales of 1 - 2 weeks during shoreline recovery, including rates most frequently between 0 - 0.3 m/day, less frequent more rapid rates of up to 1.8 m/day and minor landward movements. Despite shorter-term variability, shoreline recovery was characterised by progradation with a mean rate on the order of 0.2 m/day.

Linear correlation analysis was used to explore the degree of dependence of this temporal variability with a set of parameters describing nearshore wave conditions, beach state morphodynamics, cross-shore proximity of the sandbar to the shoreline, and the rate of cross-shore sandbar migration. Variability in shoreline recovery rates were found to be significantly correlated to nearshore wave steepness, instantaneous dimensionless fall velocity, and a temporal disequilibrium in the dimensionless fall velocity. Additionally, significant correlations were observed between shoreline recovery rates and sandbar-shoreline proximity as well as concurrent rates of sandbar migration.

These extensive observations of shoreline recovery at a dynamic and high energy site are generalised in a new conceptual model describing the observed phases and rates of shoreline recovery through various stages of onshore sandbar migration following a storm, from fully detached storm-deposited sandbar morphology through to complete sandbar welding with the shoreline. Gradual shoreline recovery rates are observed for conditions with detached and semi-attached sandbars. In contrast, more rapid rates of shoreline recovery are observed when sandbars are attached to the shoreline, with rates on average 3 - 4 times greater than for detached sandbars. Negative correlations of shoreline recovery rates with the forcing of nearshore wave steepness and dimensionless fall velocity, and coupling with concurrent rates of onshore sandbar migration are observed in particular conditions with attached and semi-attached sandbars, but not with detached sandbars.

Whereas this chapter has analysed in one-dimension the cross-shore movement of a single shoreline contour during recovery, Chapter 5 examines in two-dimensions the recovery of the broader subaerial beach profile including the beachface and berm. Furthermore, in Chapter 6 the alongshore variability of subaerial beach volume recovery is investigated along the broader Narrabeen-Collaroy embayment and at other nearby embayments.

Chapter 5

The morphodynamics and forcing of berm recovery following removal by a storm: high frequency observations from a continuously scanning Lidar

Content of this chapter is in preparation for publication in:

Phillips, M. S., Blenkinsopp, C. E., Splinter, K. D., Harley, M. D., Turner, I. L. and Cox, R. J., *in prep*. Beachface and berm morphodynamics during post-storm beach recovery: observations from a continuous scanning Lidar. Geophysical Research Letters.

Chapter overview: After nearshore sediment has returned to the shoreline during post-storm beach recovery (Chapter 4), swash processes then rework inter-tidal zone sediment up onto the subaerial beach to rebuild the berm. This chapter analyses the entire rebuilding of a berm at the timescale of each and every tidal cycle. A continuously scanning Lidar (5 Hz) enables swash and subaerial beach profile measurements to be obtained throughout a complete berm recovery period. Tide-by-tide rates of subaerial volume change, patterns of berm crest growth and behavioural modes of subaerial profile variability throughout berm recovery are examined and distinguished by swash, nearshore wave and ocean water level conditions.

5.1 Introduction

The sandy beach berm is characterised by the near-planar region of the subaerial beach, extending seaward of the foredune toe and separated from the steeper and more seaward beachface often by a distinctive change in gradient, known as the berm crest (Masselink and Hughes, 2003). The rebuilding of the berm by swash processes marks the most landward extent of wave-driven processes during beach recovery, beyond which more gradual aeolian-driven processes rebuild eroded morphology in the backshore and dunes (Section 2.4). Previous investigations of swash-driven beachface and berm morphodynamics during recovery are often limited by the temporal resolution of post-storm morphological datasets, that have more commonly observed morphological and volumetric changes during recovery at monthly to yearly timescales (e.g., Morton et al., 1994; Corbella and Stretch, 2012; Kobayashi and Jung, 2012; Yu et al., 2013; Houser et al., 2015; Scott et al., 2016).

Fewer studies have observed post-storm recovery at finer temporal resolutions (sub-daily) spanning weeks to months, to examine beachface and berm morphodynamics associated with wave, swash and ocean water level hydrodynamics (e.g., Dubois, 1988; Katoh and Yanagishima, 1992; Austin and Masselink, 2006). Using daily beach profile measurements during the initial four months following a storm, Dubois (1988) observed two main behavioural modes in profile variability, namely the progradation (seaward growth) of the beachface and aggradation (vertical growth) of the berm. Though the study did not conduct simultaneous swash measurements, they suggested that swash exceedance of the berm crest was a primary factor distinguishing these two modes. Similar findings were later observed by swash measurement campaigns of berm regrowth following coastal lagoon openings, demonstrating the importance of swash exceedance above the elevation of the berm crest (Weir et al., 2006; Baldock et al., 2008). These and additional studies have provided valuable insight into smaller-scale (swash-by-swash to tide cycle) swash zone processes and morphodynamics over relatively shorter monitoring durations of days to a few weeks (e.g., Austin and Masselink, 2006; Jensen et al., 2009; Russell et al., 2009; Blenkinsopp et al., 2011). However, there remains a knowledge gap to better understand the role of swash zone processes in the longer-term context of entire berm recovery periods following significant storm events (Puleo and Torres-Freyermuth, 2016).

Addressing research objective 2 of this thesis (Section 1.3), this chapter uses the unique deployment of a continuously scanning Lidar, mounted on the rooftop of a beachside building, to obtain high frequency (5Hz) beach profile and swash measurements throughout the entire 2.5 month recovery period of a berm, following its complete removal by a significant storm. Methodology including Lidar monitoring setup and data processing is described in Section 5.2. Patterns of berm crest growth, rates of subaerial volume change and behavioural modes of subaerial profile variability are analysed at timesteps of each and every tidal cycle throughout berm recovery with results presented in Section 5.3. Using a decision tree analysis, behavioural modes of berm recovery are characterised and distinguished by swash, nearshore wave and ocean water level conditions, presented and discussed in Section 5.4. Chapter conclusions are summarised in Section 5.5.

5.2 Methodology

5.2.1 Study site

The detailed observations of berm recovery in the present chapter were undertaken at a single beach transect approximately 700 m north of the southern (Collaroy) end of Narrabeen-Collaroy Beach, SE Australia as shown in Figure 3.2. The monitoring location is partially exposed to predominant SSE wave energy with nearshore H_s averaging 0.8 m at the -10 m depth contour (Table 3.1) with semi-diurnal tides characterised by mean spring and neap ranges of 1.3 m and 0.8 m. Modal beach morphology is of low tide terrace state. The analyses presented in this chapter focuses on wave-driven cross-shore sediment exchanges between the subaerial and subaqueous beach. For a more detailed site description of Narrabeen-Collaroy Beach please refer to Section 3.2.1

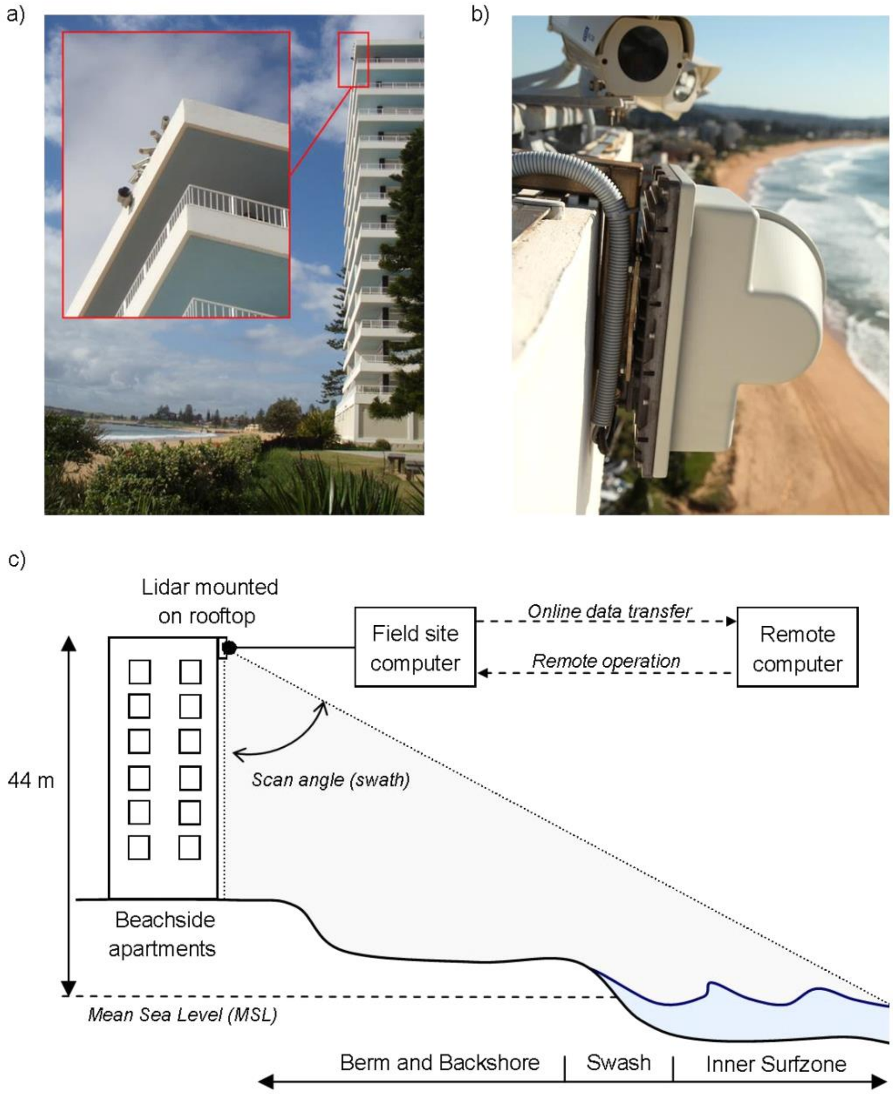

Figure 5.1: Fixed Lidar monitoring system photographs a) and b) showing Lidar instrument mounted on rooftop of beachside apartment building just below the coastal imaging station (described in Section 4.2.1) at Narrabeen-Collaroy Beach, SE Australia. c) Schematic of Lidar field setup.

5.2.2 Fixed Lidar monitoring setup

In May 2014, a near-infrared, extended-range Lidar (*SICK LD-LRS 2110*) was permanently installed on the rooftop (44 m above MSL) of a beachside building at Narrabeen-Collaroy as shown in Figure 5.1. The elevated and permanent Lidar deployment at Narrabeen-Collaroy operates by emitting a pulse of light that is reflected off the surface of the beach, swash and surf zone beneath, and returned to the instrument to be recorded as a distance based on travel time. Measurements are recorded at 0.25º angular increments along a cross-shore transect (approx. shore-normal bearing of 74º), equivalent to a cross-shore resolution of approximately 0.2 - 0.5 m across the berm and beachface, and 0.5 - 2 m within the surf zone. The Lidar swath extends from the base of the building to the offshore limit of signal return (Figure 5.1). This offshore limit was observed to vary with the degree of surf zone aeration required to obtain a valid signal reflection from the water surface (Blenkinsopp et al., 2010). The maximum range of the instrument was on the order of 130 m. Continuous scanning of the transect was undertaken at a frequency of 5 Hz since deployment, with brief and infrequent outages of up to a few days, due to local computer issues at the field site. The Fixed Lidar monitoring system enabled continuous data collection during daylight, as well as non-daylight hours as shown in Figure 5.4, in contrast to many beach monitoring techniques that are limited to collecting data solely during daylight hours. The system was designed as shown in Figure 5.1c to enable remote user operation of the Lidar, scan scheduling and automated online data transfer. Lower-elevation, short-term (days) Lidar deployments for the measurement of swash and subaerial morphology are also reported in the literature (e.g., Blenkinsopp et al., 2010; Brodie et al., 2012).

5.2.3 April 2015 storm and post-storm recovery analysis

On the 20th - 22nd April 2015, the study region was impacted by an intense extratropical cyclone known as an East Coast Low (ECL). Hourly deepwater wave data acquired from the Sydney waverider buoy recorded a peak H_s of 8.1 m during the storm, corresponding to a 20-year annual recurrence interval in terms of deepwater H_s (Shand et al., 2010). The storm approached the coast from an average SSE (161 °TN) direction and coincided with spring high tides. The impact of the storm was significant, identified as the fourth most erosive storm event on record in the last 40 years of routine monitoring (1976 - 2016) at Narrabeen-Collaroy Beach (Harley et al., 2016; Harley et al., 2017). These unique datasets from both the continuously scanning Lidar (analysed in the present chapter) and RTK-GPS profile monitoring of embayments in the region (analysed in the following Chapter 6) fortuitously captured both the impact of this significant event, as well as the complete recovery of the subaerial beach to pre-storm conditions in the months following.

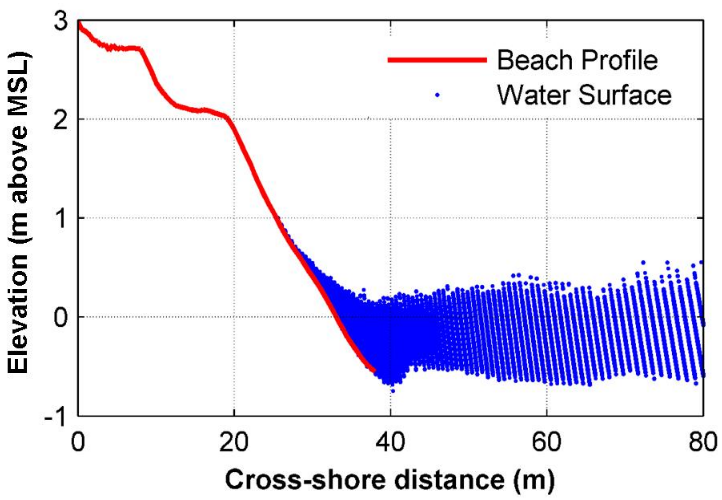

Figure 5.2: Example of profile, swash and surf zone water surface Lidar measurements during a 30 min scan at low tide (10:47 - 11:17, 29th May 2015).

5.2.4 Subaerial beach profile data extraction

In the present chapter, subaerial beach profiles were analysed at tidal intervals (i.e., low tide to low tide) throughout the entire recovery of berm morphology at the Lidar transect following the April 2015 storm event. Subaerial beach profiles were extracted from 30 min subsamples of the continuous Lidar dataset centred about each low tide, as shown in Figure 5.2. Pre-processing of the raw data to obtain detailed profile (and swash zone) information required several steps. First, raw distance data relative to the fixed location of the Lidar were transformed from polar coordinates to Cartesian (cross-shore distance and elevation) coordinates. Based on RTK-GPS ground control surveys of the measured transect, elevations were then converted to the local Australian Height Datum (m AHD, equivalent to mean sea level) and cross-shore distance (m) relative to a fixed landward benchmark. Elevation data were then linearly interpolated to regular 0.5 m cross-shore intervals. For every 30 min subsample at semi-diurnal low tides, the beach profile was determined by the minimum elevation at each cross-shore interval in order to extract a profile surface that extended down into the swash zone as shown in Figure 5.2. As the final step to distinguish the seaward limit of the measured beachface from the lower swash zone water surface, the seaward limit of the profile was defined as the minimum run down of the swash edge (refer Section 5.2.5 for details) that was then checked and verified by manual inspection. Comparisons with RTK-GPS profile surveys undertaken approximately each month throughout 2015 (12 surveys in total) found that the vertical root-mean-square error of the Lidar-measured

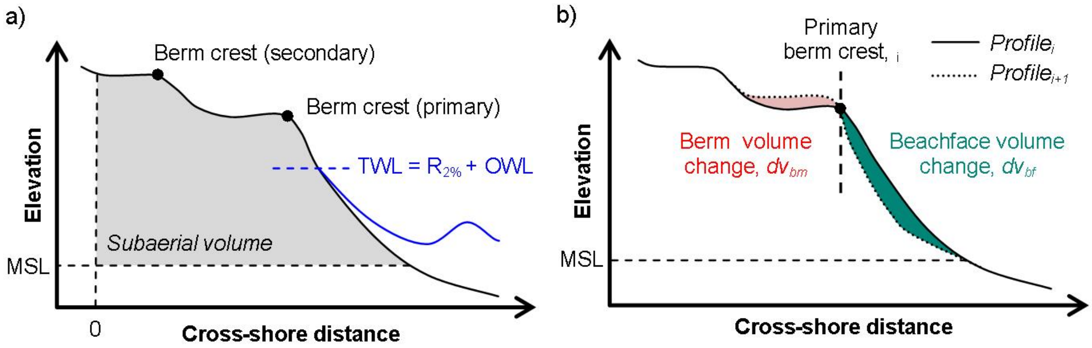

Figure 5.3: a) Profile schematic showing primary (most seaward) and secondary (landward) berm crests as well as TWL. b) Berm and beachface volume change were taken as the volume change either side of the primary berm crest on the initial profile, *i*.

profiles was 0.04 m relative to (and within the accuracy of) the RTK-GPS-measured profiles. RTK-GPS and Lidar measured profiles throughout the recovery period examined in the present chapter are presented in Appendix B.

Using these profile data obtained at every low tide, subaerial sand volume (m^3/m) was calculated as the integrated profile area above the elevation of mean sea level (0 m AHD), extending landward to the fixed cross-shore origin. Rates of subaerial volume change, dv/dt (m^3/m/day), between consecutive low tides measurements, *i*, were calculated as,

$$\frac{\boldsymbol{dv}}{\boldsymbol{dt}} = \frac{Volume_{i+1} - Volume_i}{Time_{i+1} - Time_i} \tag{5.1}$$

The position (cross-shore and elevation) of berm crests on the beach profile where extracted in a two-step process. First, potential berm crests were manually identified via visual inspection of the beach profile. Second, within a specified cross-shore region (±3 m) of each manually identified berm crest, the point of maximum change in the profile gradient was calculated where a flattening occurred in the landward direction. Where the corresponding change in profile gradient exceeded a threshold of 0.05, the point of maximum change in profile gradient was recorded as the position of the berm crest. As shown in Figures 5.3a and 5.4, where two or more berm crests were present, the most seaward of these features was identified as the 'primary crest', to distinguish this from the more landward 'secondary crest'. Rates of volume change in regions seaward (beachface, dv_{bf}/dt) and landward (berm, dv_{bm}/dt) of the primary berm crest were also calculated as illustrated in Figure 5.3b.

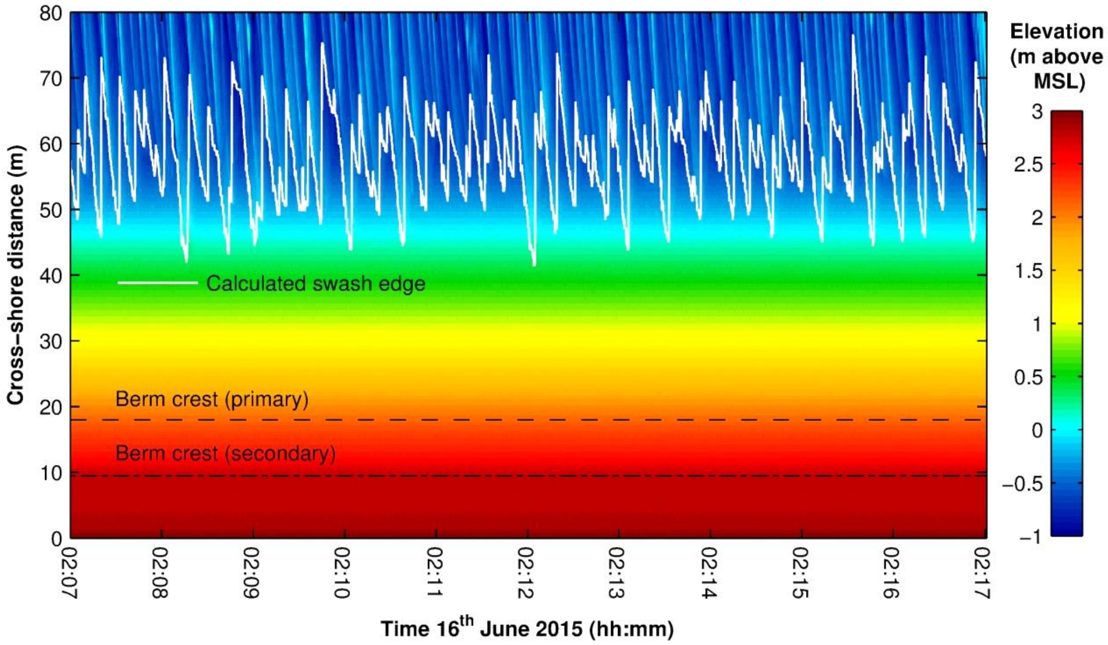

Figure 5.4: Example time series of subaerial beach profile and water surface Lidar measurements collected over a 10 minute period on 16th June 2015. The positions of the extracted swash edge and berm crests are shown. Note the capability of the Lidar to collect profile, swash and inner surf zone data outside of daylight hours, providing continuous, high temporal resolution monitoring over extending periods of time.

5.2.5 Swash and total water level data extraction

Swash water surface elevation data throughout the analysed recovery period were also obtained by the Fixed Lidar monitoring system. The time-varying leading edge of the swash, as shown in Figure 5.4, was extracted by applying a threshold technique, as described by Turner et al. (2008), to the rate of change between two successive Lidar scans. First, the dataset was smoothed using a running median filter (2 seconds) to reduce inherent noise (±0.03 m) in individual Lidar cross-shore point measurements. Second, gradients of change at each cross-shore interval between successive Lidar scans were calculated. A threshold gradient of 0.02 m/s was found to effectively distinguish the stationary bed measurements (≤ 0.02 m/s) from non-stationary water surface measurements (> 0.02 m/s). The leading edge of the swash for each scan was then defined as the point of transition between bed and water surface measurements, sampled at 5 Hz. The time series of the swash edge was referenced to the measured still ocean water levels (OWL) to give the wave runup time series throughout the recovery period.

Swash statistics were analysed for each semi-diurnal (approx. 12 hours) tidal cycle between consecutive low tides. The time series of the swash edge was used to calculate the percentage of wave runup events exceeding the primary berm crest elevation (i.e., 'swash exceedance') for each tidal cycle. Additionally the 2% exceedance elevation of wave runup events $R_{2\%}$ for each tidal cycle was calculated.

The total water level (TWL) for each tidal cycle is then given by,

$$TWL = R_{2\%} + OWL_{max} \tag{5.2}$$

where OWL_{max} was the maximum measured ocean water level (OWL) for each tidal cycle. Ocean water levels OWL, were measured every 15 minutes at the HMAS Penguin tide gauge in Port Jackson, Sydney, approximately 12 km south of the study site (Figure 3.2).

Hourly deepwater wave data H_s, T_p and θ, were acquired from the Sydney waverider buoy during the April 2015 storm and subsequent recovery. These were transformed using a MIKE21 spectral wave model to the -10 m depth contour in the nearshore directly offshore of the Fixed Lidar monitoring system, as described in Section 3.2. Dimensionless fall velocity Ω, was also quantified at the -10 m depth contour following Equation 4.2.

5.3 Results

5.3.1 Lidar observations: April 2015 storm and post-storm recovery:

During the April 2015 storm, modelled nearshore H_s at the -10 m contour of the Lidar monitoring profile are shown in Figure 5.5a to have peaked at 3.7 m. The arrival of the storm coincided with spring high tides and resulted in Lidar-recorded total water levels of up to 3.7 m above MSL (Figure 5.6a). The resulting impact on pre-storm berm and convex morphology at the Lidar profile is shown in Figure 5.5d. During the storm, the berm was completely removed, leaving a dissipative, concave post-storm subaerial profile, with minimal observed change in the foredune. This corresponded to rapid subaerial volume erosion of 55 m^3/m at the Lidar profile shown in Figure 5.5b. Approximately 56% of this erosion (31 m^3/m) was observed during the first tidal cycle (approximately first 12 hours) following the onset of storm wave conditions (Figure B.2a, Appendix B). Similar subaerial erosion observations within the broader embayment during the event were reported by Harley et al. (2016), noting an alongshore-averaged loss of 58 m^3/m of which over 90% was primarily from the berm

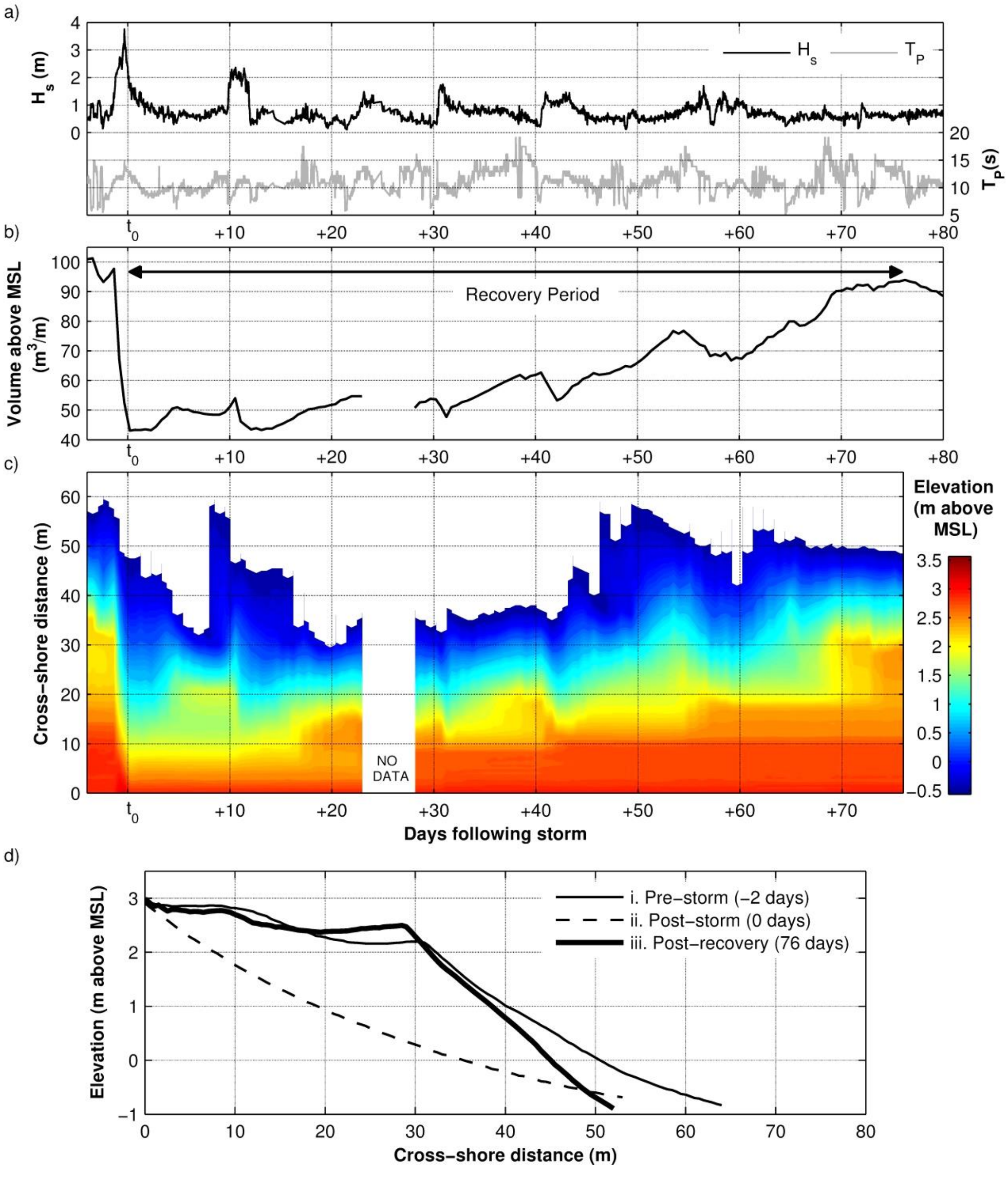

Figure 5.5: Beach recovery following 20 - 22 April 2015 storm. Time series during the storm and subsequent recovery period are shown for a) hourly measured nearshore significant wave height (H_s) and peak wave period (T_p), b) tide-by-tide measurements of subaerial beach sediment volume, and c) tide-by-tide beach profile evolution. d) Beach profiles immediately before the storm (pre-storm), immediately after the storm (post-storm) and at the end of the recovery period (post-recovery). No data was collected between days 23 and 28 due to a technical issue with the field site computer.

below the 3 m elevation contour. The April 2015 storm impact and recovery along the broader Narrabeen-Collaroy embayment and nearby embayments are presented in further detail in Chapter 6.

In the 2.5 months following the storm, wave conditions shown in Figure 5.5a were predominantly mild, with 70% of nearshore H_s below the 12-year site mean of ~0.8 m, and intermittently punctuated with larger H_s (H_s > 1 m). The mean H_s for the recovery period was 0.7 m. Nearshore Ω was also predominantly mild during this period, with approximately 80% of observations less than the 12-year site mean ($\bar{\Omega} \approx 2.0$), indicative of generally mild wave energy and accretionary beach conditions. By the 7th of July, 2015, 76 days after the storm, berm and convex profile morphology closely resembling pre-storm conditions were observed (Figure 5.5d), and virtually all (51 m^3/m) of the eroded sand volume had returned to the subaerial beach (Figure 5.5b). Tide-by-tide subaerial volume and beach profile evolution during the recovery period are shown in Figures 5.5b and 5.5c, respectively. Over the entire 76-day recovery period, subaerial volume returned at a net rate of ~0.7 $m^3/m/day$, with larger wave events causing minor intermittent erosion as the beach progressively recovered. For the first 1.5 months (days 0 to 45 of the recovery period) the net rate of subaerial volume recovery was more gradual (~0.4 $m^3/m/day$). In the final month (days 45 to 76), recovery progressed more rapidly (net rate of ~1.1 $m^3/m/day$) as nearshore sandbar morphology attached and welded to the beachface (see Figure 5.9b). Similar phases of shoreline recovery with enhanced rates as sandbars attach to the beachface are detailed in Chapter 4 and Phillips et al. (2017).

5.3.2 Berm crest formation and growth during recovery

The time series of ocean water levels (OWL), total water levels (TWL) and berm crest elevations throughout the recovery period are shown in Figure 5.6a. A close relationship is observed between the formation and vertical growth of the primary berm crest during recovery with neap-spring variations in total water levels. This was particularly apparent in the latter half of the recovery period (days 30 and onwards). The formation of a new berm crest on lower regions of the beach profile was seen during neap tides, i.e., a neap berm (e.g., days 33 to 35, Figure 5.6a). During subsequent 7-day periods of neap to spring tides (that occur approximately twice per month) and rising TWL, the berm crest underwent vertical growth (e.g., days 35 to 42). For these time periods, the increasing berm crest elevation closely correlated to the rising TWL ($R = 0.94$, $P<0.0001$), as the TWL extended higher up the beachface. Rates of vertical berm crest growth during these periods were found to be similarly correlated

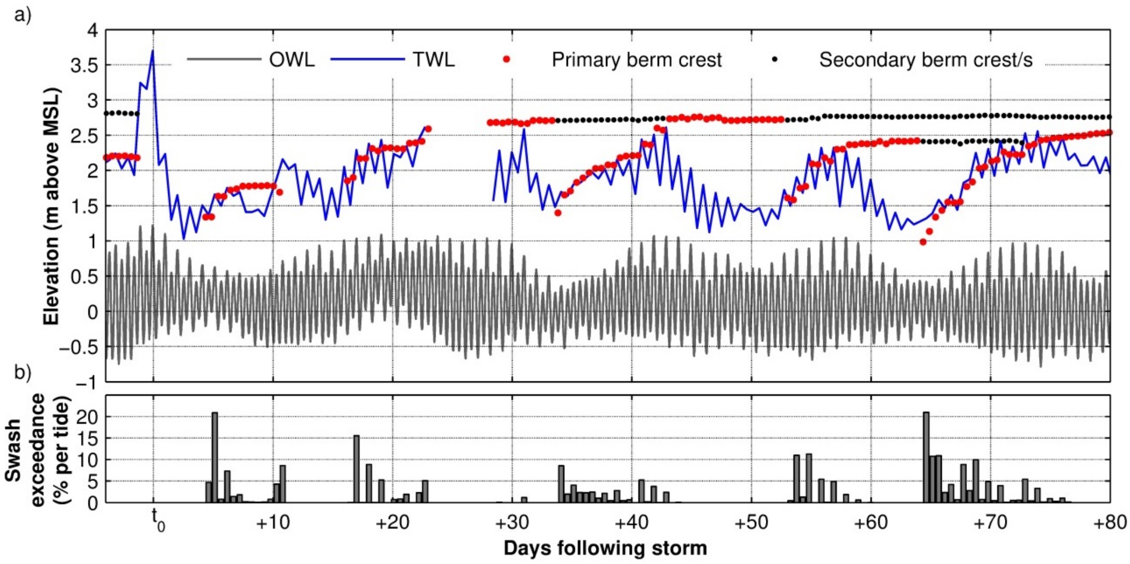

Figure 5.6: a) Elevation time series of ocean water levels (OWL), total water level (*TWL*), primary (most seaward) berm crest and secondary (landward, inactive) berm crests throughout the recovery period. Patterns of berm crest formation and vertical growth are noted with neap-spring variations in total water levels. b) The percentage of wave runup events exceeding the berm crest for each tidal cycle (approx. 12 h period) throughout recovery.

($R = 0.82$, $P<0.0001$) to the swash exceedance of the berm crest per tidal cycle (Figure 5.6b). The observed vertical growth of the berm crest then ceased during spring tides (e.g., days 42 to 43) at the maximum TWL. The TWL then decreased in elevation during spring to neap tides (e.g., days 43 to 50), stranding the berm crest and limiting swash deposition to the beachface. At the subsequent neap tide, this deposition was typically observed to form a new primary berm crest, seaward of the prior and now secondary berm crest; with this cycle reoccurring throughout the remainder of the recovery period.

5.3.3 Rates of subaerial volume change during recovery

Figure 5.7a shows the frequency distribution of the observed tide-by-tide rates of subaerial volume change throughout the entire 76-day recovery period. The distribution is found to be unimodal with a positive peak at 1 - 2 m^3/m/day and slightly negatively skewed. Considerable variability is revealed in these rates of subaerial volume change observed at tidal intervals, including the occurrence of gains (positive) and losses (negative) of sand on the order of several m^3/m/day, with magnitudes up to several orders larger than the observed and more gradual net rate of underlying recovery (approximately 0.7 m^3/m/day). This indicates that during beach recovery and predominantly mild wave conditions, significant fluctuations (positive and negative) in rates of subaerial beach volume change can take place at the timescale of individual tides.

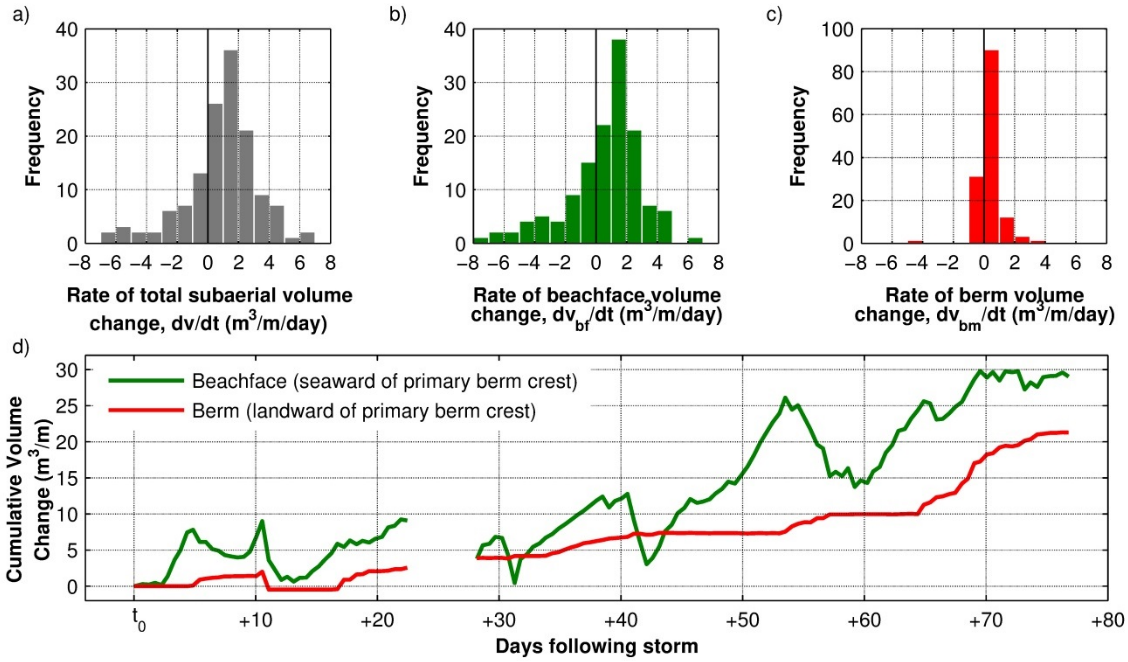

Figure 5.7: Histograms showing the distribution of tide-by-tide rates of volume change for regions of the a) total subaerial beach, b) beachface (seaward of the primary berm crest) and c) berm (landward of the primary berm crest). Note change in y-axis scaling d) Cumulative volume changes on the beachface and berm during post-storm recovery.

Figures 5.7b and 5.7c separate the respective distributions of beachface and berm volume changes during the same recovery period. The similarity of distributions in Figures 5.7a and 5.7b indicate that observed variability in measured rates of subaerial volume changes occurred predominantly on the beachface. In comparison, more uniform and gradual deposition (most frequently 0 - 1 m^3/m/day) was observed on the berm (Figure 5.7c). Figure 5.7d shows the cumulative volume changes for the beachface and berm over the recovery period. Berm deposition in Figure 5.7d occurred intermittently throughout the 76-day recovery period, when swash exceeded the berm crest. By the end of this recovery period, beachface and berm deposition accounted for 59% and 41%, respectively, of the volume returned to the subaerial beach.

These same observations are presented in Figure 5.8, this time showing the cross-shore location of berm crests (primary and secondary) and rates of subaerial erosion/deposition. Highly variable rates of volume change per tide were predominantly observed at the beachface (i.e., seaward of the primary berm crest). In contrast, intermittent deposition across the berm (landward of the primary crest) was more gradual, characteristic in this higher region of the subaerial profile. Also noted in Figure 5.8 are temporal patterns in subaerial volume changes across the beach profile. For example, between days 48 and 52 during neap tides, deposition (shown in green) was

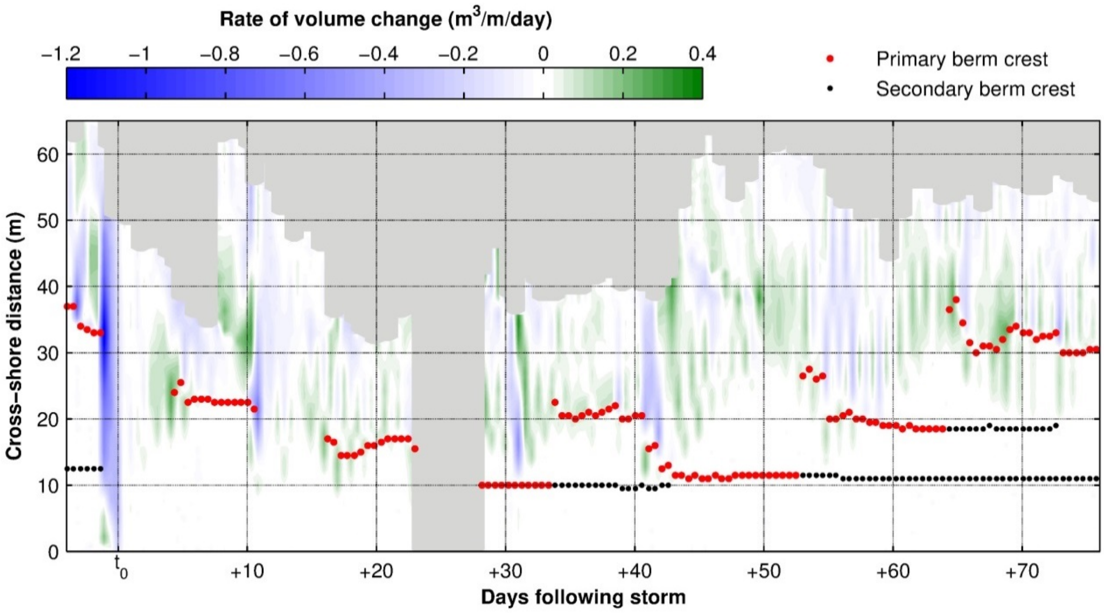

Figure 5.8: Rates of volume change (erosion and deposition) across the subaerial beach profile throughout the recovery period. The cross-shore positions of primary and secondary berm crests are also marked.

observed in the seaward (lower) regions of the profile, leading to the formation of a new neap berm. Between days 52 and 58 as the tide range increased towards springs, this deposition moved landward, concentrating in regions in the lee of the newly formed berm crest. This observation was seen to result in a landward migration of the berm crest in Figure 5.8, coinciding with its vertical growth up the beach profile (Figure 5.6a). On day 58, this deposition reached a maximum landward extent at the peak of the spring tide, establishing the cross-shore position and elevation of the berm crest.

5.3.4 Modes of profile variability during berm recovery

To begin to synthesize and characterise the results presented above, Figure 5.9 presents the observed rates of daily beachface volume change against the corresponding berm volume change for the entire 76-day recovery period. This figure reveals that the observations can be usefully separated into four main regions, corresponding to different behavioural modes of subaerial beach profile variability during berm recovery. To assist the interpretation of these four distinct modes, example phases when each of these modes was dominant during recovery are shown in Figure 5.9b.

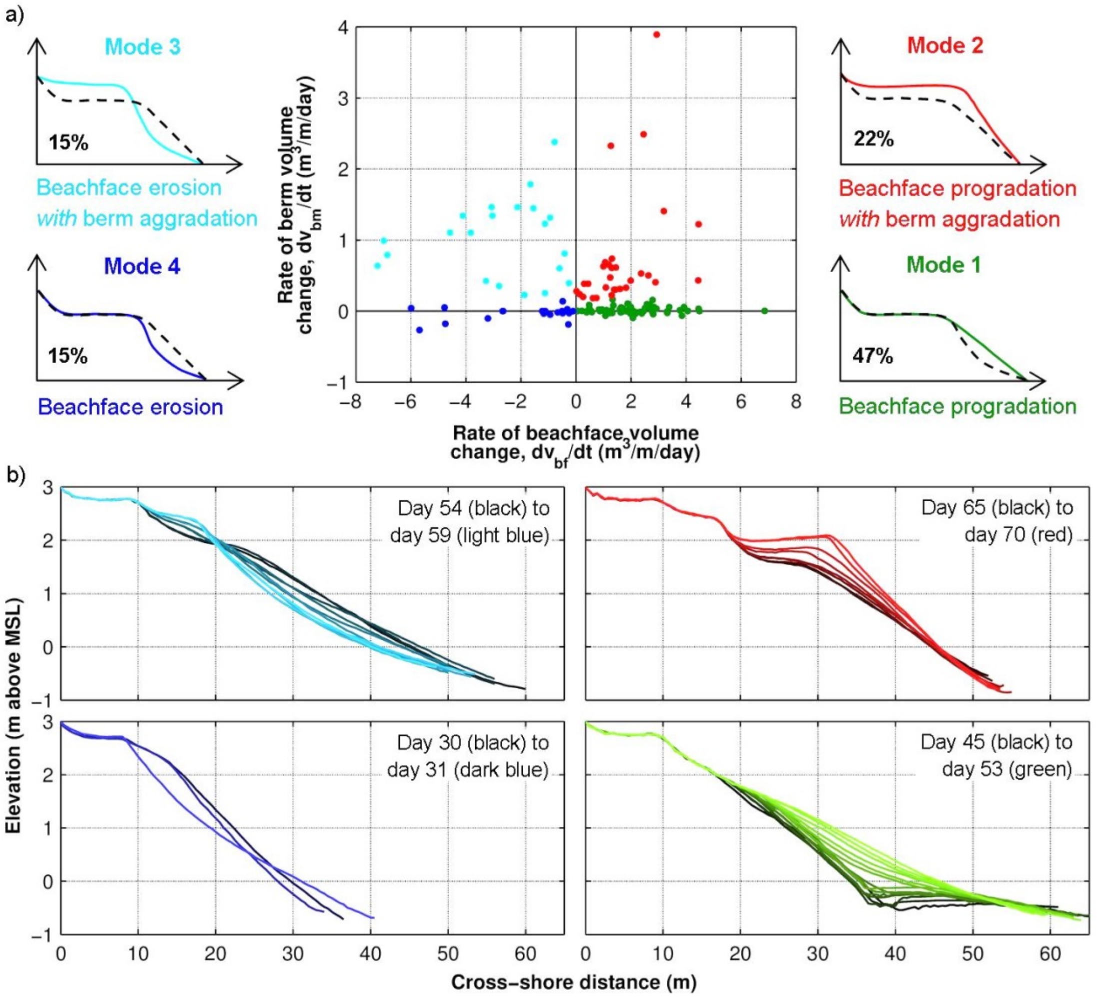

Figure 5.9: a) Classification of four principal modes of subaerial beach profile variability throughout berm recovery based on tide-by-tide Lidar measurements. Corresponding profile changes are illustrated and labelled with the dashed profile indicating initial conditions. Percentages of observations for each mode are also shown. b) Example phases during recovery showing profile development for each mode.

Mode 1) Beachface progradation

Beachface progradation (mode 1, shown in green in Figure 5.9) was the most frequently observed mode during the recovery period, accounting for nearly half (47%) of the observations. During this mode, sediment is transported from the inner surf zone to the lower beachface, causing a seaward growth of the beachface with no berm deposition. In some cases, this coincided with the welding of sandbars to the lower beachface, leading to rapid shoreline advancement (as shown in Figure 5.9b). Tide-by-tide rates of subaerial volume change during beachface progradation averaged 2.0 m^3/m/day (s.d. = 1.3 m^3/m/day) and reached up to 6.9 m^3/m/day. Beachface progradation often led to the formation of a new neap berm crest as seen during days 59 to 65 of recovery in Figure 5.10.

Mode 2) Beachface progradation with berm aggradation

The second most frequent (22% of observations) mode of profile change during recovery was beachface progradation with berm aggradation (mode 2, red in Figure 5.9). This mode involves the seaward growth of the upper beachface and vertical growth of the berm (Figure 5.9b), with sediment transport from the inner surf zone and lower beachface. Daily rates of subaerial volume change averaged 2.3 m^3/m/day (s.d. = 1.6 m^3/m/day). For mode 2, the deposition was observed higher up the beach profile than for mode 1 and led to the vertical growth of the berm crest with rates averaging 0.10 m/day (s.d. = 0.15 m/day). When mode 2 was observed to persist over several days, the beachface steepened about a nodal-point on the lower profile, as seen in Figure 5.10. In the final weeks of recovery from day 65 onwards (Figure 5.10), mode 2 was particularly prevalent. This led to a significant vertical growth by 1.5 m of a newly formed berm crest due to overwash deposition. During this aggradation of the berm, the intertidal zone gradually steepened by a factor of three, reinforcing higher wave runup and overwash deposition. This rapid steepening indicates an exhausting of intertidal sandbar welding capacity and reduction in sediment feed from the inner nearshore toward the completion of the post-storm recovery period.

Mode 3) Berm aggradation with beachface erosion

Observed slightly less frequently (15% of observations) throughout the total recovery period was berm aggradation coinciding with beachface erosion (mode 3, light blue in Figure 5.9). During mode 3, sediment is transported from the beachface and deposited on the berm and lower intertidal zone. Mode 3 was found to lead to beachface concavity (Figure 5.9b) and typically resulted in net offshore sediment transport from the subaerial beach, with rates averaging -1.8 m^3/m/day (s.d. = 2.3 m^3/m/day). Rapid vertical berm growth was also observed, averaging 0.29 m/day (s.d. = 0.18 m/day) and reaching up to 0.58 m/day. In Figure 5.9a, the growth of the berm was almost only observed with some degree of change to the beachface, whether progradation (mode 2) or erosion (mode 3). This is not surprising considering sediment must first be transported across the beachface prior to deposition on the berm and some degree of beachface deposition or erosion is likely in this active region of the profile.

Mode 4) Beachface erosion without berm aggradation

Beachface erosion without berm aggradation (mode 4, dark blue in Figure 5.9) was also observed (15% of observations). This involves the offshore transport of sediment from the subaerial beach to the inner surf zone, here observed at an average rate of -

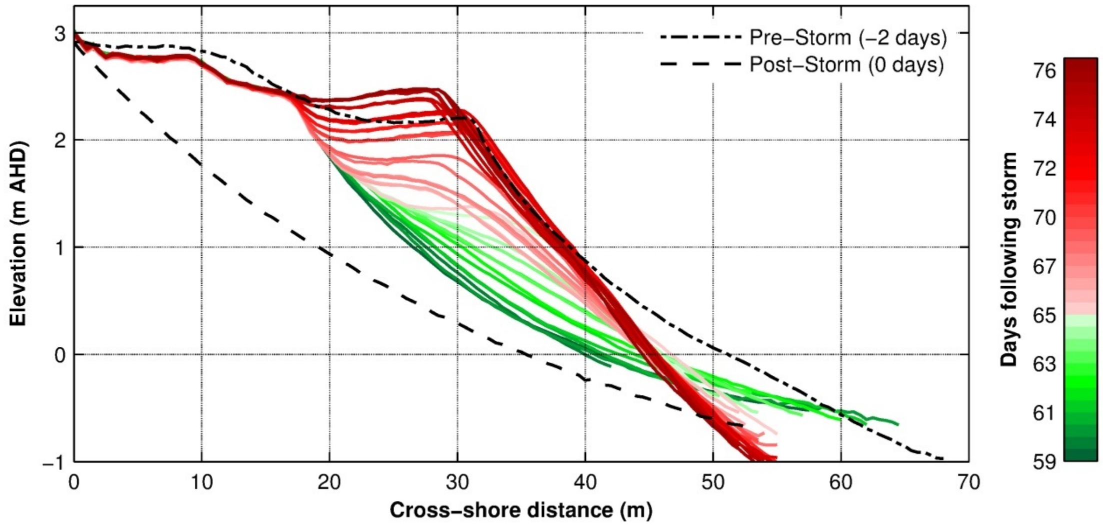

Figure 5.10: Tide-by-tide beach profile changes during the final 17 days of berm recovery. Beachface progradation (mode 1) is shown in green from day 59 to 65 leading to the formation of a neap berm. This is followed by significant berm aggradation (predominantly mode 2 with some mode 3) shown in red from day 65 to 76.

1.9 m^3/m/day (s.d. = 2.0 m^3/m/day).

Though not shown in Figure 5.9, an additional and less common mode of profile change was also observed, accounting for less than 1% of observations (day 11 only) during the recovery period. This corresponded to the removal of a neap-tide berm deposit, temporarily resetting morphology to prior post-storm conditions. Though infrequent, this mode led to rapid changes with an observed rate of subaerial volume change of -15 m^3/m/day; -10 m^3/m/day on the beachface and -4.6 m^3/m/day on the berm, respectively.

5.4 Discussion

Following the complete removal of the berm and ‘resetting’ of the beachface by a significant storm, the present findings provide detailed insight into the nature and characteristics of berm recovery, through the use of a fixed and continuous scanning Lidar to quantify at high resolutions the complete return of the subaerial profile to its pre-storm configuration. When observed at the timescale of each and every tide, a high degree of variability is revealed in rates of subaerial volume change throughout the observed 76-day recovery period (Figure 5.7a), including losses and gains on the order of several m^3/m/day, substantially larger in magnitude than the more gradual rate of net gain for the entire recovery period (here observed at 0.7 m^3/m/day). Importantly, this shows that during beach recovery following a storm (most often considered a period characterised by gradual accumulation of sand volume), in fact significant fluctuations (positive and negative) in rates of subaerial beach volume change can take place. These new data obtained at high temporal resolution show that erosion, as well as deposition, may occur on the timescale of individual tides during berm recovery, and that these rates can be several orders of magnitude larger than the observed and more gradual net rate (observed here to be approximately 0.7 m^3/m/day) of underlying recovery.

Similar results were observed in Chapter 4, highlighting fortnightly and weekly variability in rates of shoreline recovery, related to different sandbar and nearshore wave conditions. The new tide-by-tide observations presented in this chapter are also comparable to previous studies that have measured similar distributions of beachface/berm variability at sub-tidal (Russell et al., 2009) and swash-by-swash (Turner et al., 2008; Blenkinsopp et al., 2011) timescales, though for much shorter durations than the entire 76-day recovery period presented here. The variability of the subaerial beach is noted when observed at finer (sub-daily) temporal resolutions; constantly changing and being reshaped by swash activity. It is the integrated effect of this shorter-term variability characterised by rates of significant magnitude in both directions, which underlies the overall and much more gradual net recovery of the subaerial beach with time.

Figures 5.7b-c and 5.8 show that the majority of variability in rates of subaerial volume change occur at the beachface in the lower swash, with more gradual and intermittent growth on the berm in the upper swash zone. These results are consistent with detailed studies of swash zone sediment flux distributions (Baldock et al., 2006; Blenkinsopp et al., 2011), which show that the largest sediment fluxes are typically observed in the low to mid swash zone, leading to greater morphological variability. In the upper swash zone where the berm forms, sediment fluxes are generally smaller and favour the deposition of suspended sediment due to small/decelerating uprush velocities and low backwash velocities (Blenkinsopp et al., 2011). This effect is enhanced by the planar or slightly landward slope of the berm in the upper swash that with swash exceedance of the berm crest, acts as a region of infiltration and deposition with low backwash acceleration. In the present chapter, the intermittent growth of the berm was found to involve a repeated cycle of berm crest formation and vertical growth in conjunction with neap-spring tide variations in total water levels. Similar neap-spring tide patterns of berm crest formation and growth were also observed by Hine (1979) along a migrating barrier spit at Nauset Beach, United States.

5.4.1 Behavioural modes of berm recovery

Behavioural modes describing the recovery of berm morphology following removal by a storm have previously been reported by Dubois (1988). Their study identified two modes of beach recovery: beachface progradation (seaward) and berm aggradation (vertical) with upper beachface deposition, corresponding to modes 1 and 2 identified in the present study (Figure 5.9a). Dubois (1988) reported these two general modes of beachface and berm response to occur in sequential stages, where berm aggradation (vertical growth) was predominant in the initial months following a storm and later followed by beachface progradation (seaward growth) once swash no longer exceeded an established berm crest. Following a lagoon entrance opening, Weir et al. (2006) also noted similar modes of berm growth, particularly during spring (neap) tides when swash exceedance conditions were present (absent).

These new and detailed tide-by-tide observations of the entire recovery of a berm following removal by a significant storm, extends this prior work by distinguishing and characterising in greater detail the morphodynamics and related forcing of berm recovery. This includes the identification of four distinct modes of berm recovery including two modes of berm aggradation with differing beachface responses (modes 2 and 3) as well as the observation of beachface erosion without berm aggradation (mode 4) during recovery. Figure 5.11a shows the time series of the four behavioural modes identified in this study, overlayed on the return of subaerial volume throughout the entire 76-day recovery period examined here. The figure shows phases when certain modes are prevalent (e.g., mode 1 on day 45 - 53 and mode 2 on day 33 - 38), as well as phases of high tide-by-tide variability between modes (e.g., day 53 - 60).

An extensive range of nearshore wave, swash, ocean water level and morphological forcing parameters were explored for their ability to distinguish conditions associated with these different modes. Based on a decision tree analysis in Figure 5.11e, it was found that recovery modes were best differentiated based on the dimensionless fall velocity Ω (Figure 5.11b), swash exceedance of the berm crest (Figure 5.11c), and ocean water levels (Figure 5.11d). In Figure 5.11b, the value of $\bar{\Omega}$ (≈ 2.0) is defined as the long-term (12-year) site mean dimensionless fall velocity. The primary differentiator was dimensionless fall velocity Ω, with branches for mild ($\Omega < \bar{\Omega}$), moderate ($\Omega > \bar{\Omega}$ and non-storm conditions) and high (storm conditions where H_s was above the 5% exceedance level for a minimum duration of one tidal cycle. During these conditions Ω in excess of 4 was observed).

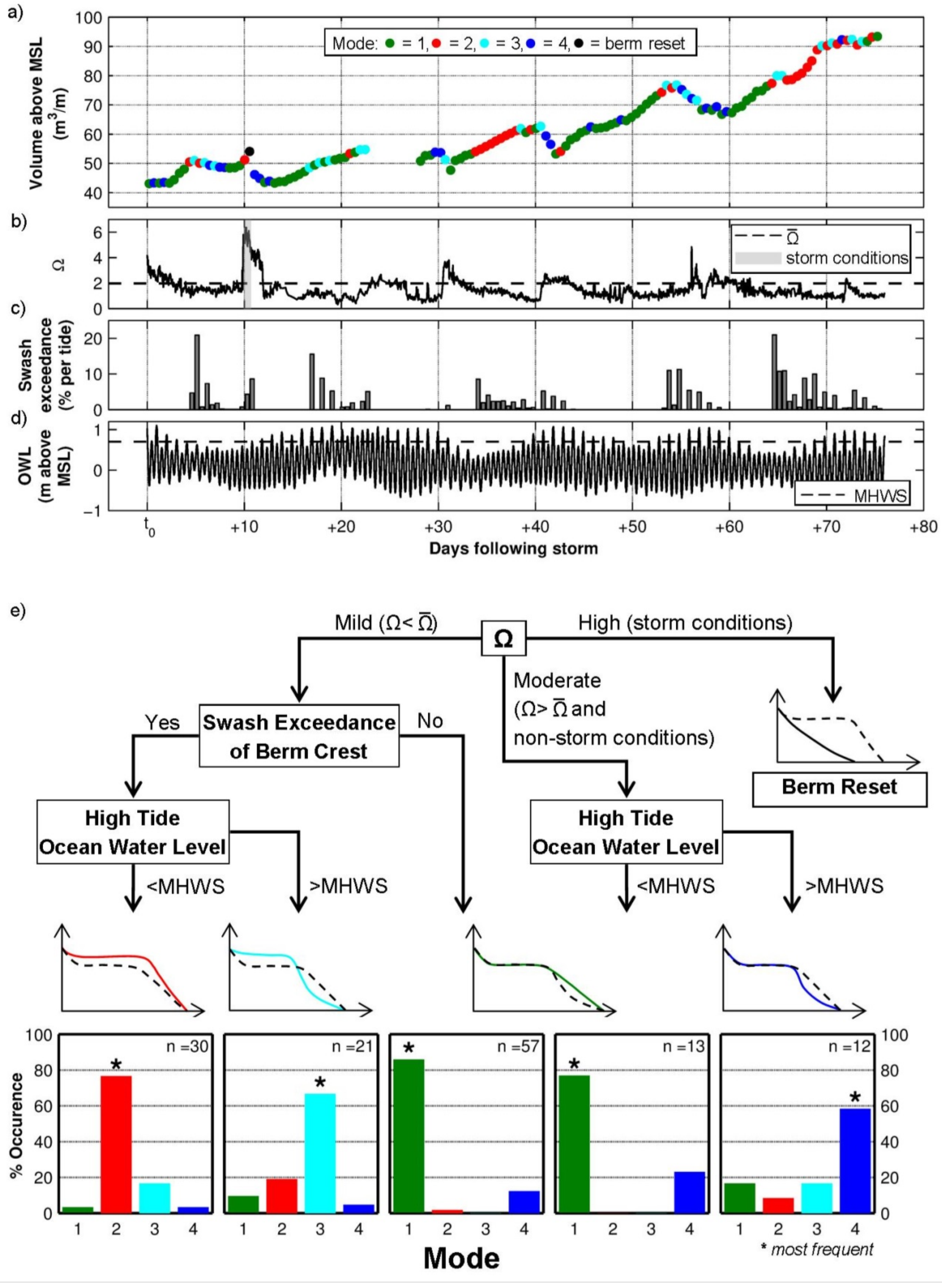

Figure 5.11: Time series throughout recovery of a) principal modes of berm recovery, b) nearshore Ω, c) swash exceedance of the berm crest per tidal cycle and d) ocean water levels. The decision tree in e) shows hydrodynamic conditions distinguishing the occurrence of each mode. $\bar{\Omega}$ refers to the 12-year site mean nearshore dimensionless fall velocity (≈ 2.0). Storm conditions refer to significant wave heights above the 5% exceedance level for a minimum duration of one tidal cycle (≈12h period), during which Ω was observed to exceed the value of 4. MHWS refers to mean high water springs (≈ 0.7 m above MSL).

Following down the branch of mild wave conditions ($\Omega < \bar{\Omega}$) in Figure 5.11e, the next defining condition was the presence/absence of swash exceedance of the berm crest. With no swash exceedance of the berm crest (Figure 5.11c) beachface progradation (mode 1) was most frequently observed (86%). Phases of several days of mode 1 and no swash exceedance are seen in Figures 5.11a and 5.11c, respectively. This mode of recovery typically occurred as the tide range declined from spring to neap (Figure 5.11d) resulting in the TWL generally not reaching the elevation of the berm crest (Figure 5.6a). Under these conditions, deposition in the upper swash zone was concentrated on the beachface, while surf/swash boundary processes acting lower on the beach profile likely enhanced suspended sediment transport from the inner surf zone (Blenkinsopp et al., 2011). Berm crest formation, often observed following mode 1 (as in Figure 5.10), may perhaps be initiated by reduced tidal shifting of swash zone processes across the beachface at neap tides, concentrating deposition at a constant elevation in the upper swash.

The left hand branches of the decision tree in Figure 5.11e show conditions of mild waves ($\Omega < \bar{\Omega}$) and swash exceedance of the berm crest, for which berm aggradation modes 2 and 3 were most frequently observed. In particular, during lower ocean water levels (OWL < MHWS) on the far left branch, 77% of observations were berm aggradation with beachface progradation (mode 2). In Figure 5.11a, phases of several days of mode 2 are observed (e.g., days 34 - 38, 65 - 69), coinciding with neap-spring tides and rising total water levels after new berm crest formation (Figure 5.11d). With these conditions, upper swash zone deposition was observed to move slightly up the beachface and onto the berm, while lower swash zone processes are seen to remove sediment from the lower beachface (Figure 4.11e). This also explains the observed steepening of the beachface about a null-point on the lower profile during this mode (Figure 5.10), also noted by Dubois (1988). In Figure 5.11a, the occurrence of mode 2 was observed to become more intermittent with the onset of spring tides (e.g., day 69 - 73), when occurring during the smaller semi-diurnal high tide.

On the left hand branch in Figure 5.11e with mild wave conditions ($\Omega < \bar{\Omega}$), swash exceedance of the berm crest and spring tide ocean water levels (OWL > MHWS), beachface erosion with berm aggradation (mode 3) was the predominant response observed (66% of observations). Interestingly, subaerial volume changes during this response indicated net offshore sediment transport, even with mild waves. This is perhaps due to more energetic lower swash zone processes shifting higher up the beachface with spring high tides, such that the majority of the beachface becomes a source of sediment. Some of this sediment is observed to be deposited on the berm via swash exceedance of the berm crest, however is predominantly transported offshore to the inner-surf zone. Reduced wave-breaking during larger high tides due to increased surf zone water depths may enhance this effect, increasing incident wave energy and sediment transport at the beachface (Guedes et al., 2011).

The middle branches of Figure 5.11e show the most prevalent modes with moderate wave conditions ($\Omega > \bar{\Omega}$ and *non-storm*) during recovery. In particular, with moderate waves and lower ocean water levels (OWL< MHWS), beachface progradation (mode 1) was again observed to be the predominant response (77% of observations). However, with moderate waves and higher ocean water levels (OWL > MHWS), beachface erosion without berm aggradation (mode 4) was most frequently observed (58% of observations). Similar to conditions with mild waves and swash exceedance, ocean water levels are again observed to be a key factor differentiating modes associated with beachface progradation and erosion at the timescale of individual tides. These results suggest the importance of tidal variations in ocean water levels shifting inner surf zone and swash zone processes to drive variability in tide-by-tide rates of volume change and profile configuration at the beachface throughout recovery.

The far right branch of the tree in Figure 5.11e indicates the temporary resetting of the berm when intermediate storm wave conditions occurred during the recovery period on day 11. The occurrence of intermediate storm erosion during recovery is a common observation on high-energy coastlines (e.g., Corbella and Stretch, 2012; Scott et al., 2016; Phillips et al., 2017). Though not observed in the present recovery period, it is noted that minor storms can also result in the formation of a higher and narrower storm berm in the beach profile (Psuty, 1965; Morton et al., 1994). While intermediate storms may lead to temporary erosion of the subaerial beach during recovery, further research is warranted into the effect of higher wave energy on the subaqueous beach during recovery, potentially transporting storm deposits in deeper waters onshore (Scott et al., 2016).

5.5 Conclusion

Tide-by-tide swash and subaerial beach profile measurements obtained from a continuously scanning Lidar at Narrabeen-Collaroy Beach, Australia, were used to analyse beachface and berm morphodynamics throughout a complete (2.5 month) recovery of berm morphology following removal by a significant storm event. Tide-by-tide rates of subaerial volume change during berm recovery were most frequently between 1 - 2 m^3/m/day, including losses and gains on the order of several m^3/m/day, substantially larger in magnitude than the more gradual rate of net gain (0.7 m^3/m/day) observed for the entire recovery period.

Patterns of berm crest formation and vertical growth were observed to be primarily governed by the neap-spring tide variations in total water levels. In particular, rates of volume change were most variable on the beachface, but were more gradual and intermittent on the berm. Beachface and berm volume changes were used to classify four principal behavioural modes of subaerial profile variability during berm recovery; beachface progradation (mode 1), beachface progradation with berm aggradation (mode 2), beachface erosion with berm aggradation (mode 3) and beachface erosion without berm aggradation (mode 4). Based on decision tree analysis, modes were differentiated according to nearshore dimensionless fall velocity, swash exceedance of the berm crest and ocean water levels. The findings provide new behavioural and parametric insight into the tide-by-tide rebuilding of the subaerial beach profile by swash activity throughout berm recovery.

Following this same significant storm event (April 2015), the subsequent Chapter 6 investigates alongshore variability in subaerial volume recovery along the broader embayed coastline of the Sydney region, including 5 additional profiles in the Narrabeen-Collaroy embayment as well as 13 profiles located at three other nearby embayments.

Chapter 6

Alongshore variability in subaerial volume recovery: within and between embayments

Content of this chapter is in preparation for publication in:

Phillips, M. S., Harley, M. D., Splinter, K. D., and Turner, I. L., *in prep*. Alongshore variability in post-storm beach recovery at spatial scales within and between embayments. Marine Geology.

Chapter overview: In addition to characterising the temporal variability of the wave-driven recovery of the subaerial beach presented in Chapters 4 and 5, the degree to which, and by what physical means, this varies spatially from one alongshore location to another is now examined. Following a significant storm event, this chapter addresses alongshore variability in the recovery of subaerial sand volume along an embayed coast. The routine monitoring of beach profiles spanning four closely-situated embayments is used to evaluate subaerial volume recovery at distinct alongshore scales, both within and between coastal embayments.

6.1 Introduction

Storms can result in widespread regional erosion of sandy beaches, creating hazards to local settlements and infrastructure along several hundred kilometres of exposed coastline. As these events reoccur with time, assessing their long-term impact requires an understanding of how beaches recover following storms across a broad array of coastal environments (e.g., Frazer et al., 2009; Anderson et al., 2010; Phillips et al., 2017). Appropriate coastal management actions are undertaken where a beach is unable to sufficiently recover from storm erosion to serve the needs (present and future) of the coastal community it supports (e.g., Dean, 2002).

In Chapters 4 and 5 of this thesis, detailed analysis was presented addressing the temporal variability of beach recovery processes within a specific region of the Narrabeen-Collaroy embayment (Figure 3.2). The findings provided new insight into characterising variability and identifying key driving parameters involved in the temporal progression of beach recovery. It is of interest to gain a broader spatial understanding of how beach recovery varies alongshore both within and between nearby embayments.

Process-based models have been applied to predict storm erosion at a range of coastal locations around the world (e.g., Roelvink et al., 2009; Bolle et al., 2011; Harley et al., 2011a) including along the Sydney coastline (e.g., Callaghan et al., 2013; Simmons et al., 2017). In contrast, the extent to which, and by what physical processes beach recovery varies from one alongshore location to another is yet to be well understood (Weymer et al., 2015). A study by Morton et al. (1994) monitored beach profiles along a 30 km stretch of barrier island coastline in Texas, United States, following Hurricane Alicia. Alongshore variability in beach recovery was observed and characterised by four contrasting responses. Recovery responses were described relative to pre-storm conditions and included: no recovery with continued erosion; partial recovery; complete recovery; and excess recovery (illustrated in Figure 2.2). Similar studies of alongshore variability in beach recovery have also been noted along other barrier island coastlines and straight, open coastlines (e.g., Birkemeier, 1979; Zhang et al., 2002; Splinter et al., 2011b; Corbella and Stretch, 2012), and to a lesser extent along embayed coastlines (Yu et al., 2013; Scott et al., 2016).

Morphological indicators commonly used to compare beach recovery between different locations (synthesised in Chapter 2) have included subaerial (above MSL) sediment volume (e.g., Morton et al., 1994), shoreline position (e.g., List et al., 2006) and dune height (e.g., Houser et al., 2015). Durations and net rates of the recovery of these indicators to pre-storm conditions have been used to evaluate and identify alongshore variability in beach recovery (e.g., Morton et al., 1994; List et al., 2006; Corbella and Stretch, 2012). In particular, Corbella and Stretch (2012) examined durations and net rates of subaerial volume recovery to a pre-storm value using beach profile measurements along approximately 100 km of straight, open coastline at Durban, South Africa. The study observed recovery durations in the range of 0.5 - 6.5 years, with net rates varying between 0.1 - 1.5 m^3/m/day. With profiles grouped and averaged into broader alongshore divisions based on their location relative to estuary entrances, the observed variability in recovery duration (1.8 - 2.8 years) and net rates (0.1 - 0.3 m^3/m/day) was found to be less. On an embayed coastline in southwest England, Scott et al. (2016) also quantified spatial variability in subaerial volume recovery. Recovery durations were on the order of several years at some locations, while at others minimal recovery was observed. This alongshore variability was noted within embayments as well as at broader scales between embayments. Further field investigation quantifying recovery durations and in particular net rates along embayed coastlines is warranted to further elucidate the extent to which beach recovery can be expected to differ within and between embayments.

Factors driving variability in recovery from one location to another are often attributed visually during field observations. On straight, open coastlines these observations have suggested the importance of local sediment supply during recovery and the related effects of numerous coastal features including rock outcrops, coastal structures, rip currents, estuary entrances, offshore storm deposits and dunes (e.g., Everts and Czerniak, 1978; List et al., 2006; Maspataud et al., 2009; Corbella and Stretch, 2012). Some studies have also noted the influence of alongshore patterns in storm overwash deposition (e.g., Houser et al., 2015; Weymer et al., 2015; Scott et al., 2016). Yu et al.

(2013) also suggested exposure to nearshore wave energy as a factor distinguishing minimal and rapid embayment recovery responses in southern China. Using nearshore wave and bathymetry measurements at an embayed coastline, Scott et al. (2016) found that sufficient nearshore wave forcing during recovery was required for the onshore sediment transport of storm deposits in deeper waters and to return alongshore storm deposition resulting in altered beach rotation.

Addressing research objective 3 of this thesis (Section 1.3), this chapter evaluates alongshore variability in subaerial (above MSL) volume recovery within and between embayed sandy beaches following a significant storm erosion event. To do so, the chapter examines the recovery at 19 beach profiles (18 RTK-GPS measured and 1 Lidar measured), located along four closely-situated embayments within a 15 km stretch of embayed coastline. Analysis is given to evaluate the extent to which subaerial volume recovery (in terms of recovery durations and net rates) following a significant storm event varies alongshore both within and between nearby embayments. The effect of alongshore variability in net rates of subaerial volume recovery on the shoreline orientation is examined. Furthermore, likely factors driving the observed alongshore variability in net rates of subaerial volume recovery are explored. The methodology of this chapter is outlined in Section 6.2, results are presented in Section 6.3 and a discussion of results is provided in Section 6.4. The conclusions of this chapter are summarised in Section 6.5.

6.2 Methodology

6.2.1 Subaerial beach profile and nearshore bathymetry data

From December 2013 to January 2017 (37 months in total) subaerial beach profile monitoring was undertaken at four sandy beach embayments situated between Broken Bay and Port Jackson (Sydney Harbour) in the Sydney metropolitan region located on the SE Australian coastline (Figure 3.2). These study embayments were Bilgola Beach, Mona Vale-Warriewood Beach, Narrabeen-Collaroy Beach, and Long Reef-Dee Why Beach. Detailed site descriptions of each of the four study embayments were previously provided in Section 3.2. To aid in the discussion of results, the embayments listed above are hereafter referred to as *Bilgola*, *Mona-Vale*, *Narrabeen* and *Dee Why* respectively.

In addition to the Lidar profile at Narrabeen that was previously described in Chapter 5, an additional 18 beach profiles were regularly surveyed within the four study embayments, on a weekly to bi-weekly basis, as well as a daily basis immediately pre- and post-individual storm events. Beach profiles were measured using RTK-GPS (vertical accuracy ≈ ± 0.03 m) with a cross-shore resolution of 0.5 m. Surveys were conducted at low tide with measurements obtained along shore-normal transects extending from the foredune to a safe wading depth on the lower beachface or inner surf zone (typically between 0.5 m to 1 m below MSL). RTK-GPS profile measurements were supplemented on a fortnightly basis with on-site photographs. Alongshore spacing of beach profiles shown in Table 6.1, varied between 100 - 900 m. This depended on the embayment length, the location of historical profiles (in the case of Narrabeen), alongshore variability in coastal morphology (particularly around lagoon entrances and offshore reefs) and also shoreline orientation. The total number of surveys undertaken each year at the four embayments are presented in Table 6.1. The time series of alongshore-averaged subaerial volume at each of the four study embayments over the entire length of the survey program is shown in Figure 6.1.

Table 6.1: RTK-GPS beach profile monitoring 2014 - 2016

Location	No. profiles surveyed	Profile spacing (m)	Number of survey dates 2014	2015	2016	Total
Bilgola	3	100 - 150	59	45	32	136
Mona Vale	5	100 - 200	55	44	30	129
Narrabeen	5	410 - 900	69	47	33	149
Dee Why	5	160 - 480	54	43	29	126

Consistent with the previous Chapter 5, the present chapter focuses on a subset of this profile dataset shown in Figure 6.1 that captured the recovery of the four embayments following a significant East Coast Low (ECL) event that occurred on the 20th - 22nd April 2015 (described in Section 5.2.3). Whereas Chapter 5 focused on a shorter 76-day post-storm recovery period specific to the Lidar monitoring profile, the present chapter analyses recovery over an extended 13-month (~400 days) post-storm study period (Figure 6.1) in order to capture the full extent of subaerial volume recovery across all study transects, up until the start of June 2016 when another significant ECL impacted the study region (Harley et al., 2017). Pre-storm profile measurements were undertaken 6 days prior to the April 2015 storm event. Mid-storm measurements were conducted on 21st April and post-storm measurements were undertaken on 22nd April. Over the following 13-month post-storm study period, 43 surveys of all profiles were

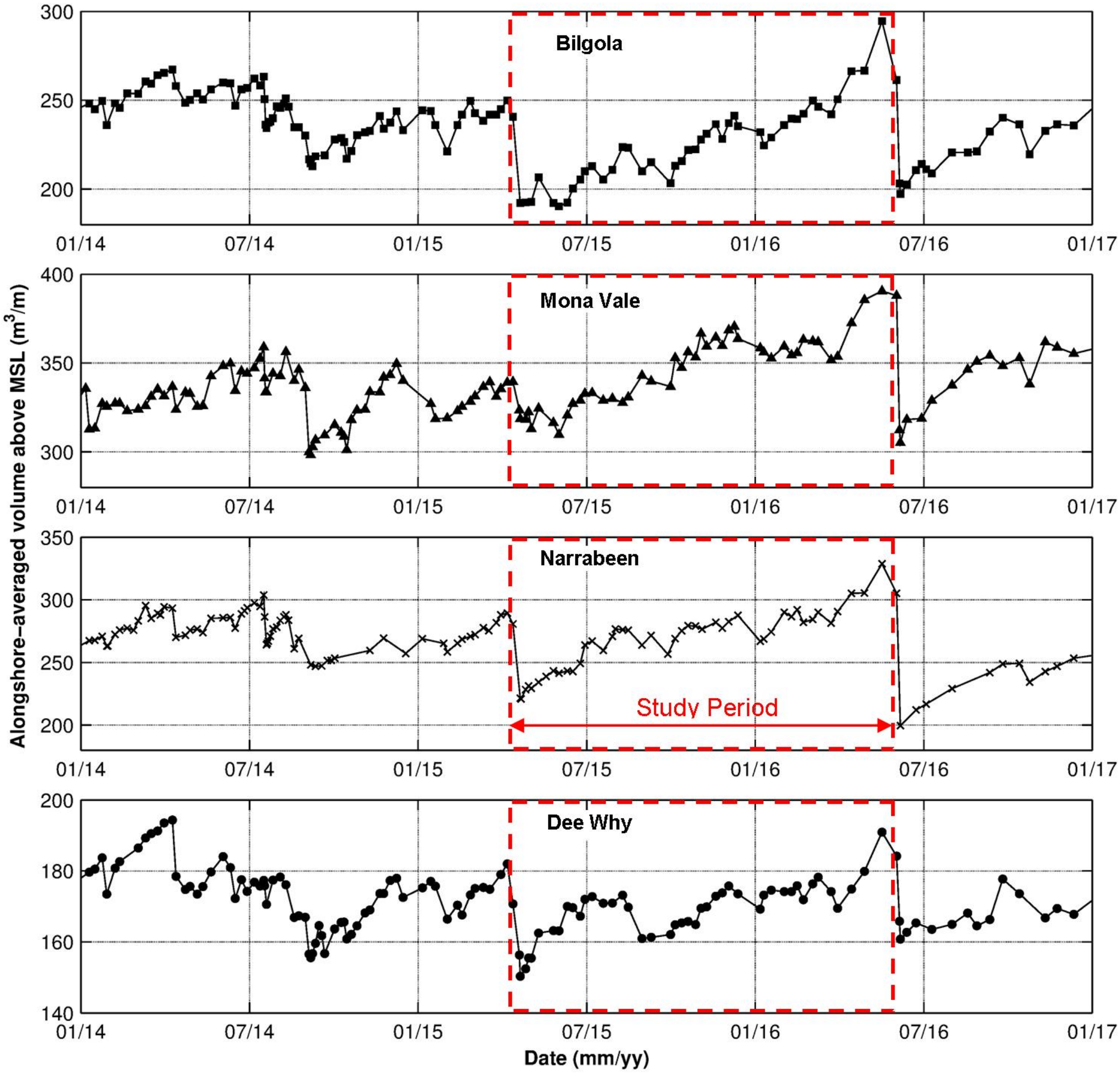

Figure 6.1: Time series of alongshore-averaged subaerial volume for each embayment over the entire beach profile monitoring dataset. Subset recovery period analysed in the present chapter is shown in red following a significant East Coast Low on 20th - 22nd April 2015.

completed at Dee Why, 44 at Bilgola and Mona Vale, and 45 at Narrabeen. Profile measurements at each low tide during the recovery period (approx. 740 low tide profile measurements in total) were also obtained by the fixed Lidar located within the southern portion of Narrabeen, noted as PFLD in Figure 3.2.

To supplement interpretation of subaerial volume and orientation measures during recovery, single-beam jet-ski mounted bathymetry surveys conducted by the NSW Office of Environment and Heritage (OEH) are also presented in this chapter. Pre-storm bathymetry surveys at all sites were obtained on 6th/7th August 2014 (i.e., approximately 8 months prior to the storm). Three bathymetry surveys during the post-storm study period (29th April 2015, 30th/31st July 2015 and 2nd June 2016) were collected at Bilgola, Mona Vale and Narrabeen, and two (7th May 2015, 31st July 2015) at Dee Why. Each bathymetry survey was combined with concurrent topographic profile measurements to provide a complete subaerial-subaqueous transect. The vertical accuracy of bathymetry surveys conducted using this technique is estimated to be on the order of 0.1 m with additional variations due to seawater temperature (MacMahan, 2001; Ruggiero et al., 2005).

6.2.2 Subaerial volume recovery and beach orientation

Analysis of beach recovery in this chapter focuses on the recovery of sediment volume to the subaerial beach. Following Chapter 5, subaerial volume per metre alongshore (m^3/m) was calculated at each of the 19 study profiles, corresponding to the integrated profile area above the mean sea level (MSL) contour and seaward of a fixed cross-shore origin. Complete recovery of subaerial volume was defined as the return of pre-storm subaerial volume, as is common amongst previous studies in the literature discussed in Sections 2.2.1 and 2.3.1. Subaerial volume was expressed relative to pre-storm conditions at each profile location. Illustrated in Figure 6.2 and similar to Corbella and Stretch (2012), the recovery duration (days) as well as a net recovery rate ($m^3/m/day$) for subaerial volume to return to a pre-storm value were calculated as:

$$\boldsymbol{Recovery\ Duration} = Date_{Recovered} - Date_{PostStorm} \quad (6.1)$$

$$\boldsymbol{Net\ Recovery\ Rate} = \frac{Volume_{Recovered} - Volume_{PostStorm}}{Recovery\ Duration} \quad (6.2)$$

Where subaerial volume did not return to a pre-storm value prior to June 2016, the recovery duration was noted as incomplete and the net recovery rate was calculated based on the volume recovered by 2nd June 2016.

In order to compare recovery durations and rates between embayments, an indicative alongshore-averaged volume (m^3/m) was also calculated for each embayment and is shown in Figure 6.1. This was calculated by averaging subaerial volumes for all profiles within each of the four embayments. At Dee Why, profile DW5 was not included due to its relatively close proximity to profile DW4 (Figure 3.2). At Mona Vale, profile measurements were concentrated in the northern region of the embayment. Here the most southern profile (MV5) was adopted as a single representative profile for the embayment, as it was located furthest away from local effects of rocky reef outcrops and orientated most similar to that of the broader embayment. Recovery duration (days) and net recovery rates ($m^3/m/day$) were also recorded and contrasted between alongshore-averaged subaerial volumes for each embayment.

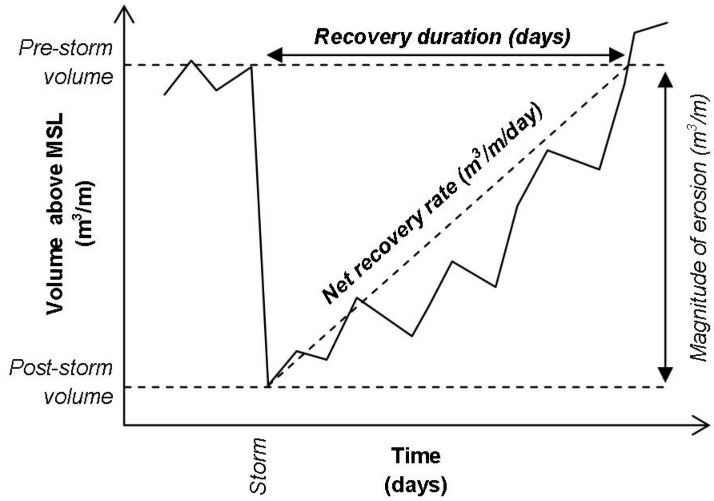

Figure 6.2: Illustration depicting storm and recovery time series of subaerial volume. Recovery duration and net recovery rate are indicated.

In addition to subaerial volume, changes during recovery in the planform rotation of each embayment (excluding Mona Vale due to limited embayment coverage) were observed by calculating beach orientation. Beach orientation (degrees) was calculated for each embayment following a similar approach to that of Ojeda and Guillén (2008). First, the cross-shore position of the MSL contour was determined and the time-averaged position for the given profile location was removed. Second, at each survey date, a linear-regression fit was applied to the demeaned cross-shore positions of the shoreline from all transects along the embayment with their subsequent positions alongshore. Finally, the beach orientation, *BO* (degrees), was taken as the angle formed by the linear-regression fit. This was expressed relative to a pre-storm orientation, positive (negative) beach orientations representing a more clockwise (anti-clockwise) rotation of the beach relative to pre-storm conditions. Additionally, the rotation magnitude at embayment extremities L_{BO} (m), was calculated as

$$L_{BO} = Embayment\ length\ \times tan(BO) \qquad (6.3)$$

This was also expressed relative to pre-storm conditions with positive (negative) values representing a wider (narrower) northern than southern extremity.

6.2.3 Wave conditions: April 2015 storm and post-storm recovery

Hourly deepwater significant wave data H_s, T_p and θ, were acquired from the Sydney waverider buoy and transformed using a MIKE21 spectral wave model to the -10 m depth contour in the nearshore directly offshore at each of the 19 measured profile

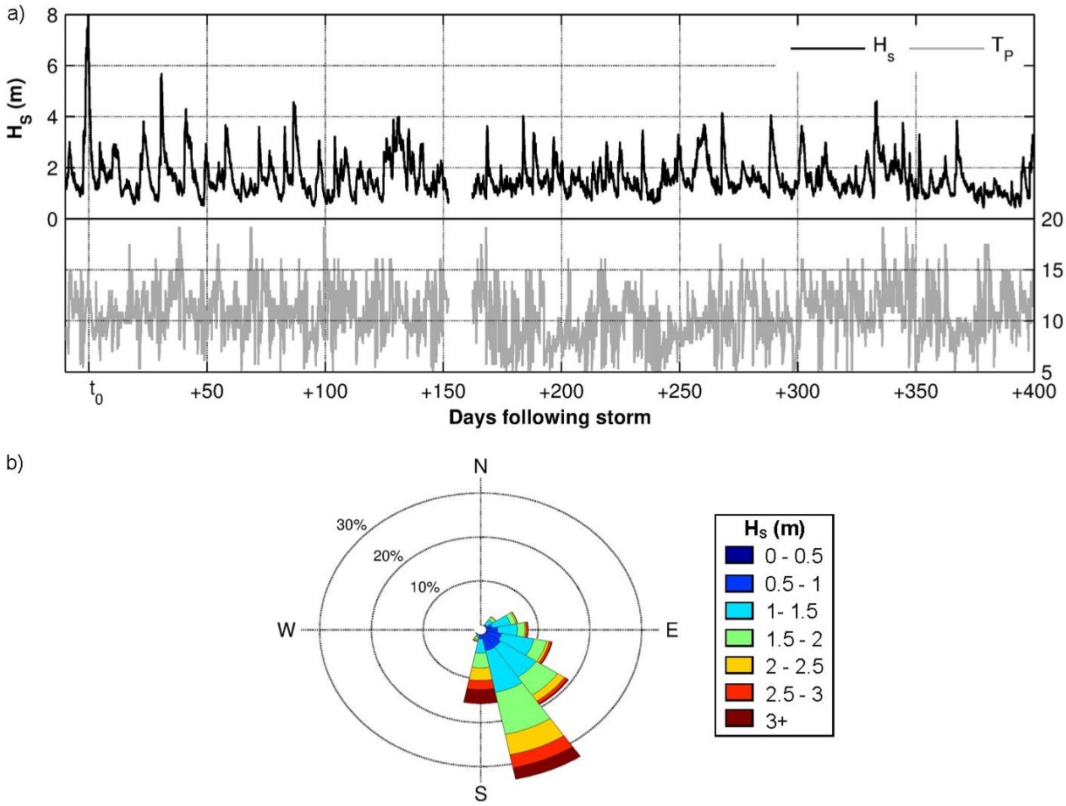

Figure 6.3: a) Deepwater wave time series for the April 2015 storm and subsequent 400-day post-storm study period to June 2016. b) Deepwater wave rose showing predominant wave direction and magnitudes during the 400-day post-storm study period.

locations, as was previously described in Section 3.2.

In Figure 6.3a, deepwater H_s can be seen to have peaked at 8.1 m during the storm, which approached the coast from an average SSE (161 °TN) direction. At the -10 m depth contour, nearshore H_s peaked between 5 - 6 m at more exposed (i.e., southerly orientated) locations including Bilgola and Mona Vale, as well as the northern ends of Narrabeen and Dee Why. The most sheltered location during the storm was the southern end of Narrabeen where nearshore H_s peaked at 3.4 m.

Deepwater wave conditions are shown in Figure 6.3a for the 400-day post-storm study period following the April 2015 storm extending to June 2016. During this period, deepwater H_s averaged 1.6 m with 75% of observations less than 2 m and 95% less than 3 m. Higher wave events accounting for the remaining 5% of the time were all notably smaller in magnitude than the April 2015 storm. The wave rose in Figure 6.3b shows the distribution of deepwater H_s and wave direction during this recovery period. Typical of this region, modal wave direction, accounting for 32% of observations was from the SSE, with 20% from SE, 15% S, 12% ESE and 8% E. Milder waves (H_s < 2 m), were predominantly from a more south-easterly direction (SSE to ESE) in comparison to larger wave events (H_s > 2 m) predominantly from a more southerly direction (S to SSE). At the -10 m depth contour, average H_s during this post-storm study period followed similar spatial patterns and magnitudes to longer-term means shown in Table 3.1, varying from 0.74 m at the sheltered southern end of Narrabeen to 1.3 m at the more exposed northern end of Dee Why.

6.3 Results

6.3.1 April 2015 storm erosion

Subaerial beach volume change at each of the 19 profile locations as a result of the April 2015 storm is shown in Figure 6.4, determined from immediately pre- and post-storm RTK-GPS profile surveys (for individual profile locations, refer to Figure 3.2). The maximum erosion observed was 82 m^3/m at profile PF6, Narrabeen. Four other profiles in the Narrabeen embayment, including PF8 at the more sheltered southern end, all eroded more than 50 m^3/m. Similar erosion also occurred at the Bilgola profiles in the range of 40 m^3/m (profile BG1) to 61 m^3/m (BG3). In contrast, erosion between 5 m^3/m (DW1) and 38 m^3/m (DW4) was observed at Dee Why. Interestingly, the more exposed locations of PF1 at Narrabeen, as well as DW1 at Dee Why, experienced the least erosion in their respective embayments. At Mona Vale, erosion was greatest (up to 21 m^3/m) on the straighter, more open section of the embayment at MV5. However, profiles in the lee of reefs fringing the Basin at Mona Vale varied in response to the storm and included minor erosion of 10 m^3/m (MV3), minimal volume change (< 1 m^3/m, MV2 and MV4) and minor accretion (2 m^3/m, MV1).

Alongshore-averaged subaerial volume changes for each embayment during the storm are presented in Table 6.2. The Narrabeen embayment was the most severely eroded, with an average 59 m^3/m of subaerial volume loss across all the surveyed profiles (approximately 3 times as much as Mona Vale and Dee Why, and 1.2 times as much as Bilgola). At most profile locations, the majority of the observed subaerial erosion occurred in the lower region of the profile between 0 and 3 m above MSL, with minimal dune erosion in the upper subaerial profile. Visual observations of berm erosion were also clearly evident in the on-site photographs from pre- and post-storm surveys shown in Appendix C.

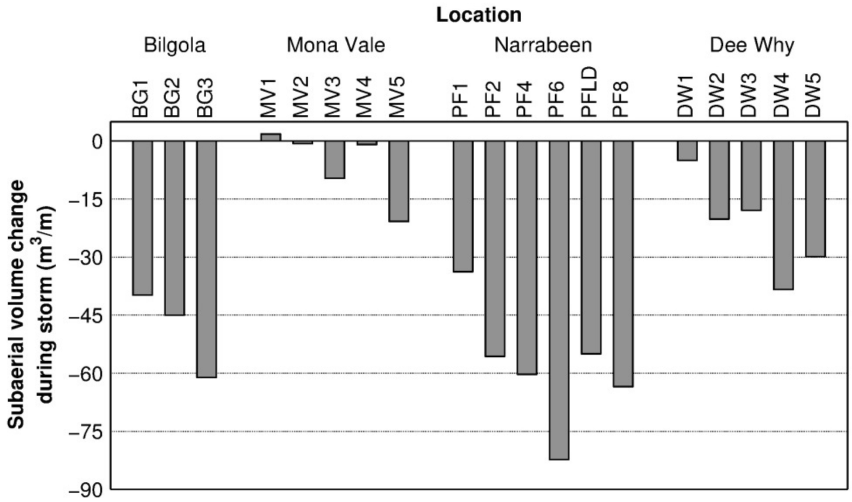

Figure 6.4: Magnitudes of subaerial volume erosion at beach profile locations during the storm on 20th - 22nd April 2015

Table 6.2: Alongshore-averaged subaerial volume erosion for each embayment during the storm on 20th - 22nd April 2015

Embayment	Bilgola	Mona Vale	Narrabeen	Dee Why
Alongshore-averaged subaerial volume change during storm (m^3/m)	- 49	- 21	- 59	- 20

6.3.2 Comparison of recovery durations and net rates within embayments

Figure 6.5 shows the recovery time series of subaerial volume at each profile location following the April 2015 storm event. The corresponding recovery duration and net recovery rate for each location is shown in Figure 6.6. A broad range of recovery rates were observed across the 19 profile locations. These included rapid recovery within a matter of days to weeks following the storm (e.g., Narrabeen PF1) with net rates in excess of 1 m^3/m/day. In contrast, more gradual recovery was also observed with net rates as low as 0.1 m^3/m/day and at some locations only partial recovery to pre-storm conditions over the 400-day post-storm study period was observed (e.g., Narrabeen PF6 and PF8). Gradual net recovery rates between 0.1 - 0.3 m^3/m/day were most common, accounting for 9 of the total 19 profile locations (BG1-3, MV3, MV5, PF6, PF8 and DW4-5). Moderate rates between 0.3 - 1 m^3/m/day was observed at 5 profiles (PF2, PF4, PFLD and DW2-3) and rapid rates in excess of 1 m^3/m/day at 2 profiles (PF1 and DW1), while 3 profiles with insignificant storm erosion (MV1, MV2 and MV4) were excluded from the recovery analysis. The overall median rate across all profile locations was 0.24 m^3/m/day.

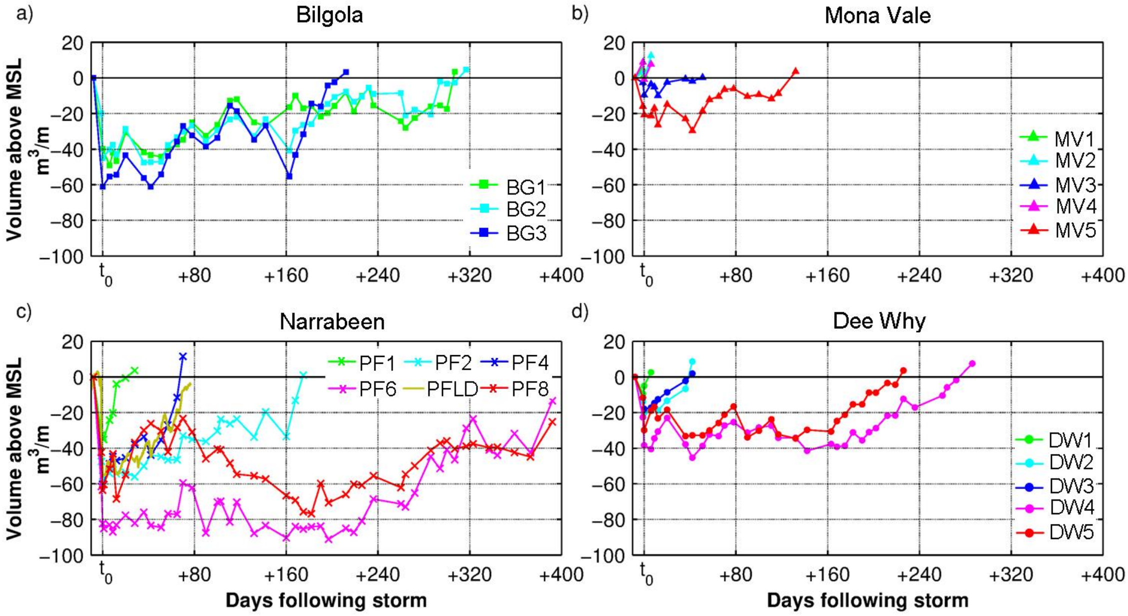

Figure 6.5: Recovery time series of subaerial volume following the April 2015 storm event for profile locations at a) Bilgola, b) Mona Vale, c) Narrabeen and d) Dee Why. Subaerial volumes are shown relative to pre-storm values and t_0 is the date of survey immediately post-storm (22[nd] April 2015).

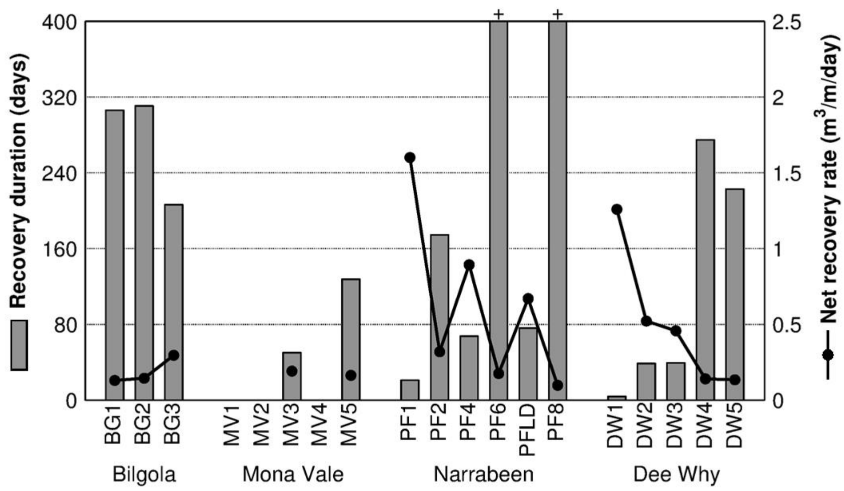

Figure 6.6: Recovery durations and net recovery rates for profile locations. A relatively high degree of alongshore variability in recovery is noted in the Narrabeen and Dee Why embayments.

The extent to which subaerial volume recovery varied alongshore within each of the embayments is seen in Figures 6.5 and 6.6. This was most pronounced within the Narrabeen embayment, with alongshore variability in subaerial volume recovery evident from north to south, as well as between adjacent profiles. At the northern end of Narrabeen, PF1 recovered rapidly to pre-storm conditions within 21 days at a net rate of 1.6 m^3/m/day. The net recovery rate at this location was the fastest across all 19 profile locations observed in this study. In contrast, at the southern end of the Narrabeen embayment (PF8), the net recovery rate of 0.10 m^3/m/day was the slowest across all profiles and approximately 16 times slower than PF1. By June 2016, the more northern profiles at Narrabeen (PF1-4) had accreted 55 - 126 m^3/m beyond pre-storm conditions, while PF6 and PF8 had only partially (80% and 60%, respectively) recovered their pre-storm volumes. Recovery at Narrabeen was also observed to vary significantly between neighbouring profiles as seen in Figure 6.6. PF2 recovered at a net rate approximately 5 times slower than neighbouring PF1 (~ 400 m north) and 3 times slower than PF4 (~ 900 m south). Similarly, PF6 recovered at rate of 0.18 m^3/m/day, approximately 4 times slower than the fixed Lidar profile (PFLD) located ~300 m further south.

Notable alongshore variability in recovery was also observed within the Dee Why embayment as shown in Figures 6.5 and 6.6. A distinct north to south trend discernible in the observed durations and rates of recovery that were observed at this embayment. The least eroded profile (DW1) situated at the northern end of the embayment recovered rapidly within 4 days at a rate of 1.3 m^3/m/day. In the middle of the Dee Why embayment, DW2 and DW3 recovered in 39 days at rates of approximately 0.5 m^3/m/day, roughly 2.5 times slower than DW1. In the southern end, DW4 and DW5 recovered in 7 - 9 months with similar and slower rates of ~0.14 m^3/m/day. Recovery to pre-storm conditions at the southern end of the embayment was on the order of 4 times slower than in the middle, and 10 times slower than at the northern end.

In contrast to Narrabeen and Dee Why, recovery within the shorter Bilgola embayment was comparably uniform alongshore with notably less variability between profiles (Figures 6.5 and 6.6). BG1 and BG2 recovered to their pre-storm conditions within 5 days of each other, roughly 10 months after the storm, with similar net rates of 0.13 and 0.15 m^3/m/day, respectively. Recovery at BG3 was slightly more rapid, returning to pre-storm conditions within 7 months at a net rate of 0.3 m^3/m/day, roughly twice as fast as BG1 and BG2. In Figure 6.5, week-by-week subaerial volume changes are seen to be consistent across the Bilgola profiles, particularly during the first half of the recovery period. This observation of a relatively uniform alongshore pattern in recovery was unique amongst the monitored embayments.

Within the Mona Vale embayment, MV5 recovered within approximately 4 months of the storm, at a relatively gradual rate of 0.16 m^3/m/day (Figures 6.5 and 6.6). Erosion at the southern end of the Basin at MV3 recovered at a similar rate of 0.19 m^3/m/day. Other Mona Vale profiles with insignificant storm impacts due to their sheltered location within the Basin were excluded from the analysis. Due to the limited profile locations along the entire embayment at this site it is not feasible to comment on the alongshore variability at Mona Vale from these findings.

6.3.3 Comparison of recovery durations and net rates between embayments

Figure 6.7 shows the recovery time series of alongshore-averaged subaerial volume for each embayment following the April 2015 storm event. Recovery duration and the corresponding net recovery rate for each embayment are given in Table 6.3. Recovery durations varied between 2 and 8 months while net rates of subaerial volume recovery were relatively consistent between embayments, varying in the relatively narrow range of 0.16 to 0.30 m^3/m/day. This resulted in embayments that exhibited lesser erosion measured immediately post-storm (Dee Why and Mona Vale) recovering earlier than more eroded embayments (Narrabeen and Bilgola). Net recovery rates for Dee Why and Narrabeen were similar and the most rapid of the four study embayments. These were approximately twice the net rate observed for Mona Vale and 1.5 times that observed for Bilgola. In contrast to the observed range of net recovery rates within embayments (≈ 1.5 m^3/m/day), the observed range of net rates between embayments based on the alongshore-averaged subaerial volume (≈ 0.14 m^3/m/day) was substantially smaller by a factor of 10.

Table 6.3: Embayment recovery durations and net recovery rates

Embayment	Bilgola	Mona Vale	Narrabeen	Dee Why
Recovery Duration (days)	231	128	208	69
Net Recovery Rate (m^3/m/day)	0.21	0.16	0.28	0.30

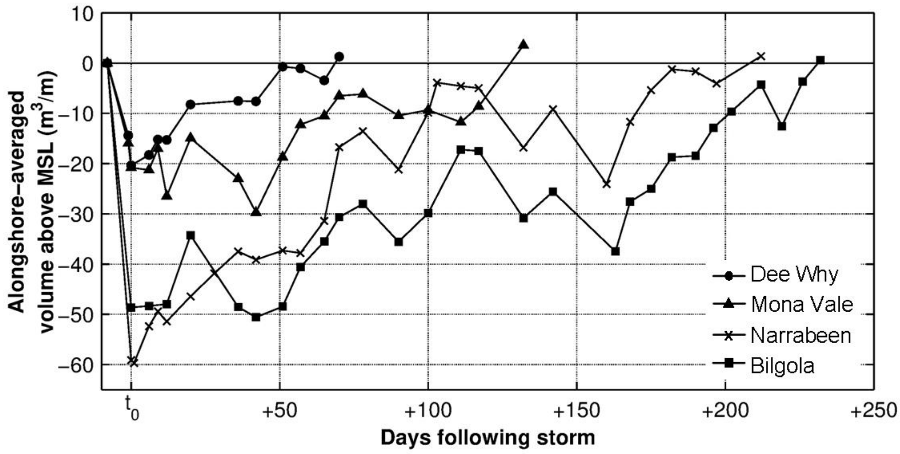

Figure 6.7: Recovery time series of alongshore-averaged subaerial volume for each embayment following the April 2015 storm event.

Figures 6.8a and 6.8b indicate changes in embayment orientation during the recovery period, as subaerial volume returned to pre-storm conditions. Corresponding changes in width between embayment extremities are shown in Figure 6.8b. At Narrabeen, a pronounced clockwise rotation in the embayment was observed to steadily develop throughout its recovery at approximately 0.006°/day. By the end of the 208-day recovery for this embayment, the beach had rotated 1.2 degrees clockwise relative to its pre-storm orientation, such that in Figure 6.8b the rotation magnitude between embayment extremities was on the order of 75 m (see also Figure C.3, Appendix C). Dee Why also rotated clockwise during its 69-day recovery, reaching a maximum rotation of 2 degrees greater than pre-storm orientation approximately mid-way through, before returning to 1 degree by the end of its recovery (~30 m greater width in north than south, Figure 6.8). In contrast, beach orientation at Bilgola was observed to fluctuate throughout its 231-day recovery between -5 and +2 degrees relative to pre-storm conditions. In Figure 6.8b, this is equivalent to differences of typically 0 - 30 m between the southern and northern ends of the 500 m long embayment, and is likely due to more localised impacts associated with the alongshore migration of rips and sandbar welding patterns in the shorter embayment.

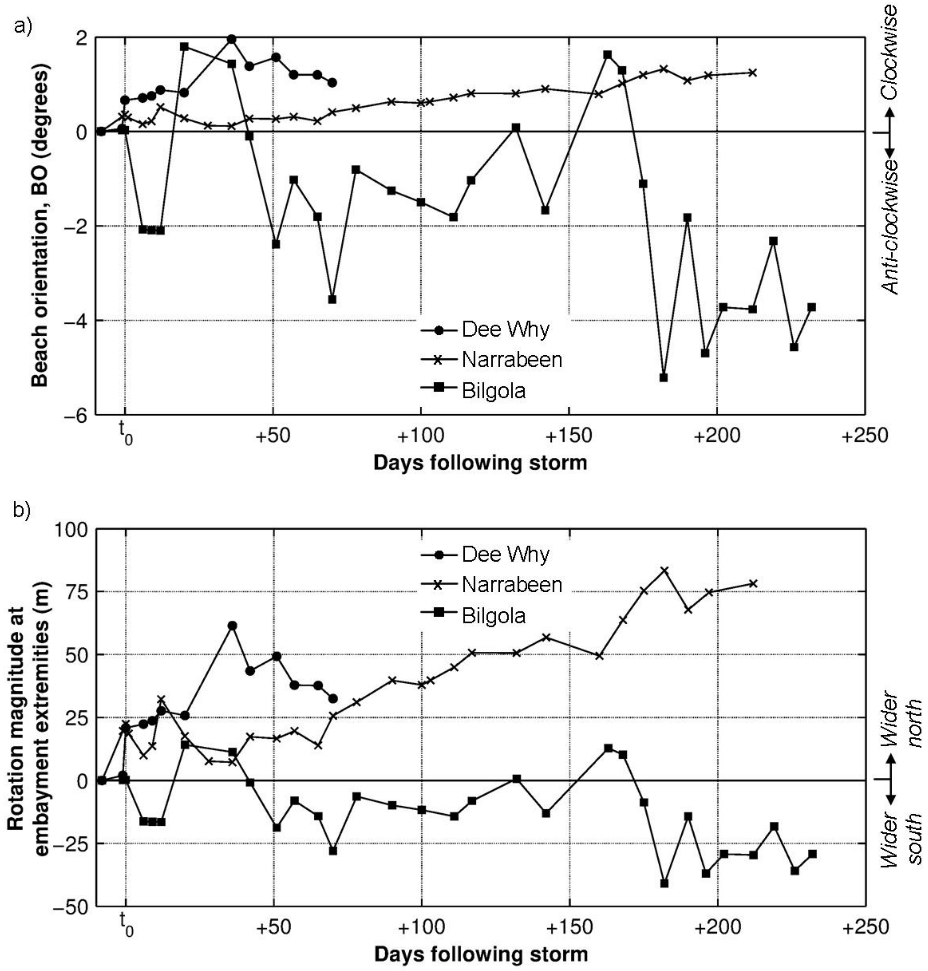

Figure 6.8: Beach rotation time series during the recovery of subaerial volume recovery in each embayment. a) Beach orientation relative to pre-storm orientation. b) Corresponding discrepancies in width between embayment extremities relative to pre-storm conditions.

6.3.4 Erosion magnitudes and recovery

The magnitude of the eroded subaerial sediment volume at each individual profile, as well as the average across each of the four study embayments, is plotted against the corresponding recovery duration and net recovery rate in Figures 6.9a and 6.9b. As expected, in general longer (shorter) recovery durations were observed for locations that experienced larger (smaller) storm erosion volume (Figure 6.9a). However, this relationship was poorly correlated (R^2 = 0.16) and occurred with a high degree of variability such that recovery durations varied by up to 200 days for a given magnitude of observed subaerial erosion. As shown in Figure 6.9b, gradual net rates (< 0.3 m^3/m/day) are predominantly observed across most locations for virtually the full range of erosion magnitudes between 10 - 82 m^3/m. The most rapid net rates of recovery (> 1 m^3/m/day) at Narrabeen and Dee Why occurred at the least eroded profiles within their

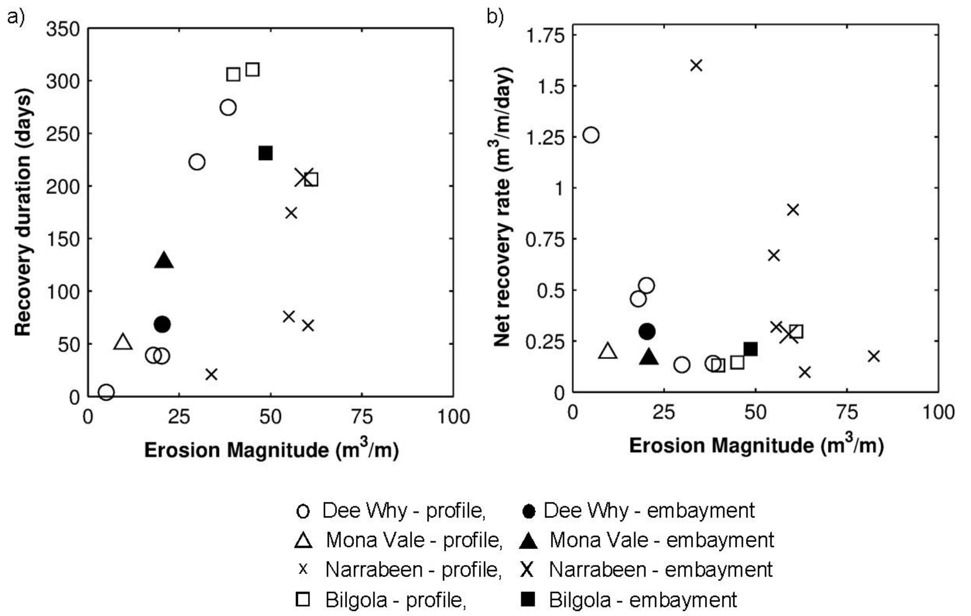

Figure 6.9: Magnitudes of storm erosion plotted against a) recovery durations and b) net recovery rates

respective embayments. At Dee Why, recovery rates increased exponentially with decreasing erosion magnitude between profiles (r^2 = 0.90). This trend at Narrabeen was more linear and occurred with greater variability (r^2 = 0.48). At Dee Why and Narrabeen, similar net recovery rates were observed despite significant differences in the magnitude of measured erosion. While general trends are evident, relationships between the alongshore variability in recovery (durations and/or net rates) and alongshore variability in the magnitude of storm erosion remain inconclusive from these results. Additional factors driving spatial variability in recovery are discussed further in the following Section 6.4.

6.4 Discussion

6.4.1 Alongshore variability in recovery: within and between embayments

The present findings evaluate the extent to which subaerial volume recovery varies alongshore on an embayed coastline following a significant storm event. In particular, alongshore variability is compared both within and between four closely-situated embayments on an embayed coastline. Differences observed at these distinctive spatial scales are summarised in Figure 6.10, showing the net recovery rate and alongshore range of net rates observed for each embayment. Despite the embayments differing in length, shoreline orientation and upper nearshore slopes (Table 3.1), net

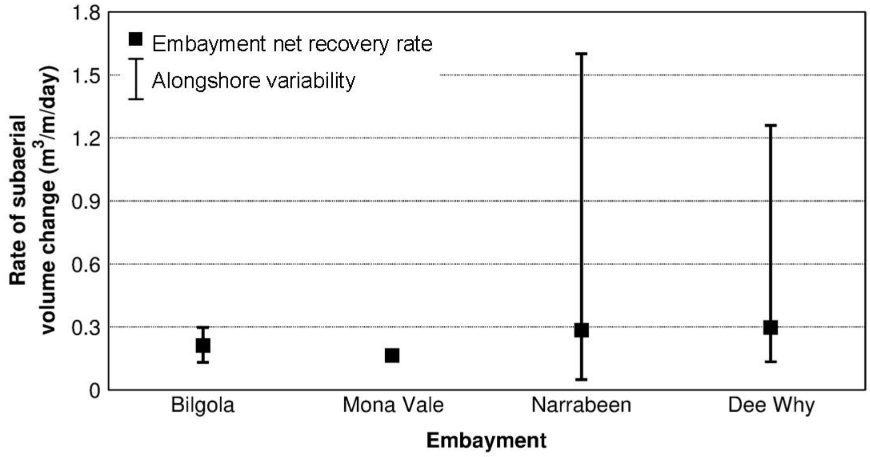

Figure 6.10: A comparison of net recovery rates at two distinctive alongshore scales: between and within embayments. Alongshore variability is notably greater within the Narrabeen and Dee Why embayments than compared to between the embayments.

rates are seen to be relatively consistent between the four study embayments, varying in the relatively narrow range between 0.16 - 0.3 m^3/m/day. In contrast, the alongshore range of net rates observed within embayments (in particular Narrabeen and Dee Why) were observed to be substantially greater by up to a factor of 10, varying between 0.1 - 1.6 m^3/m/day. Recovery durations at these locations also ranged from just several days to more than a year (Figure 6.6). These observations suggest the importance of localised processes in driving alongshore variability in beach recovery at embayed coastlines. An exception to this was in the short, pocket embayment of Bilgola where observed recovery was gradual and more alongshore uniform.

To place these observations in the context of what has been reported elsewhere, Corbella and Stretch (2012) observed comparable magnitudes and alongshore patterns of beach recovery along the more straight, open coastline of Durban, South Africa. Their study noted a very similar alongshore range in net rates (0.1 - 1.5 m^3/m/day) though over typically longer, multi-year recovery durations. Likewise, when averaged and compared between broader alongshore regions separated by estuary entrances, it was reported that this variability reduced to a range of 0.1 - 0.3 m^3/m/day. On both straight, open (Corbella and Stretch, 2012) and embayed coastlines (the present chapter), net recovery rates between alongshore locations spaced only a few hundred metres apart can be notably disparate and significantly greater than differences between averages of broader coastline divisions or embayments.

In addition to variability between neighbouring profiles, the present findings from an embayed coastline also highlight the presence of alongshore gradients in net rates, not reported on a straight, open coast by Corbella and Stretch (2012). Moderate to rapid net rates (up to 1.6 m^3/m/day) were observed in the middle to northern and more exposed regions of longer embayments (Figure 6.6), while more gradual rates were typically observed at the southern, more sheltered ends (< 0.2 m^3/m/day). The alongshore gradients in net rates were found to result in rotational effects (here observed as a clockwise rotation) during recovery (Figure 6.8). This is consistent with previous studies of embayed beach rotation that have highlighted the significance of alongshore variability in cross-shore sediment fluxes on seasonal-scale rotation signals (Ranasinghe et al., 2004a; Harley et al., 2011b; Harley et al., 2015). The present findings demonstrate that following erosion, though an embayment may recover to a pre-storm subaerial volume, its shoreline orientation may deviate from pre-storm conditions due to alongshore gradients in rates of recovery within the embayment.

6.4.2 Storm deposition and subaqueous sediment supply during recovery

For the subaerial beach to recover at any location, a sufficient local sediment supply is required. Sediment sources for beach recovery are often deposited by preceding storm activity, when eroded sediment is displaced to varying extents offshore and alongshore in the subaqueous beach, and potentially also in the backshore as overwash deposition (Weymer et al., 2015; Scott et al., 2016). Sediment discharge at estuary entrances can also provide an additional source during recovery (Corbella and Stretch, 2012). In particular, the role of subaqueous sediment supply in governing temporal variations in recovery was highlighted in Chapter 4. Specifically, the proximity of the offshore storm deposits, in the form of cross-shore migrating sandbars, was found to be a key parameter determining temporal variations in rates of shoreline recovery. Increased subaqueous sediment supply with closer sandbar-shoreline proximity and attachment was observed to enhance the rate at which the shoreline returned to its pre-storm position. In contrast when sandbars were displaced at greater distances and detached from the shoreline, rates of shoreline recovery were more gradual.

Storm deposition in the subaqueous beach is a factor likely also driving alongshore variability in net rates of subaerial sediment volume recovery. This was apparent from the observed recovery period in the present chapter, examining the combined topographic and bathymetry profile measurements presented in Figures 6.11, 6.12 and 6.13. A number of qualitative observations can be made, distinguishing patterns of subaqueous storm deposition at profiles associated with rapid (> 1 m^3/m/day), moderate (0.3 - 1.0 m^3/m/day) and gradual (0.3 < m^3/m/day) net recovery rates.

Profiles with rapid net recovery rates are shown in Figures 6.11b (PF1 at Narrabeen) and 6.12b (DW1 at Dee Why). These show notable deposition directly offshore at these locations following the April 2015 storm, extending from depths of -8 m through to the shallower surf zone at depths between the 0 m and -2 m contours. In addition to cross-shore sediment transport, the observed high energy storm that impacted the coastline from an oblique (SSE) direction, likely also resulted in some degree of alongshore sediment transport, with deposition at these locations situated updrift of headlands at the northern end of embayments. Sediment discharge at a nearby lagoon entrance also potentially added to the deposition in Figure 6.11b. Rapid onshore transport of these deposits to the subaerial beach is observed in the initial months following the storm. This provides an immediate subaqueous sediment supply, enhancing net rates and excess recovery in the subaerial beach. Similar observations are seen at profiles with moderate net rates in Figures 6.11c (PF4, Narrabeen) and 6.12c (DW2, Dee Why), though with relatively less storm deposition at shallower depths and more progressive onshore sediment transport during recovery.

In contrast, patterns of storm deposition at profiles with gradual net rates are indicated in Figures 6.11d (PF8, Narrabeen), 6.12d (DW5, Dee Why) and 6.13b-d (BG1 and BG2, Bilgola). Offshore deposits are either almost entirely absent (PF8), predominantly situated in deeper waters below the -5 m depth contour (BG1 and BG2) or show minimal flattening of the profile at shallower depths between the 0 and -2 m contours (DW5). At PF8 (Figure 6.11d), subaerial erosion during the storm coincided with limited offshore deposition (approximate loss of 25 m^3/m between 0 m and -10 m depth contours), indicating that eroded sediment was displaced alongshore. Subsequent bathymetry surveys show that the alongshore return of this sediment was minimal throughout recovery and likely resulted in the partial beach recovery observed at this location. Conversely at the updrift neighbouring profile (PFLD, Figure 6.6), this additional sediment supply likely enhanced recovery in this localised region. At Bilgola (Figures 6.13b-c), deposits in deeper waters below the -5 m depth contour were observed to move steadily onshore during recovery with more gradual recovery in the subaerial beach. The lack of deposition (sediment supply) immediately offshore in shallower depths above the -2 m contour likely reduced net rates at these locations.

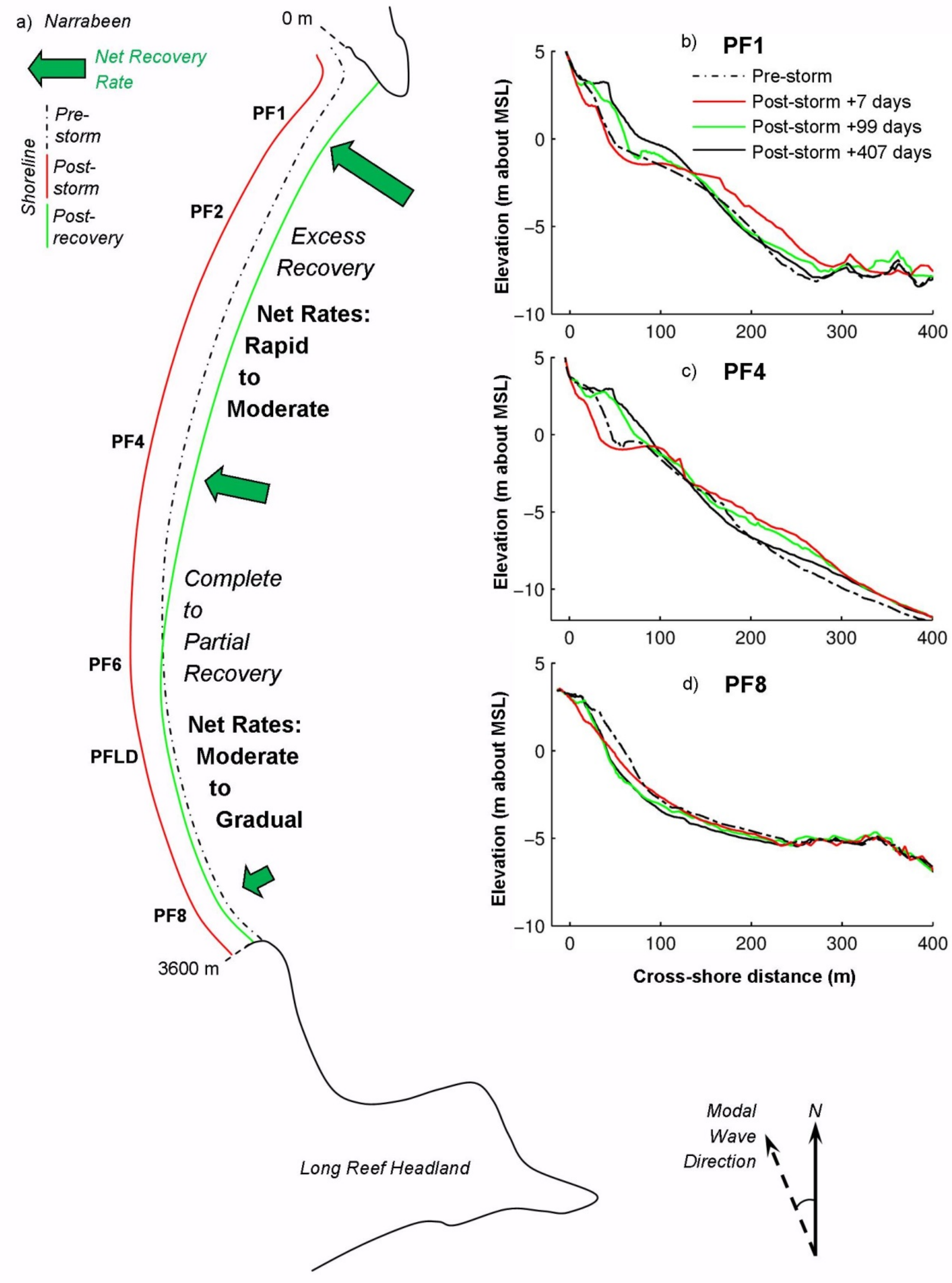

Figure 6.11: a) Alongshore recovery characteristics within the longer, partially exposed (to predominant wave energy) embayment of Narrabeen. Combined topographic and bathymetry surveys during recovery at profiles b) PF1, c) PF4 and d) PF8.

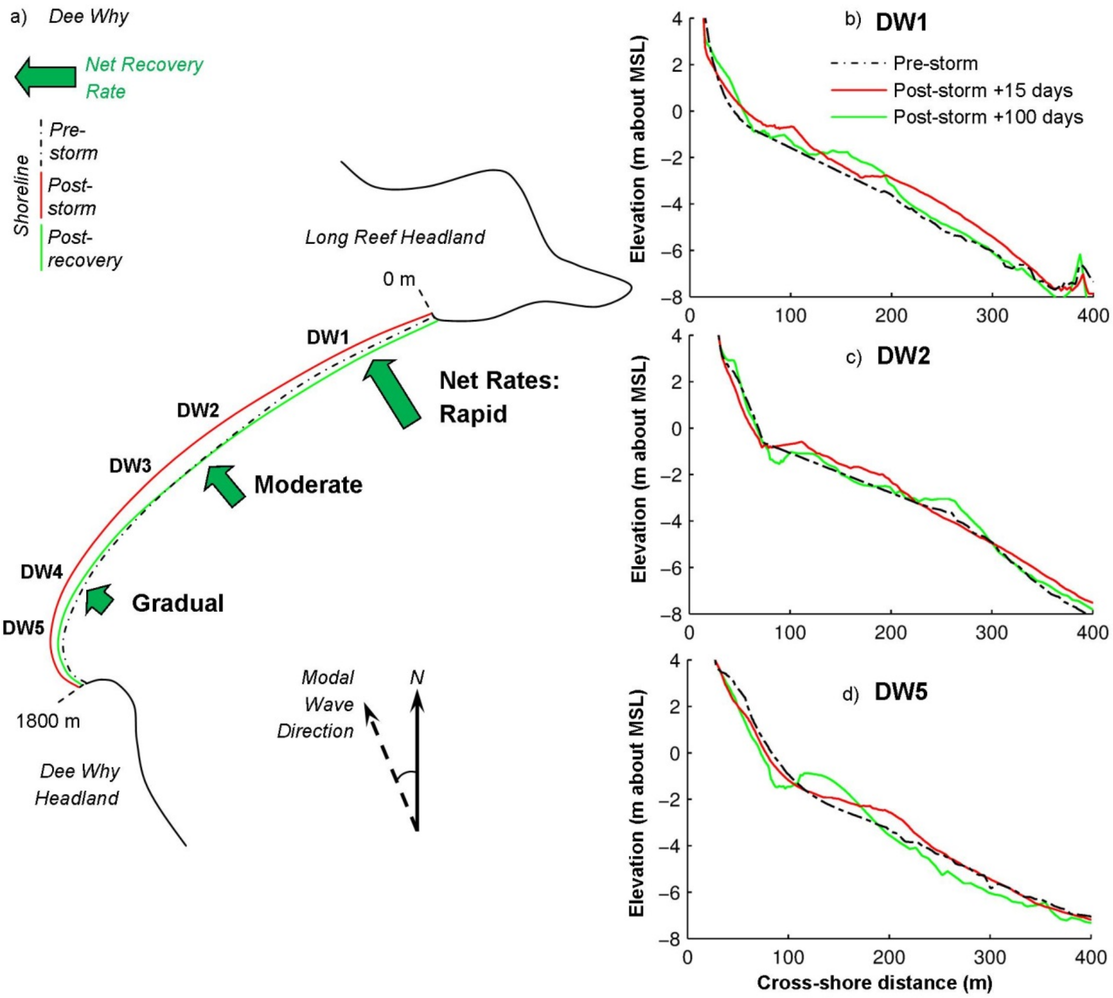

Figure 6.12: a) Alongshore recovery characteristics within the Dee Why embayment, more exposed to predominant wave energy. Combined topographic and bathymetry surveys during recovery at profiles b) DW1, c) DW2 and d) DW5.

Though not observed in the present study, minimal or partial recovery has also been noted at locations where storms result in significant overwash deposition (Weymer et al., 2015; Scott et al., 2016). With overwash deposition, sediment is entirely removed from the nearshore and can only return to the beach (by natural means) by generally slower aeolian processes. On coasts with perpendicular coastal structures (e.g., groynes, stormwater outlets) recovery may be enhanced at updrift locations where nearshore deposition is accumulated, and conversely slowed at downdrift locations where lacking (Corbella and Stretch, 2012).

The observations presented here reinforce the findings of Chapter 4 that the location to which sand is displaced in the subaqueous beach during a storm will then subsequently influence the duration and rate at which subaerial beach recovery occurs. Net recovery rates in the subaerial beach are enhanced at locations where eroded

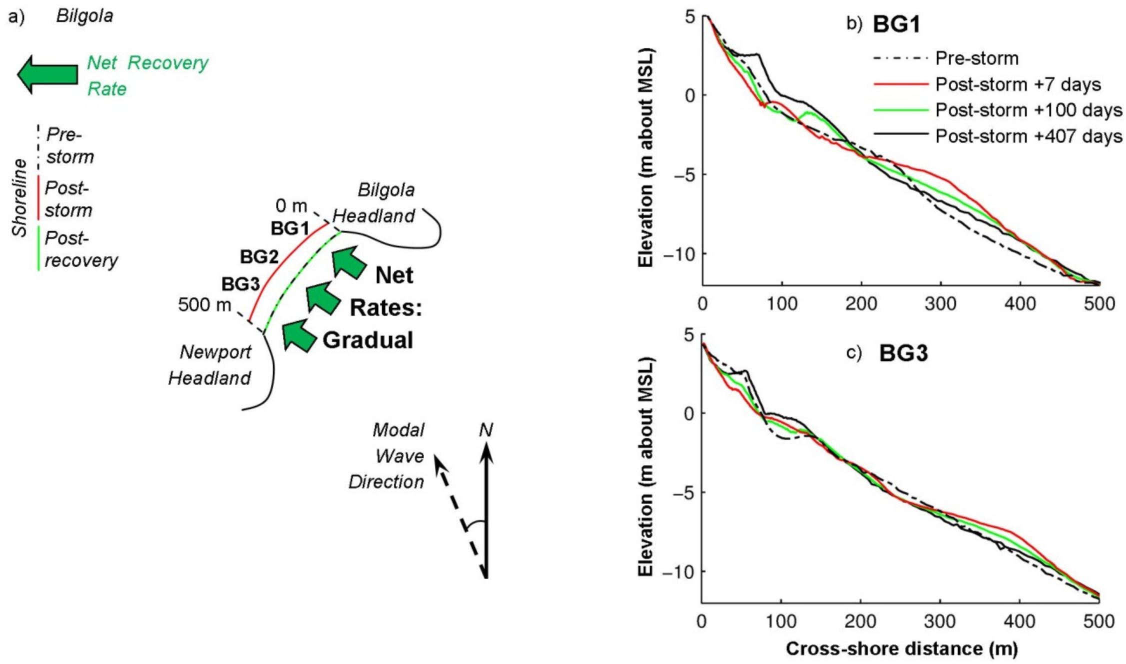

Figure 6.13:a) Alongshore recovery characteristics within the shorter and exposed pocket embayment of Bilgola. Combined topographic and bathymetry surveys during recovery at profiles b) BG1 and c) BG3.

sediment is deposited immediately offshore and is situated in shallower depths to readily return onshore by wave action. In contrast, at locations where eroded sediment is not deposited immediately offshore or predominantly deposited in deeper waters, net rates are slower. The sediment supply role of the subaqueous beach is considered a factor of primary importance in driving both temporal (Chapter 4) and alongshore (present chapter) variability in rates of beach recovery.

6.4.3 Alongshore variability in wave exposure during recovery

In addition to considerations of sediment supply, previous studies have also suggested the requirement of sufficient nearshore wave energy during recovery to mobilise and return offshore storm deposits to the subaerial beach (e.g., Scott et al., 2016, Yu et al., 2013). Along embayed coastlines, alongshore variability in wave exposure can be pronounced due to varying degrees of sheltering of oblique wave energy by headlands and reefs (Short and Wright, 1981; Harley et al., 2015). Alongshore variability in nearshore $\overline{H}_s$ (at the -10 m depth contour) at each embayment for the observed recovery period is shown in Figure 6.14. These follow similar alongshore trends to longer-term averages previously described in Section 6.2.3, with nearshore $\overline{H}_s$ varying at profile locations between 0.7 - 1.3 m.

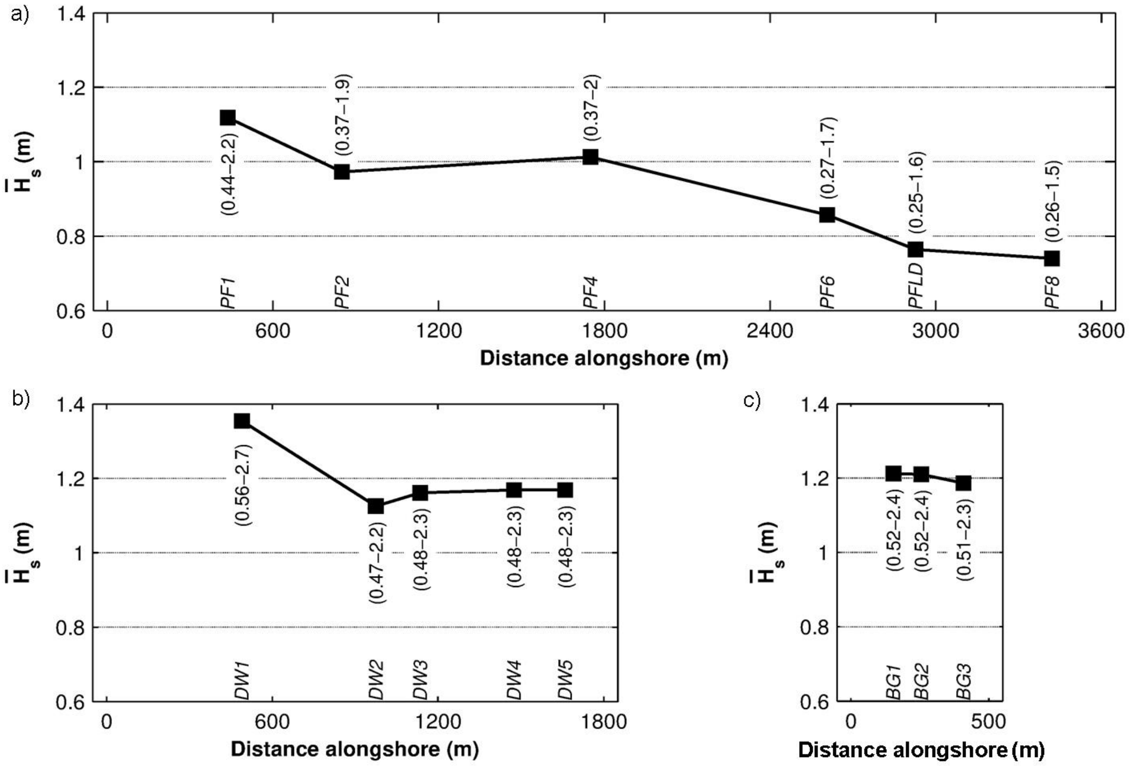

Figure 6.14: Mean nearshore $\overline{H}_s$ for alongshore profile locations at a) Narrabeen, b) Dee Why and c) Bilgola. The 95% confidence interval is given in brackets

The effect of alongshore variability in nearshore wave exposure on the observed net recovery rates in the subaerial beach is difficult to assess in isolation, without consideration of subaqueous sediment deposition previously described in Section 6.4.2. Net rates at more exposed locations (PF1-4 in Figure 6.14a and all profiles in Figure 6.14b-c) varied from gradual to rapid (0.1 - 1.6 m^3/m/day) while net rates at sheltered locations (PF6-8 in Figure 6.14b) varied from gradual to moderate (0.1 - 0.7 m^3/m/day). The effect of more exposed (or sheltered) wave exposure during recovery does not necessarily correspond with rapid (or gradual) net recovery rates. A more sheltered local wave climate may still exhibit sufficient energy to move onshore a shallow storm deposit (e.g., PFLD Narrabeen) at a faster net recovery rate, than a more exposed location with storm deposition situated in deeper offshore waters (e.g., BG1-3 Bilgola).

Greater wave exposure during recovery acts to mobilise onshore sediment transport of storm deposits in deeper offshore waters, observed here to depths of approximately -10 m AHD (Figure 6.5). In contrast, a more sheltered wave climate is less effective in mobilising storm deposits in deeper waters. In more sheltered locations, storm deposition in deeper waters (offshore or alongshore) may remain relatively immobile until sufficient wave energy triggers onshore sediment transport into shallower nearshore waters (Yu et al., 2013; Scott et al., 2016). At more sheltered locations (Figure 6.5), when storm deposits in shallower waters (if present) have returned to the subaerial beach, rates of recovery decline and partial recovery may prevail for extended periods of time (Phillips et al., 2015; Phillips et al., 2017). Further research toward predicting beach recovery along embayed coastlines is anticipated to account for both the sediment supply effect of subaqueous storm deposition, and available nearshore wave energy to return this deposition to the subaerial beach.

6.5 Conclusion

Following a significant storm event, alongshore variability in the recovery of subaerial volume to pre-storm conditions was evaluated along an embayed coast at 19 beach profile locations spanning four closely-located embayments. Recovery durations and net recovery rates were quantified and compared at distinct alongshore scales within coastal embayments (comparing subaerial volume recovery between individual profile locations) and between coastal embayments (comparing alongshore-averaged subaerial volume recovery between embayments). The net recovery rates of alongshore-averaged subaerial volume at all four study embayments were relatively consistent and varied in the range of 0.1 - 0.3 m^3/m/day with a typical duration of several months. In contrast, the range of variability in net recovery rates at profile locations within individual embayments was found to be substantially larger by a factor of 10. Net recovery rates at profiles within the longer (1.8 - 3.6 km) embayments ranged between 0.1 - 1.6 m^3/m/day and recovery durations from several days to more than one year. Variability in net recovery rates was characterised by alongshore gradients between embayment extremities, as` well as locations spaced only a few hundred metres apart differing widely in their rate of recovery. Alongshore gradients in net recovery rates resulted in embayments deviating from a pre-storm orientation during recovery. Factors considered driving alongshore variability in subaerial beach recovery on an embayed coast include spatial patterns of subaqueous storm deposition (local sediment supply) as well as the sheltering of nearshore wave energy during recovery (alongshore-variable wave forcing) by headlands and reefs.

Chapter 7

Conclusion

Following the rapid and destructive impacts of storm erosion, beach recovery is a key natural process of restoration, returning eroded sediment to the subaerial beach and rebuilding coastal morphology to continue to support the needs of present-day coastal communities. When viewed holistically as presented in Chapter 2, beach recovery is seen to comprise of various processes and morphological adjustments observed to occur over a range of durations at varying rates. On wave-dominated sandy beaches these include wave-driven processes such as the onshore transport of lower shoreface storm deposits [O(several years)], onshore sandbar migration [O(days to weeks)], shoreline/berm recovery [O(months to 1 - 2 years)] and subaerial sediment volume recovery [O(months to several years)], as well as aeolian-driven processes that primarily dictate the recovery of backshore and dune systems [O(several years to 1 - 2 decades)]. While a more detailed empirical and process-based understanding of storm erosion has been developed, the focus of this thesis has been to advance a conceptual understanding of the wave-driven processes associated with recovery of the subaerial beach following storm events.

In this regard, the central aim of this thesis was to *provide quantitative and parametric insight into wave-driven recovery processes of the subaerial beach following storms on microtidal, wave-dominated sandy beaches*. Using various field monitoring approaches, this thesis has addressed three different wave-driven processes of beach recovery; namely the nearshore forcing of shoreline recovery (Chapter 4), the swash-related morphodynamics and forcing of berm recovery (Chapter 5), and the spatial variability of subaerial volume recovery along an embayed coastline (Chapter 6). Rates, durations and behavioural characteristics related to these processes were quantified and key governing parameters were examined. This was approached by investigating three specific research objectives outlined in Section 1.3, for which the key outcomes are summarised below.

1. *Examine the influence of sandbar morphodynamics and nearshore wave parameters on shoreline recovery at a microtidal, wave-dominated sandy beach.*

The results of Chapter 4 highlight the temporal variability of shoreline recovery following storms and give new insight into key driving parameters. This was achieved using a 10-year dataset of daily shoreline and sandbar positions from a Coastal Imaging station at Narrabeen-Collaroy Beach, Australia. Rates of shoreline recovery to a pre-storm position were quantified following a total of 82 individual storm events. Observed rates during shoreline recovery were characterised by an overall mean of ~0.2 m/day. Temporal variability in rates was most evident at shorter timescales of 1 - 2 weeks and included rates most frequently between 0 - 0.3 m/day, less frequent more rapid rates of up to 2 m/day and also minor landward movements. As such, temporal variability during shoreline recovery was found to be characterised by both accretion and erosion, with net progradation of the shoreline a result of the integrated effect of these shorter-term fluctuations.

This temporal variability was significantly correlated with nearshore wave parameters related to wave steepness, the cross-shore proximity (and attachment) of the sandbar to the shoreline and the observed rate of cross-shore sandbar migration. More gradual shoreline recovery rates were associated with fully detached and semi-attached sandbar conditions. In contrast, more rapid rates of shoreline recovery were observed when sandbars were closer and/or attached to the shoreline, on average 3 - 4 times greater than rates with detached sandbars. In conditions with attached and semi-attached sandbars, shoreline recovery rates were negatively correlated to the forcing of nearshore wave steepness and dimensionless fall velocity, and coupled with concurrent rates of onshore sandbar migration.

These findings are summarised in a new conceptual model (Figure 4.9) that characterises temporal phases and rates of shoreline recovery corresponding to stages of onshore sandbar migration following a storm, from fully detached storm-deposited sandbar morphology through to complete sandbar welding with the shoreline.

2. *At the timescale of individual tides, classify and evaluate parameters governing beachface and berm morphodynamics throughout the entire recovery of a berm following a significant storm event at a microtidal, wave-dominated sandy beach.*

Whereas the results of Chapter 4 explored relationships between observations of subaqueous morphology and wave processes related to the one-dimensional (cross-shore) recovery of a single alongshore-averaged shoreline contour, the findings of Chapter 5 give insight into the morphodynamics and forcing of the two-dimensional recovery of the subaerial beach profile including the broader beachface and berm. Tide-by-tide swash and beach profile measurements collected from a continuously scanning Lidar at Narrabeen-Collaroy Beach, Australia, were used to analyse the complete (2.5 month) recovery of berm morphology to pre-storm conditions, following removal by a significant storm. Tide-by-tide rates of subaerial volume change during berm recovery were most frequently between 1 - 2 m^3/m/day but varied substantially with losses and gains on the order of several cubic metres of sediment per metre of shoreline per day. The rates of volume change observed at tidal intervals during recovery reached up to several orders of magnitude larger than the more gradual net gain (0.7 m^3/m/day) observed for the entire 2.5 month recovery period. The findings reinforce the results of Chapter 4, again showing that it is the integrated effect of shorter-term variability with rates of relative large magnitude that results in the overall (more gradual) net recovery of a beach with time.

The results of Chapter 5 reveal that the beachface and berm do not necessarily behave synchronously during their recovery. In particular, rates of volume change were most variable at the beachface but were more gradual and intermittent at the berm. Berm crest elevation during recovery were found to be primarily governed by neap-spring variations in total water levels. The inception of new berm crests was observed around neap tides and subsequently followed by vertical growth significantly correlated with rising neap-to-spring total water levels. This pattern repeated throughout the observed recovery period, involving the formation and vertical growth of multiple berm crests.

The position of the berm crest was used to distinguish rates of beachface and berm volume change to then identify four principal behavioural modes of subaerial profile variability during berm recovery (Figure 5.9); namely beachface progradation (mode 1), beachface progradation with berm aggradation (mode 2), beachface erosion with berm aggradation (mode 3) and beachface erosion (mode 4). Using decision tree analysis, the occurrence of each mode was differentiated according to particular conditions associated with nearshore dimensionless fall velocity, swash exceedance of the berm crest and ocean water levels (Figure 5.11). The findings provide new behavioural and parametric insight into the tide-by-tide rebuilding of the subaerial beach profile by swash activity throughout berm recovery.

3. *Evaluate the alongshore variability in subaerial volume recovery within and between embayments following a significant storm event along a microtidal, wave-dominated, embayed coastline.*

Following the same significant storm event analysed in detail in Chapter 5 at a single cross-shore profile location, Chapter 6 detailed the observed alongshore variability of subaerial volume recovery along the broader embayed coastline. Data from the routine profile monitoring at 19 locations spanning four closely-situated embayments was used to quantify recovery durations and net recovery rates, with comparisons made at distinct alongshore scales including within coastal embayments (comparing subaerial volume recovery between individual profile locations) and between coastal embayments (comparing alongshore-averaged subaerial volume recovery between embayments).

A key finding was that the range of variability in net recovery rates was substantially larger (by a factor of 10) within embayments compared to between embayments. In particular, net recovery rates varied most within longer (1.8 - 3.6 km) embayments and ranged between 0.1 - 1.6 m^3/m/day with recovery durations from several days to more than one year. Variability in net recovery rates was characterised by alongshore gradients between embayment extremities, as well as differences between locations spaced only a few hundred metres apart. Alongshore gradients in net recovery rates resulted in embayments deviating from a pre-storm orientation during recovery. As such, the findings of this thesis demonstrate that though an embayment may recover to a pre-storm subaerial volume following erosion, its shoreline orientation may concurrently deviate from pre-storm conditions. In contrast, comparisons of embayment-scaled recovery were relatively consistent and gradual. Net recovery rates varied in the range of 0.1 - 0.3 m^3/m/day between embayments with typical durations of several months.

The findings suggest the primary importance of localised processes occurring within embayments in driving alongshore variability in beach recovery along embayed coastlines. Evident in bathymetry surveys and nearshore wave statistics, driving factors of alongshore variability in beach recovery are considered to include spatial patterns in subaqueous storm deposition (local sediment supply) as well as the sheltering of nearshore wave energy during recovery (alongshore-variable wave forcing) by headlands and reefs. In agreement with the results of Chapter 4, net recovery rates of subaerial volume were enhanced at locations where offshore deposition was abundant with deposits at shallower depths able to readily return onshore by wave action. On the contrary, at locations where offshore deposition was limited or predominantly located in deeper waters, net rates tended to be slower. The results of Chapters 4 and 6 point towards the likely importance of the subaqueous beach as a primary sediment source driving both temporal and spatial variability in beach recovery respectively.

7.1 Implications and further research

While field investigations in this work have been undertaken on microtidal wave-dominated sandy beaches, further research examining and comparing processes of beach recovery is also warranted at beaches with differing sediment characteristics (e.g., gravel), tidal range settings (e.g., mesotidal, macrotidal) and wave climates. This thesis has indicated through field observations the strong links between wave-driven processes and morphology during recovery in both the subaqueous and subaerial environment. This was made possible by beach monitoring techniques that are able to capture subaqueous beach interactions with the subaerial beach during recovery, such as video imagery, routine topographic and bathymetric surveys, as well as the detailed insight given through high resolution profile and swash data collected by Fixed Lidar monitoring systems.

As a next step, advances to numerically model beach recovery following storm events is an important requirement for assessing vulnerability and resilience to storm erosion and coastal inundation as coastlines evolve over timescales of multiple storms, years and decades. The conceptual understanding and key driving parameters identified in this thesis can contribute insight to further research that is now warranted to develop behavioural and/or numerical models to predict wave-driven sediment transport at the beachface and berm during post-storm beach recovery. A sophisticated model of beach recovery is likely to ultimately involve integrating the various wave and aeolian sediment transport processes that comprise the overall progression of beach recovery described in Chapter 2.

In developing tools to accurately predict post-storm beach recovery, it is considered important that further research seek to engage with coastal management and the economic, social and ecological values of local coastal communities. Studies should work toward predicting the recovery of a beach to a condition, using appropriate recovery indicators, based on site-specific criteria that best characterise the desired state of a beach according to community values. This insight is valuable to post-storm beach remediation works by informing of how to best work with natural recovery processes to enhance the return of the beach to such a condition following a storm. Engaging and educating coastal communities of beach recovery processes (which may often go unnoticed following the vivid impact and media attention given to storm erosion) is also likely to be beneficial toward informing community expectations and perceptions of broader coastal variability and change in post-storm situations.

References

Aagaard, T., Davidson-Arnott, R., Greenwood, B. and Nielsen, J., 2004. Sediment supply from shoreface to dunes: linking sediment transport measurements and long-term morphological evolution. Geomorphology, 60(1–2), 205-224. doi: 10.1016/j.geomorph.2003.08.002.

Aagaard, T., Greenwood, B. and Hughes, M., 2013. Sediment transport on dissipative, intermediate and reflective beaches. Earth-Science Reviews, 124, 32-50. doi: 10.1016/j.earscirev.2013.05.002.

Aarninkhof, S. G. J., Turner, I. L., Dronkers, T. D. T., Caljouw, M. and Nipius, L., 2003. A video-based technique for mapping intertidal beach bathymetry. Coastal Engineering, 49(4), 275-289. doi: 10.1016/S0378-3839(03)00064-4.

Anderson, T. R., Frazer, L. N. and Fletcher, C. H., 2010. Transient and persistent shoreline change from a storm. Geophysical Research Letters, 37(8). doi: 10.1029/2009GL042252.

Angnuureng, D. B., Almar, R., Senechal, N., Castelle, B., Addo, K. A., Marieu, V. and Ranasinghe, R., 2017. Shoreline resilience to individual storms and storm clusters on a meso-macrotidal barred beach. Geomorphology, 290, 265-276. doi: 10.1016/j.geomorph.2017.04.007.

Aubrey, D. G., 1979. Seasonal patterns of onshore/offshore sediment movement. Journal of Geophysical Research: Oceans, 84(C10), 6347-6354. doi: 10.1029/JC084iC10p06347.

Aubrey, D. G. and Ross, R. M., 1985. The quantitative description of beach cycles. Marine Geology, 69(1–2), 155-170. doi: 10.1016/0025-3227(85)90139-2.

Austin, M. J. and Masselink, G., 2006. Observations of morphological change and sediment transport on a steep gravel beach. Marine Geology, 229(1–2), 59-77. doi: 10.1016/j.margeo.2006.02.003.

Bagnold, R. A., 1940. Beach Formation by Waves: Some Model Experiments in a Wave Tank. Journal of the Institution of Civil Engineers, 15(1), 27-52. doi: 10.1680/ijoti.1940.14279.

Baldock, T. E., Barnes, M. P. and Hughes, M. G., 2006. Field observations of instantaneous cross-shore free surface profiles and flow depths in the swash zone. In Procceedings: International Conference on Coastal Dynamics 2005, Barcelona, Spain, 1-14. doi: 10.1061/40855(214)101.

Baldock, T. E., Weir, F. and Hughes, M. G., 2008. Morphodynamic evolution of a coastal lagoon entrance during swash overwash. Geomorphology, 95(3–4), 398-411. doi: 10.1016/j.geomorph.2007.07.001.

Bamford, M., Watkins, D., Bancroft, W., Tischler, G. and Wahl, J., 2008. Migratory shorebirds of the east Asian-Australasian flyway; population estimates and internationally important sites, Wetlands International - Oceania, Canberra, Australia.

Barnard, P. L., Short, A. D., Harley, M. D., Splinter, K. D., Vitousek, S., Turner, I. L., Allan, J., Banno, M., Bryan, K. R., Doria, A., Hansen, J. E., Kato, S., Kuriyama, Y., Randall-Goodwin, E., Ruggiero, P., Walker, I. J. and Heathfield, D. K., 2015. Coastal vulnerability across the Pacific dominated by El Nino/Southern Oscillation. Nature Geoscience, 8(10), 801-807. doi: 10.1038/ngeo2539.

Bascom, W., 1964. Waves and beaches - the dynamics of the ocean surface. Anchor Books, New York, United States.

Bascom, W. N., 1954. Characteristics of natural beaches. In Procceedings: 4th Conference on Coastal Engineering, Chicago, United States, 163-180. doi: 10.9753/icce.v4.10.

Bauer, B. O. and Davidson-Arnott, R. G., 2003. A general framework for modeling sediment supply to coastal dunes including wind angle, beach geometry, and fetch effects. Geomorphology, 49(1), 89-108. doi: 10.1016/S0169-555X(02)00165-4.

Bergillos, R. J., Ortega-Sánchez, M., Masselink, G. and Losada, M. A., 2016. Morpho-sedimentary dynamics of a micro-tidal mixed sand and gravel beach, Playa Granada, southern Spain. Marine Geology, 379, 28-38. doi: 10.1016/j.margeo.2016.05.003.

Birkemeier, W. A., 1979. The effects of the 19 December 1977 coastal storm on beaches in North Carolina and New Jersey. Shore and Beach, 47, 7-15.

Blackwell, B. D., 2007. The ecoservice values for some of Australia's natural coastal assets: How much are our coasts worth and what's missing from the mosaic? In Procceedings: Australia and New Zealand Society of ecological Economics Conference, Noosaville, Australia.

Blenkinsopp, C. E., Mole, M. A., Turner, I. L. and Peirson, W. L., 2010. Measurements of the time-varying free-surface profile across the swash zone obtained using an industrial LIDAR. Coastal Engineering, 57(11–12), 1059-1065. doi: 10.1016/j.coastaleng.2010.07.001.

Blenkinsopp, C. E., Turner, I. L., Masselink, G. and Russell, P. E., 2011. Swash zone sediment fluxes: Field observations. Coastal Engineering, 58(1), 28-44. doi: 10.1016/j.coastaleng.2010.08.002.

Bolle, A., Mercelis, P., Roelvink, D., Haerens, P. and Trouw, K., 2011. Application and validation of XBeach for three different field sites. Coastal Engineering Proceedings, SI(32), 40. doi: 10.9753/icce.v32.sediment.40.

Bramato, S., Ortega-Sánchez, M., Mans, C. and Losada, M. A., 2012. Natural Recovery of a Mixed Sand and Gravel Beach after a Sequence of a Short Duration Storm and Moderate Sea States. Journal of Coastal Research, 28(1), 89-101. doi: 10.2112/jcoastres-d-10-00019.1.

Brodie, K. L., Slocum, R. K. and McNinch, J. E., 2012. New insights into the physical drivers of wave runup from a continuously operating terrestrial laser scanner. In Procceedings: Oceans 2012, Hampton Roads, United States, 1-8. doi: 10.1109/OCEANS.2012.6404955.

Callaghan, D. P., Nielsen, P., Short, A. and Ranasinghe, R., 2008. Statistical simulation of wave climate and extreme beach erosion. Coastal Engineering, 55(5), 375-39010.1016/j.coastaleng.2007.12.003.

Callaghan, D. P., Ranasinghe, R. and Roelvink, D., 2013. Probabilistic estimation of storm erosion using analytical, semi-empirical, and process based storm erosion models. Coastal Engineering, 82, 64-75. doi: 10.1016/j.coastaleng.2013.08.007.

Castelle, B., Bujan, S., Ferreira, S. and Dodet, G., 2017. Foredune morphological changes and beach recovery from the extreme 2013/2014 winter at a high-energy sandy coast. Marine Geology, 385, 41-55. doi: 10.1016/j.margeo.2016.12.006.

CERC, 1984. Shore Protection Manual, Coastal Engineering Research Center, Department of the Army Corps of Engineers, Waterways Experiment Station, Washington, D.C., United States.

Choowong, M., Phantuwongraj, S., Charoentitirat, T., Chutakositkanon, V., Yumuang, S. and Charusiri, P., 2009. Beach recovery after 2004 Indian Ocean tsunami from Phang-nga, Thailand. Geomorphology, 104(3–4), 134-142. doi: 10.1016/j.geomorph.2008.08.007.

Coco, G., Bryan, K., Green, M., Ruessink, B., van Enckevort, I. J. and Turner, I. L., 2005. Video Observations of Shoreline and Sandbar Coupled Dynamics. In Procceedings: Australasian Port and Harbour Conference, Adelaide, Australia, 471-476.

Coco, G., Senechal, N., Rejas, A., Bryan, K. R., Capo, S., Parisot, J. P., Brown, J. A. and MacMahan, J. H. M., 2014. Beach response to a sequence of extreme storms. Geomorphology, 204, 493-501. doi: 10.1016/j.geomorph.2013.08.028.

Cooper, N. J., Hooke, J. M. and Bray, M. J., 2001. Predicting coastal evolution using a sediment budget approach: a case study from southern England. Ocean & Coastal Management, 44(11), 711-728. doi: 10.1016/S0964-5691(01)00079-5.

Corbella, S. and Stretch, D., 2012. Shoreline recovery from storms on the east coast of Southern Africa. Natural Hazards and Earth System Science, 12(1), 11-22. doi: 10.5194/nhess-12-11-2012.

Costas, S., Alejo, I., Vila-Concejo, A. and Nombela, M. A., 2005. Persistence of storm-induced morphology on a modal low-energy beach: A case study from NW-Iberian Peninsula. Marine Geology, 224(1–4), 43-56. doi: 10.1016/j.margeo.2005.08.003.

Couriel, E., Alley, K. and Modra, B., 2012. OEH NSW Tidal Planes Analysis 1990–2010 Harmonic Analysis. Report MHL2053, Manly Hydraulics Laboratory, NSW Office of Environment and Heritage, Sydney, Australia.

Coutts-Smith, A. J., 2004. The significance of mega-rips along an embayed coast. Ph.D. Thesis, University of Sydney, Australia.

Cowell, P., Thom, B., Carter, R. and Woodroffe, C., 1994. Morphodynamics of coastal evolution. Cambridge University Press, Cambridge, United Kingdom.

Dabrio, C. J., 1982. Sedimentary structures generated on the foreshore by migrating ridge and runnel systems on microtidal and mesotidal coasts of S. Spain. Sedimentary Geology, 32(1–2), 141-151. doi: 10.1016/0037-0738(82)90018-5.

Davidson-Arnott, R. G. D., 1988. Temporal and spatial controls on beach/dune interaction, Long Point, Lake Erie. Journal of coastal research, SI(3), 131-136.

Davidson-Arnott, R. G. D. and Law, M. N., Seasonal patterns and controls on sediment supply to coastal foredunes, Long Point, Lake Erie. In: Nordstrom, K. F., Putsy, N. P. and Carter, R. W. G. (Eds.), 1990. Coastal Dunes: Form and Process. John Wiley & Sons Ltd, Chichester, England, pp. 177-200.

Davidson, M. A., Splinter, K. D. and Turner, I. L., 2013. A simple equilibrium model for predicting shoreline change. Coastal Engineering, 73, 191-202. doi: 10.1016/j.coastaleng.2012.11.002.

Davies, J., 1964. A morphogenic approach to world shorelines. Zeitschrift fur Geomorphologie, 8, 127-142.

Davies, J. L., 1980. Geographical Variation in Coastal Development. Longman Group Ltd, New York, United States.

Davis, R. A., Fox, W. T., Hayes, M. O. and Boothroyd, J. C., 1972. Comparison of ridge and runnel systems in tidal and non-tidal environments. Journal of Sedimentary Research, 42(2), 413-42110.1306/74d7256d-2b21-11d7-8648000102c1865d.

Davis, R. A. and Hayes, M. O., 1984. What is a wave-dominated coast? Marine Geology, 60(1), 313-329. doi: 10.1016/0025-3227(84)90155-5.

Day, J. W., Boesch, D. F., Clairain, E. J., Kemp, G. P., Laska, S. B., Mitsch, W. J., Orth, K., Mashriqui, H., Reed, D. J., Shabman, L., Simenstad, C. A., Streever, B. J., Twilley, R. R., Watson, C. C., Wells, J. T. and Whigham, D. F., 2007. Restoration of the Mississippi Delta: Lessons from Hurricanes Katrina and Rita. Science, 315(5819), 1679-1684. doi: 10.1126/science.1137030.

Dean, R. G., 1973. Heuristic Models of Sand Transport in the Surf Zone. In Procceedings: Conference on Engineering Dynamics in the Coastal Zone, Sydney, Australia, 215-221.

Dean, R. G., 2002. Beach nourishment: theory and practice. World Scientific Publishing, Singapore.

Defeo, O., McLachlan, A., Schoeman, D. S., Schlacher, T. A., Dugan, J., Jones, A., Lastra, M. and Scapini, F., 2009. Threats to sandy beach ecosystems: A review. Estuarine, Coastal and Shelf Science, 81(1), 1-12. doi: 10.1016/j.ecss.2008.09.022.

Delgado-Fernandez, I. and Davidson-Arnott, R., 2011. Meso-scale aeolian sediment input to coastal dunes: The nature of aeolian transport events. Geomorphology, 126(1), 217-232. doi: 10.1016/j.geomorph.2010.11.005.

DHI, 2014. MIKE21 SW. Spectral Wave FM Module User Guide, Danish Hydraulics Lab, Hørsholm, Denmark.

Dubarbier, B., Castelle, B., Marieu, V. and Ruessink, G., 2015. Process-based modeling of cross-shore sandbar behavior. Coastal Engineering, 95, 35-50. doi: 10.1016/j.coastaleng.2014.09.004.

Dubois, R. N., 1988. Seasonal changes in beach topography and beach volume in Delaware. Marine Geology, 81(1–4), 79-96. doi: 10.1016/0025-3227(88)90019-9.

Everts, C. H. and Czerniak, M. T., 1978. Spatial and temporal changes in New Jersey Beaches. In Procceedings: Coastal Sediments '77, Charleston, United States, 444-459.

Farris, A. S. and List, J. H., 2007. Shoreline Change as a Proxy for Subaerial Beach Volume Change. Journal of Coastal Research, 23(3), 740-748. doi: 10.2112/05-0442.1.

Fernández-Mora, A., Calvete, D., Falqués, A. and de Swart, H. E., 2015. Onshore sandbar migration in the surf zone: New insights into the wave-induced sediment transport mechanisms. Geophysical Research Letters, 42(8), 2869-2877. doi: 10.1002/2014GL063004.

Ferreira, Ó., 2006. The role of storm groups in the erosion of sandy coasts. Earth Surface Processes and Landforms, 31(8), 1058-1060. doi: 10.1002/esp.1378.

Forbes, D. L., Parkes, G. S., Manson, G. K. and Ketch, L. A., 2004. Storms and shoreline retreat in the southern Gulf of St. Lawrence. Marine Geology, 210(1–4), 169-204. doi: 10.1016/j.margeo.2004.05.009.

Frampton, A. P. R., 2010. A Review of Amenity Beach Management. Journal of Coastal Research, 26(6), 1112-1122. doi: 10.2112/JCOASTRES-D-09-00008.1.

Frazer, L. N., Anderson, T. R. and Fletcher, C. H., 2009. Modeling storms improves estimates of long-term shoreline change. Geophysical Research Letters, 36(20), L20404. doi: 10.1029/2009GL040061.

Gallagher, E. L., Elgar, S. and Guza, R. T., 1998. Observations of sand bar evolution on a natural beach. Journal of Geophysical Research: Oceans, 103(C2), 3203-3215. doi: 10.1029/97JC02765.

Gordon, A., 2015. When did you last NABE a beach? Beach scraping demystified for fun and profit. In Procceedings: 24th New South Wales Coastal Conference, Forster, Australia.

Gourlay, M. R., 1968. Beach and Dune Erosion Tests. Report M935/M936, Delft Hydraulics Laboratory, Delft, Netherlands.

Guedes, R. M. C., Bryan, K. R., Coco, G. and Holman, R. A., 2011. The effects of tides on swash statistics on an intermediate beach. Journal of Geophysical Research: Oceans, 116(C4), C04008. doi: 10.1029/2010JC006660.

Hallermeier, R. J., 1980. A profile zonation for seasonal sand beaches from wave climate. Coastal engineering, 4, 253-277. doi: 10.1016/0378-3839(80)90022-8.

Harley, M., Armaroli, C. and Ciavola, P., 2011a. Evaluation of XBeach predictions for a real-time warning system in Emilia-Romagna, Northern Italy. Journal of Coastal Research, SI(64), 1861.

Harley, M., Turner, I., Short, A. and Ranasinghe, R., 2011b. A reevaluation of coastal embayment rotation: The dominance of cross-shore versus alongshore sediment transport processes, Collaroy-Narrabeen Beach, southeast Australia. Journal of Geophysical Research: Earth Surface, 116(F4), F04033. doi: 10.1029/2011JF001989.

Harley, M. D. and Turner, I. L., 2008. A simple data transformation technique for pre-processing survey data at embayed beaches. Coastal Engineering, 55(1), 63-68. doi: 10.1016/j.coastaleng.2007.07.001.

Harley, M. D., Turner, I. L., Kinsela, M. A., Middleton, J. H., Mumford, P. J., Splinter, K. D., Phillips, M. S., Simmons, J. A., Hanslow, D. J. and Short, A. D., 2017. Extreme coastal erosion enhanced by anomalous extratropical storm wave direction. Scientific Reports, 7(1), 6033. doi: 10.1038/s41598-017-05792-1.

Harley, M. D., Turner, I. L. and Short, A. D., 2015. New insights into embayed beach rotation: The importance of wave exposure and cross-shore processes. Journal of Geophysical Research: Earth Surface, 120(8), 1470–1484. doi: 10.1002/2014JF003390.

Harley, M. D., Turner, I. L., Short, A. D. and Ranasinghe, R., Monitoring beach processes using conventional, RTK-GPS and image-derived survey methods: Narrabeen Beach, Australia. In: Woodroffe, C. D., Bruce, E. M., Puotinen, M. and Furness, R. A. (Eds.), 2007. GIS for the Coastal Zone: a Selection of Papers from CoastGIS 2006. Univeristy of Wollongong, Australia, pp. 151-164.

Harley, M. D., Turner, I. L., Short, A. D. and Ranasinghe, R., 2009. An empirical model of beach response to storms-SE Australia. In Procceedings: Australasian Coasts and Ports Conference, Wellington, New Zealand, 600-606.

Harley, M. D., Turner, I. L., Short, A. D. and Ranasinghe, R., 2011c. Assessment and integration of conventional, RTK-GPS and image-derived beach survey methods for daily to decadal coastal monitoring. Coastal Engineering, 58(2), 194-205. doi: 10.1016/j.coastaleng.2010.09.006.

Harley, M. D., Turner, I. L., Splinter, K. D., Phillips, M. S. and Simmons, J. A., 2016. Beach response to Australian East Coast Lows: A comparison between the 2007 and 2015 events, Narrabeen-Collaroy Beach. Journal of Coastal Research, SI(75), 388-392. doi: 10.2112/SI75-078.1.

Henderson, S. M., Allen, J. S. and Newberger, P. A., 2004. Nearshore sandbar migration predicted by an eddy-diffusive boundary layer model. Journal of Geophysical Research: Oceans, 109(C6), C06024. doi: 10.1029/2003JC002137.

Hine, A. C., 1979. Mechanisms of berm development and resulting beach growth along a barrier spit complex. Sedimentology, 26(3), 333-351. doi: 10.1111/j.1365-3091.1979.tb00913.x.

Hoefel, F. and Elgar, S., 2003. Wave-induced sediment transport and sandbar migration. Science, 299(5614), 1885-1887. doi: 10.1126/science.1081448.

Holland, K. T., Holman, R. A., Lippmann, T. C., Stanley, J. and Plant, N., 1997. Practical use of video imagery in nearshore oceanographic field studies. Oceanic Engineering, IEEE Journal of, 22(1), 81-92. doi: 10.1109/48.557542.

Holman, R. A. and Stanley, J., 2007. The history and technical capabilities of Argus. Coastal Engineering, 54(6–7), 477-491. doi: 10.1016/j.coastaleng.2007.01.003.

Houser, C., 2009. Synchronization of transport and supply in beach-dune interaction. Progress in Physical Geography, 33(6), 733-746. doi: 10.1177/0309133309350120.

Houser, C. and Hamilton, S., 2009. Sensitivity of post-hurricane beach and dune recovery to event frequency. Earth Surface Processes and Landforms, 34(5), 613-628. doi: 10.1002/esp.1730.

Houser, C. and Mathew, S., 2011. Alongshore variation in foredune height in response to transport potential and sediment supply: South Padre Island, Texas. Geomorphology, 125(1), 62-72. doi: 10.1016/j.geomorph.2010.07.028.

Houser, C., Wernette, P., Rentschlar, E., Jones, H., Hammond, B. and Trimble, S., 2015. Post-storm beach and dune recovery: Implications for barrier island resilience. Geomorphology, 234, 54-63. doi: 10.1016/j.geomorph.2014.12.044.

Iwagaki, Y. and Noda, H., 1963. Laboratory study of scale effects in two-dimensional beach processes In Procceedings: 8th Conference on Coastal Engineering Mexico City, Mexico, 194-210. doi: 10.9753/icce.v8.14.

Jensen, S. G., Aagaard, T., Baldock, T. E., Kroon, A. and Hughes, M., 2009. Berm formation and dynamics on a gently sloping beach; the effect of water level and swash overtopping. Earth Surface Processes and Landforms, 34(11), 1533-1546. doi: 10.1002/esp.1845.

Jongman, B., Ward, P. J. and Aerts, J. C., 2012. Global exposure to river and coastal flooding: Long term trends and changes. Global Environmental Change, 22(4), 823-835. doi: 10.1016/j.gloenvcha.2012.07.004.

Kana, T. W., 1977. Beach erosion during minor storm. Journal of the Waterway Port Coastal and Ocean Division, 103(4), 505-518.

Karunarathna, H., Pender, D., Ranasinghe, R., Short, A. D. and Reeve, D. E., 2014. The effects of storm clustering on beach profile variability. Marine Geology, 348, 103-112. doi: 10.1016/j.margeo.2013.12.007.

Katoh, K. and Yanagishima, S.-i., 1992. Berm formation and berm erosion. In Procceedings: International Conference on Coastal Engineering, Venice, Italy, 2136-2149. doi: 10.1061/9780872629332.163.

Katuna, M. P., 1991. The Effects of Hurricane Hugo on the Isle of Palms, South Carolina: From Destruction to Recovery. Journal of Coastal Research, SI(8), 263-273. doi: 10.2307/25735420.

Kobayashi, N. and Jung, H., 2012. Beach Erosion and Recovery. Journal of Waterway, Port, Coastal, and Ocean Engineering, 138(6), 473-483. doi: 10.1061/(ASCE)WW.1943-5460.0000147.

Kriebel, D. and Dean, R., 1993. Convolution Method for Time-Dependent Beach-Profile Response. Journal of Waterway, Port, Coastal, and Ocean Engineering, 119(2), 204-226. doi: 10.1061/(ASCE)0733-950X(1993)119:2(204).

Kriebel, D. L., 1987. Beach recovery following hurricane Elena. In Procceedings: Coastal Sediments, New Orleans, United States, 990-1005.

Larson, M. and Kraus, N. C., 1989. SBEACH: Numerical model for simulating storm-induced beach change- Report 1. Empirical foundation and model development. CERC-89-9, Coastal Engineering Research Center, Department of the Army Corps of Engineers, Washington, D.C., United States.

Leadon, M. E., 1999. Beach, dune and offshore profile response to a severe storm event. In Procceedings: International Symposium on Coasting Engineering and Science of Coastal Sediment Processes, Hauppauge, United States, 2534-2549.

Lee, G.-h., Nicholls, R. J. and Birkemeier, W. A., 1998. Storm-driven variability of the beach-nearshore profile at Duck, North Carolina, USA, 1981–1991. Marine Geology, 148(3–4), 163-177. doi: 10.1016/S0025-3227(98)00010-3.

Liew, S. C., Gupta, A., Wong, P. P. and Kwoh, L. K., 2010. Recovery from a large tsunami mapped over time: The Aceh coast, Sumatra. Geomorphology, 114(4), 520-529. doi: 10.1016/j.geomorph.2009.08.010.

Lippmann, T. and Holman, R., 1990. The spatial and temporal variability of sand bar morphology. Journal of Geophysical Research: Oceans, 95(C7), 11575-11590. doi: 10.1029/JC095iC07p11575.

Lippmann, T. C. and Holman, R. A., 1989. Quantification of sand bar morphology: A video technique based on wave dissipation. Journal of Geophysical Research: Oceans, 94(C1), 995-1011. doi: 10.1029/JC094iC01p00995.

List, J. H., Farris, A. S. and Sullivan, C., 2006. Reversing storm hotspots on sandy beaches: Spatial and temporal characteristics. Marine Geology, 226(3), 261-279. doi: 10.1016/j.margeo.2005.10.003.

Loureiro, C., Ferreira, Ó. and Cooper, J. A. G., 2012. Extreme erosion on high-energy embayed beaches: Influence of megarips and storm grouping. Geomorphology, 139–140, 155-171. doi: 10.1016/j.geomorph.2011.10.013.

Maccarone, A. D. and Mathews, P. L., 2011. Changes in ghost crab (Ocypode Quadrata) abundance and distribution at a Texas beach two years after hurricane Ike. Texas Journal of Science, 63(3/4), 199-210.

Machado, P. M., Costa, L. L., Suciu, M. C., Tavares, D. C. and Zalmon, I. R., 2016. Extreme storm wave influence on sandy beach macrofauna with distinct human pressures. Marine Pollution Bulletin, 107(1), 125-135. doi; 10.1016/j.marpolbul.2016.04.009.

Mackenzie, A. D., 1939. Coastal erosion in Victoria. Transactions of the Institution of Engineers, Australia, 20, 229-236.

MacMahan, J., 2001. Hydrographic surveying from personal watercraft. Journal of surveying engineering, 127(1), 12-24. doi: 10.1061/(ASCE)0733-9453(2001)127:1(12).

Maspataud, A., Ruz, M. H. and Hequette, A., 2009. Spatial Variability in Post-Storm Beach Recovery along a Macrotidal Barred Beach, Southern North Sea. Journal of Coastal Research, SI(56), 88-92. doi: 10.2307/25737543.

Masselink, G., Austin, M., Scott, T., Poate, T. and Russell, P., 2014. Role of wave forcing, storms and NAO in outer bar dynamics on a high-energy, macro-tidal beach. Geomorphology, 226, 76-93. doi: 10.1016/j.geomorph.2014.07.025.

Masselink, G. and Hughes, M. G., 2003. Introduction to coastal processes and geomorphology. Hodder Arnold, London, United Kingdom.

Masselink, G., Kroon, A. and Davidson-Arnott, R. G. D., 2006. Morphodynamics of intertidal bars in wave-dominated coastal settings — A review. Geomorphology, 73(1–2), 33-49. doi: 10.1016/j.geomorph.2005.06.007.

Masselink, G. and Short, A. D., 1993. The effect of tide range on beach morphodynamics and morphology: a conceptual beach model. Journal of Coastal Research, 9(3), 785-800.

Masselink, G. and van Heteren, S., 2014. Response of wave-dominated and mixed-energy barriers to storms. Marine Geology, 352, 321-347. doi: 10.1016/j.margeo.2013.11.004.

McLean, R. and Shen, J.-S., 2006. From Foreshore to Foredune: Foredune Development over the Last 30 Years at Moruya Beach, New South Wales, Australia. Journal of Coastal Research, 22(1), 28-36. doi: 10.2307/4300263.

Morris, B. D. and Turner, I. L., 2010. Morphodynamics of intermittently open–closed coastal lagoon entrances: New insights and a conceptual model. Marine Geology, 271(1–2), 55-66. doi: 10.1016/j.margeo.2010.01.009.

Mortlock, T. R. and Goodwin, I. D., 2016. Impacts of enhanced central Pacific ENSO on wave climate and headland-bay beach morphology. Continental Shelf Research, 120, 14-25. doi: 10.1016/j.csr.2016.03.007.

Morton, R. A., Gibeaut, J. C. and Paine, J. G., 1995. Meso-scale transfer of sand during and after storms: implications for prediction of shoreline movement. Marine Geology, 126(1–4), 161-179. doi: 10.1016/0025-3227(95)00071-6.

Morton, R. A. and Paine, J. G., 1985. Beach and vegetation-line changes at Galveston Island, Texas: erosion, deposition, and recovery from Hurricane Alicia. University of Texas, Bureau of Economic Geology Geological Circular, 85-5, 1-39.

Morton, R. A., Paine, J. G. and Gibeaut, J. C., 1994. Stages and Durations of Post-Storm Beach Recovery, Southeastern Texas Coast, U.S.A. Journal of Coastal Research, 10(4), 884-908. doi: 10.2307/4298283.

Morton, R. A. and Sallenger, A. H., 2003. Morphological Impacts of Extreme Storms on Sandy Beaches and Barriers. Journal of Coastal Research, 19(3), 560-573. doi: 10.2307/4299198.

Mulcahy, N., Kennedy, D. M. and Blanchon, P., 2016. Hurricane-induced shoreline change and post-storm recovery: northeastern Yucatan Peninsula, Mexico. Journal of Coastal Research, SI(75), 1192-1196. doi: 10.2112/SI75-239.1.

Mulder, J. P., Hommes, S. and Horstman, E. M., 2011. Implementation of coastal erosion management in the Netherlands. Ocean & coastal management, 54(12), 888-897. doi: 10.1016/j.ocecoaman.2011.06.009.

Nielsen, A. F. and Lord, D. B., 1993. Subaqueous beach fluctuations on the Australian South-Eastern seaboard. In Procceedings: Australasian Conference on Coastal and Ocean Engineering, Townsville, Australia, 645-650.

Ojeda, E. and Guillén, J., 2008. Shoreline dynamics and beach rotation of artificial embayed beaches. Marine Geology, 253(1), 51-62. doi: 10.1016/j.margeo.2008.03.010.

Orme, A. R., 1985. The behavior and migration of longshore bars. Physical Geography, 6(2), 142-164. doi: 10.1080/02723646.1985.10642268.

Ostrowski, R., Pruszak, Z. and Zeidler, R., 1990. Multi-Scale Nearshore & Beach Changes. In Procceedings: International Conference on Coastal Engineering, Delft, Netherlands, 2101-2116. doi: 10.1061/9780872627765.161.

Owens, E. and Frobel, D., 1977. Ridge and runnel systems in the Magdalen Islands, Quebec. Journal of Sedimentary Research, 47(1), 191-198.

Pape, L., Plant, N. G. and Ruessink, B. G., 2009. Cross-shore sandbar response to waves. Journal of Coastal Research, SI(56), 1030-1034.

Pape, L., Plant, N. G. and Ruessink, B. G., 2010. On cross-shore migration and equilibrium states of nearshore sandbars. Journal of Geophysical Research: Earth Surface, 115(F3), F03008. doi: 10.1029/2009JF001501.

Pender, D. and Karunarathna, H., 2013. A statistical-process based approach for modelling beach profile variability. Coastal Engineering, 81, 19-29. doi: 10.1016/j.coastaleng.2013.06.006.

Phillips, M. S., Harley, M. D., Turner, I. L., Splinter, K. D. and Cox, R. J., 2017. Shoreline recovery on wave-dominated sandy coastlines: the role of sandbar morphodynamics and nearshore wave parameters. Marine Geology, 385, 146-159. doi: 10.1016/j.margeo.2017.01.005.

Phillips, M. S., Turner, I. L., Cox , R. J., Splinter, K. D. and Harley, M. D., 2015. Will the sand come back? Observations and characteristics of beach recovery In Procceedings: Australasian Coasts & Ports Conference, Auckland, New Zealand.

Plant, N. G., Holman, R. A., Freilich, M. H. and Birkemeier, W. A., 1999. A simple model for interannual sandbar behavior. Journal of Geophysical Research: Oceans, 104(C7), 15755-15776. doi: 10.1029/1999JC900112.

Plant, N. G., Todd Holland, K. and Holman, R. A., 2006. A dynamical attractor governs beach response to storms. Geophysical Research Letters, 33(17), L17607. doi: 10.1029/2006GL027105.

Poate, T., Masselink, G., Russell, P. and Austin, M., 2014. Morphodynamic variability of high-energy macrotidal beaches, Cornwall, UK. Marine Geology, 350, 97-111. doi: 10.1016/j.margeo.2014.02.004.

Price, T. D. and Ruessink, B. G., 2013. Observations and conceptual modelling of morphological coupling in a double sandbar system. Earth Surface Processes and Landforms, 38(5), 477-489. doi: 10.1002/esp.3293.

Priestas, A. M. and Fagherazzi, S., 2010. Morphological barrier island changes and recovery of dunes after Hurricane Dennis, St. George Island, Florida. Geomorphology, 114(4), 614-626. doi: 10.1016/j.geomorph.2009.09.022.

Psuty, N. P., 1965. Beach-ridge development in Tabasco, Mexico. Annals of the Association of American Geographers, 55(1), 112-124. doi: 10.1111/j.1467-8306.1965.tb00509.x.

Puleo, J. A. and Torres-Freyermuth, A., 2016. The second international workshop on swash-zone processes. Coastal Engineering, 115, 1-7. doi: 10.1016/j.coastaleng.2015.09.007.

Quartel, S., Kroon, A. and Ruessink, B., 2008. Seasonal accretion and erosion patterns of a microtidal sandy beach. Marine Geology, 250(1), 19-33. doi: 10.1016/j.margeo.2007.11.003.

Rakocinski, C. F., LeCroy, S. E., McLelland, J. A. and Heard, R. W., 2000. Possible sustained effects of Hurricanes Opal and Erin on the macrobenthos of nearshore habitats within the Gulf Islands National Seashore. Gulf and Caribbean Research, 12(1), 19-30. doi: 10.18785/gcr.1201.03.

Ranasinghe, R., Holman, R., de Schipper, M., Lippmann, T., Wehof, J., Duong, T. M., Roelvink, D. and Stive, M., 2012. Quantifying nearshore morphological recovery time scales using ARGUS video imaging: Palm Beach, Sydney and Duck, North Carolina. In Procceedings: International Conference on Coastal Engineering, Santander, Spain. doi: 10.9753/icce.v33.sediment.24.

Ranasinghe, R., McLoughlin, R., Short, A. and Symonds, G., 2004a. The Southern Oscillation Index, wave climate, and beach rotation. Marine Geology, 204(3–4), 273-287. doi: 10.1016/S0025-3227(04)00002-7.

Ranasinghe, R., Symonds, G., Black, K. and Holman, R., 2004b. Morphodynamics of intermediate beaches: a video imaging and numerical modelling study. Coastal Engineering, 51(7), 629-655. doi: 10.1016/j.coastaleng.2004.07.018.

Rector, R. L., 1954. Laboratory study of equilibrium profiles of beaches. Technical Memorandum No.41, Beach Erosion Board, Coastal Engineering Research Center, Department of the Army Corps of Engineers, Waterways Experiment Station, Washington, D.C., United States.

Revell, D. L., Dugan, J. E. and Hubbard, D. M., 2011. Physical and Ecological Responses of Sandy Beaches to the 1997–98 El Niño. Journal of Coastal Research, 27(4), 718-730. doi: 10.2112/JCOASTRES-D-09-00179.1.

Ritchie, W. and Penland, S., 1988. Rapid dune changes associated with overwash processes on the deltaic coast of South Louisiana. Marine Geology, 81(1), 97-122. doi: 10.1016/0025-3227(88)90020-5.

Roberts, T. M., Wang, P. and Puleo, J. A., 2013. Storm-driven cyclic beach morphodynamics of a mixed sand and gravel beach along the Mid-Atlantic Coast, USA. Marine Geology, 346, 403-421. doi: 10.1016/j.margeo.2013.08.001.

Roelvink, D., Reniers, A., van Dongeren, A., van Thiel de Vries, J., McCall, R. and Lescinski, J., 2009. Modelling storm impacts on beaches, dunes and barrier islands. Coastal Engineering, 56(11–12), 1133-1152. doi: 10.1016/j.coastaleng.2009.08.006.

Rosati, J. D., 2005. Concepts in Sediment Budgets. Journal of Coastal Research, 21(2), 307-322. doi: 10.2112/02-475A.1.

Roy, P. S., Thom, B. G. and Wright, L. D., 1980. Holocene sequences on an embayed high-energy coast: an evolutionary model. Sedimentary Geology, 26(1), 1-19. doi: 10.1016/0037-0738(80)90003-2.

Ruessink, B. G. and Jeuken, M. C. J. L., 2002. Dunefoot dynamics along the Dutch coast. Earth Surface Processes and Landforms, 27(10), 1043-1056. doi: 10.1002/esp.391.

Ruessink, B. G., Kuriyama, Y., Reniers, A. J. H. M., Roelvink, J. A. and Walstra, D. J. R., 2007. Modelling cross-shore sandbar behavior on the timescale of weeks. Journal of Geophysical Research: Earth Surface, 112(F3), F03010. doi: 10.1029/2006JF000730.

Ruessink, B. G., Pape, L. and Turner, I. L., 2009. Daily to interannual cross-shore sandbar migration: Observations from a multiple sandbar system. Continental Shelf Research, 29(14), 1663-1677. doi: 10.1016/j.csr.2009.05.011.

Ruggiero, P., Kaminsky, G. M., Gelfenbaum, G. and Voigt, B., 2005. Seasonal to interannual morphodynamics along a high-energy dissipative littoral cell. Journal of Coastal Research, 21(3), 553-57810.2112/03-0029.1.

Russell, P. E., Masselink, G., Blenkinsopp, C. and Turner, I. L., 2009. A Comparison of Berm Accretion in the Swash Zone on Sand and Gravel Beaches at the Timescale of Individual Waves. Journal of Coastal Research, SP(56), 1791-1795.

Sallenger, A. H., Holman, R. A. and Birkemeier, W. A., 1985. Storm-induced response of a nearshore-bar system. Marine Geology, 64(3–4), 237-257. doi: 10.1016/0025-3227(85)90107-0.

Sallenger, A. H., Jr., 2000. Storm Impact Scale for Barrier Islands. Journal of Coastal Research, 16(3), 890-895. doi: 10.2307/4300099.

Scott, T., Masselink, G., O'Hare, T., Saulter, A., Poate, T., Russell, P., Davidson, M. and Conley, D., 2016. The extreme 2013/2014 winter storms: Beach recovery along the southwest coast of England. Marine Geology, 382, 224-241. doi: 10.1016/j.margeo.2016.10.011.

Scott, T., Masselink, G., O'Hare, T., Davidson, M. and Russell, P., 2015. Multi-annual sand and gravel beach response to storms in the southwest of England. In Procceedings: Coastal Sediments, San Diego, United States. doi: 10.1142/9789814689977_0256

Senechal, N., Coco, G., Castelle, B. and Marieu, V., 2015. Storm impact on the seasonal shoreline dynamics of a meso- to macrotidal open sandy beach (Biscarrosse, France). Geomorphology, 228, 448-461. doi: 10.1016/j.geomorph.2014.09.025.

Sexton, W. J. and Hayes, M. O., 1991. The Geologic Impact of Hurricane Hugo and Post-Storm Shoreline Recovery Along the Undeveloped Coastline of South Carolina, Dewees Island to the Santee Delta. Journal of Coastal Research, SI(8), 275-290. doi: 10.2307/25735421.

Shand, T., Goodwin, I., Mole, M., Carley, J., Coghlan, I., Harley, M. and Peirson, W., 2010. NSW coastal inundation hazard study: coastal storms and extreme waves. Report 16, Water Research Laboratory , UNSW Australia, Sydney, Australia.

Shepard, F. P., 1950. Beach cycles in southern California, Beach Erosion Board, Coastal Engineering Research Center, Department of the Army Corps of Engineers, Washington, D.C., United States.

Shepard, F. P. and LaFond, E. C., 1940. Sand movements along the Scripps Institution pier. American Journal of Science, 238(4), 272-285.

Short, A. D., 1979. Three Dimensional Beach-Stage Model. The Journal of Geology, 87(5), 553-571. doi: 10.1086/628445.

Short, A. D., 1985. Rip-current type, spacing and persistence, Narrabeen Beach, Australia. Marine Geology, 65(1–2), 47-71. doi: 10.1016/0025-3227(85)90046-5.

Short, A. D., 1999. Handbook of beach and shoreface morphodynamics. John Wiley & Sons, Chichester, United Kingdom.

Short, A. D., 2006. Australian Beach Systems—Nature and Distribution. Journal of Coastal Research, 22(1), 11-27. doi: 10.2112/05a-0002.1.

Short, A. D., 2007. Beaches of the New South Wales coast: a guide to their nature, characteristics, surf and safety. Sydney University Press, Sydney, Australia.

Short, A. D. and Hesp, P. A., 1982. Wave, beach and dune interactions in southeastern Australia. Marine Geology, 48(3–4), 259-284. doi: 10.1016/0025-3227(82)90100-1.

Short, A. D. and Trenaman, N. L., 1992. Wave climate of the Sydney region, an energetic and highly variable ocean wave regime. Marine and Freshwater Research, 43(4), 765-791. doi: 10.1071/MF9920765.

Short, A. D. and Woodroffe, C. D., 2009. The coast of Australia. Cambridge University Press, New York, United States.

Short, A. D. and Wright, L. D., 1981. Beach systems of the Sydney region. Australian Geographer, 15(1), 8-16. doi: 10.1080/00049188108702791.

Silva, J. S., Leal, M. M. V., Araújo, M. C. B., Barbosa, S. C. T. and Costa, M. F., 2008. Spatial and Temporal Patterns of Use of Boa Viagem Beach, Northeast Brazil. Journal of Coastal Research, 24(1A), 79-86. doi: 10.2112/05-0527.1.

Simmons, J. A., Harley, M. D., Marshall, L. A., Turner, I. L., Splinter, K. D. and Cox, R. J., 2017. Calibrating and assessing uncertainty in coastal numerical models. Coastal Engineering, 125, 28-41. doi: 10.1016/j.coastaleng.2017.04.005.

Small, C. and Nicholls, R. J., 2003. A global analysis of human settlement in coastal zones. Journal of Coastal Research, 19(3), 584-599.

Smith, A. M., Mather, A. A., Bundy, S. C., Cooper, J. A. G., Guastella, L. A., Ramsay, P. J. and Theron, A., 2010. Contrasting styles of swell-driven coastal erosion: examples from KwaZulu-Natal, South Africa. Geological Magazine, 147(6), 940-953. doi: 10.1017/S0016756810000361.

Sonu, C. J., 1968. Collective movement of sediment in littoral environment. In Procceedings: International Conference on Coastal Engineering, London, United Kingdom. doi: 10.1061/9780872620131.024.

Sonu, C. J., 1973. Three-Dimensional Beach Changes. The Journal of Geology, 81(1), 42-64. doi: 10.2307/30060693.

Sonu, C. J. and Beek, J. L. V., 1971. Systematic Beach Changes on the Outer Banks, North Carolina. The Journal of Geology, 79(4), 416-425. doi: 10.2307/30063058.

Speer, M. S., Wiles, P. and Pepler, A., 2009. Low pressure systems off the New South Wales coast and associated hazardous weather: establishment of a database. Australian Meteorological and Oceanographic Journal, 58(1), 29.

Splinter, K. D., Holman, R. A. and Plant, N. G., 2011a. A behavior-oriented dynamic model for sandbar migration and 2DH evolution. Journal of Geophysical Research: Oceans, 116, C01020. doi: 10.1029/2010JC006382.

Splinter, K. D., Strauss, D. R. and Tomlinson, R. B., 2011b. Assessment of Post-Storm Recovery of Beaches Using Video Imaging Techniques: A Case Study at Gold Coast, Australia. IEEE Transactions on Geoscience and Remote Sensing, 49(12), 4704-4716. doi: 10.1109/TGRS.2011.2136351.

Stone, G. W., Liu, B., Pepper, D. A. and Wang, P., 2004. The importance of extratropical and tropical cyclones on the short-term evolution of barrier islands along the northern Gulf of Mexico, USA. Marine Geology, 210(1–4), 63-78. doi: 10.1016/j.margeo.2004.05.021.

Suanez, S., Cariolet, J.-M., Cancouët, R., Ardhuin, F. and Delacourt, C., 2012. Dune recovery after storm erosion on a high-energy beach: Vougot Beach, Brittany (France). Geomorphology, 139–140, 16-33. doi: 10.1016/j.geomorph.2011.10.014.

Sunamura, T. and Takeda, I., 1984. Landward migration of inner bars. Marine Geology, 60(1–4), 63-78. doi: 10.1016/0025-3227(84)90144-0.

Tătui, F., Vespremeanu-Stroe, A. and Preoteasa, L., 2014. Alongshore variations in beach-dune system response to major storm events on the Danube Delta coast. Journal of Coastal Research, SI(70), 693-699. doi: 10.2112/SI70-117.1.

Terwindt, J., Hulsbergen, C. and Kohsiek, L., 1984. Structures in deposits from beach recovery, after erosion by swell waves around the southwestern coast of Aruba (Netherlands Antilles). Marine geology, 60(1-4), 283-311. doi: 10.1016/0025-3227(84)90154-3.

Thom, B. and Hall, W., 1991. Behaviour of beach profiles during accretion and erosion dominated periods. Earth Surface Processes and Landforms, 16(2), 113-127. doi: 10.1002/esp.3290160203.

Thom, B. G., 1984. Transgressive and regressive stratigraphies of coastal sand barriers in southeast Australia. Marine Geology, 56(1), 137-158. doi: 10.1016/0025-3227(84)90010-0.

Turner, I. L., Harley, M. D., Short, A. D., Simmons, J. A., Bracs, M. A., Phillips, M. S. and Splinter, K. D., 2016. A multi-decade dataset of monthly beach profile surveys and inshore wave forcing at Narrabeen, Australia. Scientific Data, 3, 160024. doi: 10.1038/sdata.2016.24.

Turner, I. L., Russell, P. E. and Butt, T., 2008. Measurement of wave-by-wave bed-levels in the swash zone. Coastal Engineering, 55(12), 1237-1242. doi: 10.1016/j.coastaleng.2008.09.009.

Uunk, L., Wijnberg, K. M. and Morelissen, R., 2010. Automated mapping of the intertidal beach bathymetry from video images. Coastal Engineering, 57(4), 461-469. doi: 10.1016/j.coastaleng.2009.12.002.

van de Lageweg, W. I., Bryan, K. R., Coco, G. and Ruessink, B. G., 2013. Observations of shoreline–sandbar coupling on an embayed beach. Marine Geology, 344, 101-114. doi: 10.1016/j.margeo.2013.07.018.

van Enckevort, I. M. J. and Ruessink, B. G., 2001. Effect of hydrodynamics and bathymetry on video estimates of nearshore sandbar position. Journal of Geophysical Research: Oceans, 106(C8), 16969-16979. doi: 10.1029/1999JC000167.

van Enckevort, I. M. J. and Ruessink, B. G., 2003. Video observations of nearshore bar behaviour. Part 1: alongshore uniform variability. Continental Shelf Research, 23(5), 501-512. doi: 10.1016/S0278-4343(02)00234-0.

van Enckevort, I. M. J., Ruessink, B. G., Coco, G., Suzuki, K., Turner, I. L., Plant, N. G. and Holman, R. A., 2004. Observations of nearshore crescentic sandbars. Journal of Geophysical Research: Oceans, 109(C6), C06028. doi: 10.1029/2003JC002214.

van Maanen, B., de Ruiter, P. J., Coco, G., Bryan, K. R. and Ruessink, B. G., 2008. Onshore sandbar migration at Tairua Beach (New Zealand): Numerical simulations and field measurements. Marine Geology, 253(3–4), 99-106. doi: 10.1016/j.margeo.2008.05.007.

Vousdoukas, M. I., Almeida, L. P. M. and Ferreira, Ó., 2012. Beach erosion and recovery during consecutive storms at a steep-sloping, meso-tidal beach. Earth Surface Processes and Landforms, 37(6), 583-593. doi: 10.1002/esp.2264.

Wainwright, D. J., Ranasinghe, R., Callaghan, D. P., Woodroffe, C. D., Jongejan, R., Dougherty, A. J., Rogers, K. and Cowell, P. J., 2015. Moving from deterministic towards probabilistic coastal hazard and risk assessment: Development of a modelling framework and application to Narrabeen Beach, New South Wales, Australia. Coastal Engineering, 96, 92-99. doi: 10.1016/j.coastaleng.2014.11.009.

Walstra, D., Van Rijn, L., Van Ormondt, M., Brière, C. and Talmon, A., 2007. The Effects of Bed Slope and Wave Skewness on Sediment Transport and Morphology. In Procceedings: International Symposium on Coastal Engineering and Science of Coastal Sediment Process, New Orleans, United States, 1-14. doi: 10.1061/40926(239)11.

Wang, P., Kirby, J. H., Haber, J. D., Horwitz, M. H., Knorr, P. O. and Krock, J. R., 2006. Morphological and Sedimentological Impacts of Hurricane Ivan and Immediate Poststorm Beach Recovery along the Northwestern Florida Barrier-Island Coasts. Journal of Coastal Research, 22(6), 1382-1402. doi: 10.2112/05-0440.1.

Wearne, A. H., 1977. Beach changes during the early accretion phase. Journal Soil Conservation Service NSW, 33, 109-116.

Weir, F. M., Hughes, M. G. and Baldock, T. E., 2006. Beach face and berm morphodynamics fronting a coastal lagoon. Geomorphology, 82(3–4), 331-346. doi: 10.1016/j.geomorph.2006.05.015.

Weymer, B. A., Houser, C. and Giardino, J. R., 2015. Poststorm Evolution of Beach-Dune Morphology: Padre Island National Seashore, Texas. Journal of Coastal Research, 31(3), 634-644. doi: 10.2112/JCOASTRES-D-13-00020.1.

Witmer, A. D. and Roelke, D. L., 2014. Human interference prevents recovery of infaunal beach communities from hurricane disturbance. Ocean & Coastal Management, 87, 52-60. doi: 10.1016/j.ocecoaman.2013.11.005.

Wright, L. D. and Short, A. D., 1984. Morphodynamic variability of surf zones and beaches: A synthesis. Marine Geology, 56(1–4), 93-118. doi: 10.1016/0025-3227(84)90008-2.

Wright, L. D., Short, A. D. and Green, M. O., 1985. Short-term changes in the morphodynamic states of beaches and surf zones: An empirical predictive model. Marine Geology, 62(3–4), 339-364. doi: 10.1016/0025-3227(85)90123-9.

You, Z.-J., Laine, R., Hanslow, D. J., Baldock, T. and Wiecek, D., 2014. Field measurements of beach-dune dynamic profiles to assess erosion hazard on the coast of NSW, Australia. In Procceedings: International Conference on Coastal Engineering, Seoul, Korea. doi: 10.9753/icce.v34.management.23.

Young, I. R. and Holland, G., 1996. Atlas of the Oceans: Wind and Wave Climate. Elsevier, Oxford, United Kingdom.

Yu, F., Switzer, A. D., Lau, A. Y. A., Yeung, H. Y. E., Chik, S. W., Chiu, H. C., Huang, Z. and Pile, J., 2013. A comparison of the post-storm recovery of two sandy beaches on Hong Kong Island, southern China. Quaternary International, 304, 163-175. doi: 10.1016/j.quaint.2013.04.002.

Zeigler, J. M., Hayes, C. R. and Tuttle, S. D., 1959. Beach Changes during Storms on Outer Cape Cod, Massachusetts. The Journal of Geology, 67(3), 318-336. doi: 10.2307/30057084.

Zhang, K., Douglas, B. and Leatherman, S., 2002. Do Storms Cause Long-Term Beach Erosion along the US East Barrier Coast? The journal of Geology, 110(4), 493-502. doi: 10.1086/340633.

Appendix A

The varying recovery of post-storm subaerial beach morphology: a demonstrative example from field data at Narrabeen-Collaroy, SE Australia

Content of this Appendix is in preparation for publication in:

Phillips, M. S., Harley, M. D., Blenkinsopp, C. E., Turner, I. L., Splinter, K. D. and Cox, R. J., *in prep*. Timescales and rates of post-storm beach recovery: a synthesis. Coastal Engineering.

The varying recovery of subaerial beach morphology is further demonstrated in Figure A.1 using beach profile data (described by Turner et al., 2016) collected from Narrabeen-Collaroy Beach, SE Australia (refer to Section 3.2.1 for a detailed site description). Figure A.1a shows beach profile changes during recovery following a storm event in June 2011. The associated recovery indicators of subaerial volume and shoreline position are shown in Figures A.1b and A.1c. These were observed to return to pre-storm conditions within several months of the conclusion of the erosion event. The volume and shoreline indices were observed to progress in a similar fashion, with an initial lag of approximately one month, followed by relatively rapid recovery rates (2.4 m^3/m/day and 1.2 m/day), which then reduced (0.4 m^3/m/day and 0.1 m/day) in the later months as the volume and shoreline approached pre-storm conditions. Overall, net rates of subaerial volume and shoreline recovery during this initial 3 to 4 month period were approximately 0.6 m^3/m/day and 0.2 m/day, respectively. These durations and rates mark the completion of shoreline and berm recovery and also the recovery of subaerial (above MSL) volume in this example.

In contrast to subaerial volume and shoreline recovery, backshore aggradation and dune recovery in Figure A.1a is observed to occur for this same storm event over longer durations of several years. In Figures A.1d and A.1e, the eroded backshore and dune toe in the upper profile have only partially recovered to pre-storm volume (60%) and elevation (73%) at the time of writing, 5 years after the storm. Recovery of dune volume (sediment volume above the dune toe contour, approximately 3 m) lagged in response until one year after the storm before proceeding at a steady rate of 2 - 3 m^3/m/year, with minor storm interruption during the second year. The recovery of dune toe elevation is observed to progress rapidly (0.01 - 0.03 m/day) immediately following storm erosion associated with wave-driven deposition, and then steadily at approximately 0.1 - 0.2 m/year due predominantly to aeolian processes. Rates and timescales of backshore aggradation and dune recovery are much slower and prolonged in comparison to shoreline and subaerial volume recovery.

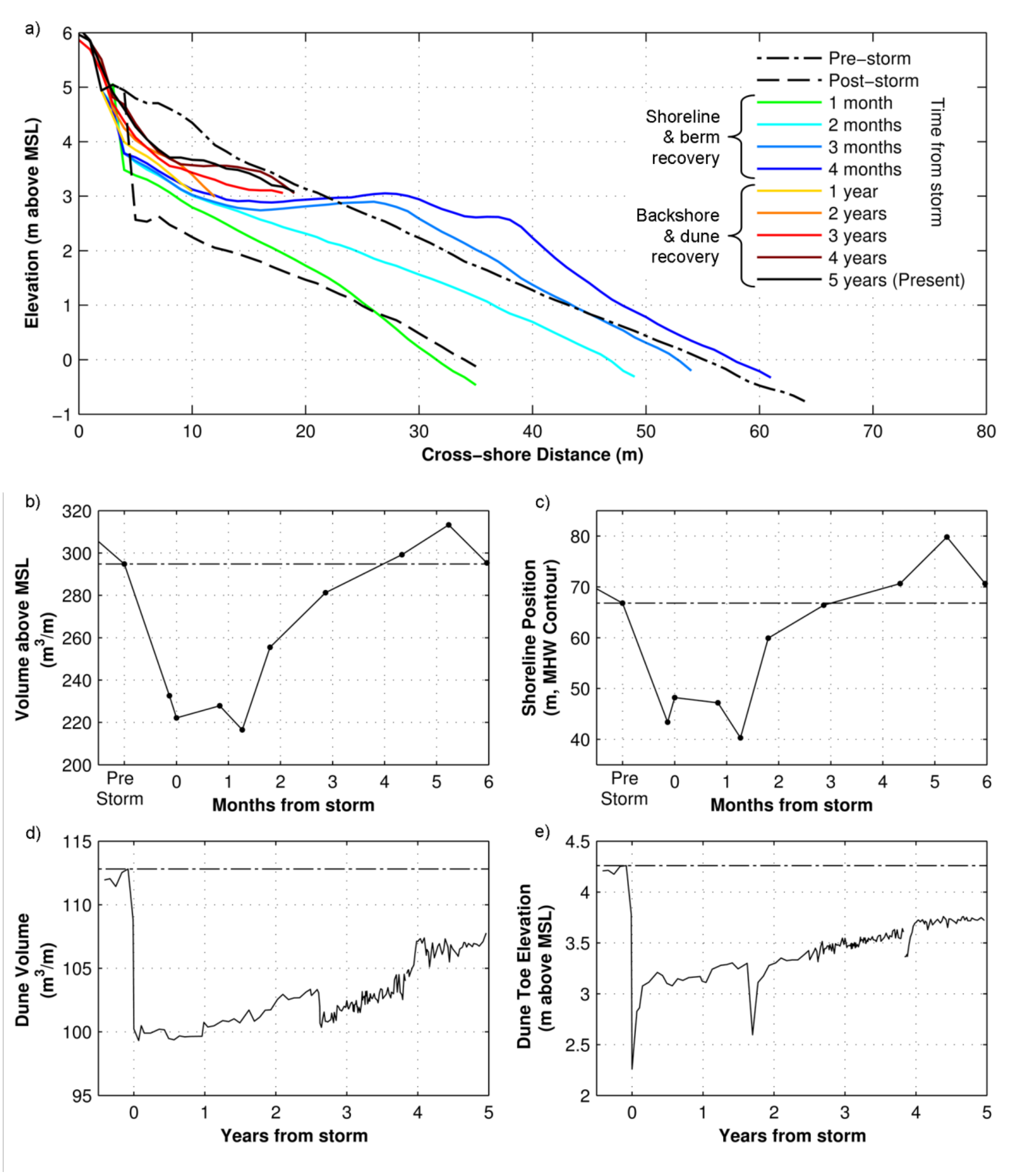

Figure A.1: Quantifying and contrasting the subaerial processes of post-storm beach recovery at Narrabeen Beach, Australia following storm activity in June 2011. a) Subaerial beach profile changes showing shorter-term wave-driven shoreline and berm recovery, and longer-term aeolian-driven backshore and dune recovery. Corresponding measurements of b) subaerial volume, c) shoreline position, d) dune volume and e) dune toe elevation. Pre-storm conditions marked by dashed-dotted line.

Appendix B

Fixed Lidar beach profile comparison with surveyed RTK-GPS beach profiles

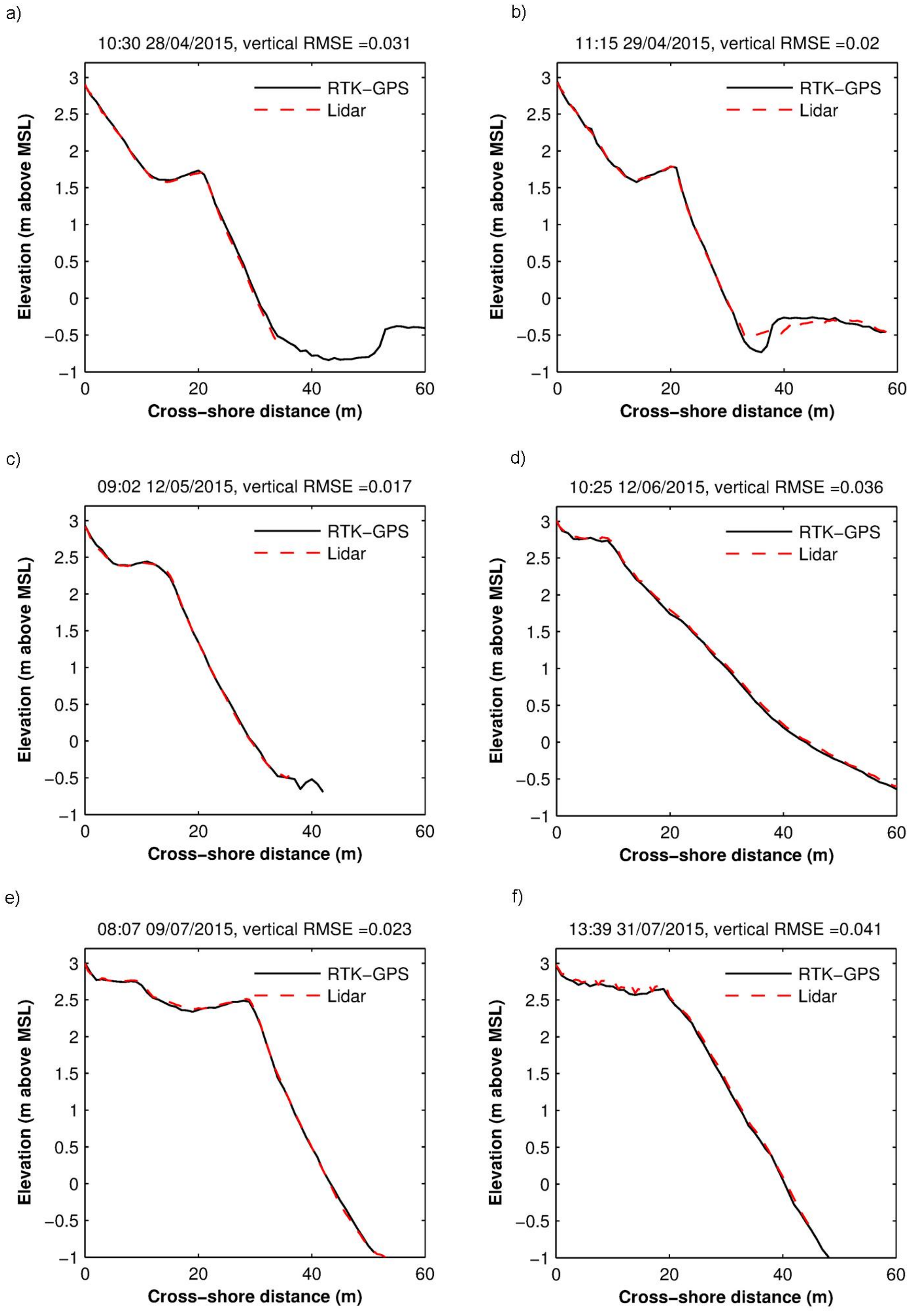

Figure B.1: Comparison of beach profiles measured from the Fixed Lidar monitoring system with concurrent RTK-GPS surveys of the exact transect measured throughout the recovery period analysed in Chapter 4. The vertical root-mean-square-error (RMSE) of the Lidar-derived profile relative to the RTK-GPS profile is noted above each graph, calculated across the subaerial (above MSL) region of the profile.

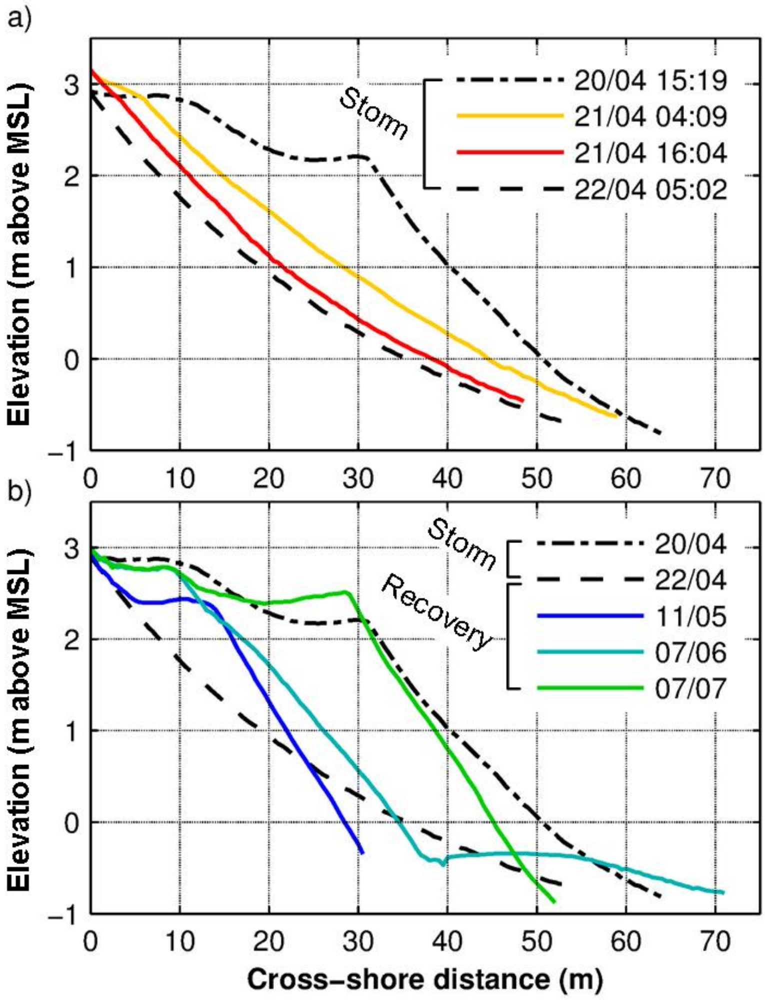

Figure B.2: Lidar measured beach profiles showing a) Rapid profile changes during the April 2015 storm and b) progressive profile changes during post-storm recovery. Note the presence of an attached sandbar in the lower regions of the beach profile on 7th June 2015 prior to more rapid rates of subaerial volume recovery during the final month of berm recovery.

Appendix C

Survey photographs: April 2015 storm and recovery

Figure C.1: Bilgola Beach a) Pre-storm 14th April 2015, b) Post-storm 22nd April 2015 and c) after recovery 29th April 2016.

Figure C.2: Mona Vale Beach a) Pre-storm 14th April 2015, b) Post-storm 22nd April 2015 and c) after recovery 29th April 2016

Figure C.3: Narrabeen Beach a) Pre-storm 14th April 2015, b) Post-storm 22nd April 2015 and c) after recovery 29th April 2016

Figure C.4: Dee Why Beach a) Pre-storm 14th April 2015, b) Post-storm 22nd April 2015 and c) after recovery 29th April 2016